

**DEVELOPMENT OF HAZARD PREDICTION MODEL FOR
TOXIC AIR POLLUTANTS RESULTING FROM TERRORIST
EVENTS**

**M.M.M.S. KUMARA
333**

Department of Chemistry, University of Colombo,
Colombo 03, Sri Lanka.

“Dissertation submitted in partial fulfillment of the requirements for the degree of
MASTER OF SCIENCE of the UNIVERSITY OF COLOMBO, SRI LANKA”

September 2012

**DEVELOPMENT OF HAZARD PREDICTION
MODEL FOR TOXIC AIR POLLUTANTS
RESULTING FROM TERRORIST EVENTS**

M.M.M.S. KUMARA

2012

2012

M. Sc. Analytical Chemistry

Kumara M.M.M.S

Abstract

Hazard prediction following an immediate release of a toxic air pollutant enables fast execution of disaster management activities. A computer code called “Hazard Prediction Model” (HPM), which is capable of predicting the atmospheric dispersion and quantifying ground level concentrations/dosages of passive gas/vapor clouds was developed. The study primarily aimed at explosive and thermal releases of six chemical agents including chlorine, sarin, tabun, sulfur mustard, hydrogen cyanide and cyanogen chloride.

To simulate the dispersal of toxic agents in the atmosphere, meteorological and geographical data were primarily in demand. In addition, it was required to account for the significant chemical reactions of each agent in the atmosphere. To compensate these needs, the development of Hazard Prediction Model involved four separate sub models; diagnostic meteorological model, geographical model, chemical model and a dispersion model. The model development was performed using visual C# programming language resulting in an interactive user interface which enables efficient operation in an emergent case. The diagnostic meteorological model was primarily consisted of a basic meteorological parameterization scheme and a diagnostic wind model. The role of the first was to process meteorological user input and to interpolate in a 3-Dimensional grid system, whereas the latter to produce terrain influenced wind field. To achieve this task, appropriate mathematical models were selected from literature and programmed. In the development of geographical model, a database was created by processing Digital Elevation Maps in ArcGIS software and computing terrain data over a 510 x 920 grid covering Sri Lanka. Furthermore, codes to calculate terrain features and to perform grid operations were also written. Under the development of dispersion model, a Lagrangian Puff Particle model was programmed. This was capable of simulating the dispersal of agent in the atmosphere and calculating concentrations/dosages at interested locations in the space. In the development of chemical model, only significant atmospheric reactions of the chemical agents; hydroxyl radical reactions of sarin, tabun and sulfur mustard were considered. Necessary algorithms were written for these chemical processes and incorporated into HPM as a chemical model.

Finally, the performance of the model was evaluated using three step approach; evaluation of the basic meteorological parameterization scheme, mass consistent wind model and total model performance. The first step involved comparison of model predictions with several derived meteorological parameters reported in well known Indianapolis tracer gas experiments. The experiment reports onsite meteorological measurements and several important derived

parameters. These derived parameters were kept as evaluation objectives and the scheme was evaluated using the onsite measurements as input to HPM. It was observed that the HPM model predictions were in good agreement with reported data. To validate the mass consistent wind model, a potential flow was simulated around a hemi spherical hill where analytical solutions for the problem were available. The accuracy of simulated wind components were statistically evaluated with analytical solutions. Furthermore, visual observation was also employed. The study showed that the wind model is capable of producing accurate wind flows. Finally, the total model performance was evaluated using Dipole Pride 26 field experiment (DP26). Hazard Prediction Model was used to simulate eight instantaneous sulfur hexafluoride releases using meteorological and geographical data provided in DP26 data set. Model predictions were statistically evaluated with reported dosages by DP26 samplers. The study showed that model predictions were in good agreement with the actual values reported by samplers. Finally, the applicability of HPM for Sri Lanka was demonstrated using a model calculation.

Acknowledgements

I would like to express my humble gratitude to my supervisor, Dr. Samantha Weerasinghe for his good counsel all the way through the entire research project and his valuable guidance without which this endeavor would not have been a success.

I convey my deepest gratitude to the Head of the Department, Prof.K.R.R.Mahanama, M. Sc. Analytical Chemistry Course Coordinator, Dr. Dilrukshi Wijayarathna and all the academic staff of the University of Colombo for the support given.

I would also like to thank Prof. J. Chang of George Mansion University and Mrs. Kumari M. Weerasinghe of National Building Research Organization for the support given by providing valuable field data sets without which this work would have been difficult.

I make this an opportunity to thank all my friends for the endless help and encouragement given all the way through.

Last but not least, I would like to express my gratitude to my parents, uncle, aunt and all the other family members for the enormous support and encouragement given throughout the study.

Declaration

This thesis is my original work and has not been submitted previously for a degree at this or any other university / institute. To the best of my knowledge it does not contain any material published or written by another person, except as acknowledged in the text.

.....
Mr. M.M.M.S. Kumara

Date.....

This is to certify that this dissertation is based on the work carried by Mr. M.M.M.S. Kumara under my supervision. The dissertation has been prepared according to the format stipulated and is of acceptable standard.

Certified by:

Supervisor : Dr. Samantha Weerasinghe

Date.....

Signature.....

Table of Contents

Abstract	I
Acknowledgements	III
Declaration	IV
Table of Contents	V
List of Tables.....	VIII
List of Figures	IX
1 Introduction	1
1.1 Behavior and the Impact of a Chemical Warfare Attack.....	2
1.1.1 Chemical warfare agents and the terrorism.....	4
1.1.1.1 Chocking agents	5
1.1.1.2 Nerve agents	6
1.1.1.3 Blood agents	8
1.1.1.4 Blister agents	9
1.1.2 Dissemination of chemical warfare agents in the atmosphere	10
1.1.3 Dispersion of chemical warfare agents in the atmosphere	11
1.1.3.1 The structure of the earth's atmosphere	11
1.1.3.2 Atmospheric turbulence.....	13
1.1.3.3 Atmospheric stability.....	13
1.1.3.4 Dispersal of chemical warfare agents	13
1.2 Modeling of Chemical Warfare Release	15
1.2.1 Atmospheric dispersion models	18
1.2.2 Meteorological models.....	21
1.2.3 Source models	23
1.3 Computer Simulation of Hazard Prediction Models	24
1.4 Objectives and Scopes of the Research	25
2 Computer Model Development.....	26

2.1	Grid System	26
2.2	The Meteorological Model	28
2.2.1	Meteorological input	29
2.2.2	Description of the meteorological model	30
2.2.2.1	Procedure for the estimation of solar elevation angle	30
2.2.2.2	Procedure for the estimation of sensible heat flux, Monin-Obukhov length and surface friction velocity.....	31
2.2.2.3	Procedure for the estimation of convective scaling velocity and boundary layer height.....	36
2.2.2.4	Formulation of gridded meteorological fields	38
2.2.2.5	Turbulence parameterization scheme	49
2.3	Geographical Model	52
3	Modeling Explosive Releases of Chemical Warfare Agents and Dispersion in the Atmosphere	54
3.1	Modeling the Sources of Chemical Warfare Agents from Terrorist Events	54
3.1.1	Modeling instantaneous explosive releases.....	55
3.1.2	Modeling continuous/semi-continuous sources	59
3.2	Modeling the Dispersion of Chemical Warfare Agents in the Atmosphere.....	62
3.3	Modeling chemical reactions.....	65
4	Model Evaluation Methodology.....	67
4.1	Evaluation of basic meteorological parameterization scheme	68
4.2	Evaluation of the Mass Consistent Wind Model.....	69
4.3	Evaluation of the Overall Performance of Hazard Prediction Model	70
4.4	Effect of chemical processes on atmospheric dispersion of GB, GA and HD	74
5	Results and Discussion.....	75
5.1	Evaluation of Basic Meteorological Parameterization Scheme	75
5.2	Evaluation of the Mass Consistent Wind Model.....	78
5.3	Evaluation of the Overall Model Performance.....	83
5.4	Effect of Chemical Reactions	87

5.5 Application of Hazard Prediction Model in Sri Lanka.....	88
6 Conclusions	93
References	94
Appendix I.....	99
Appendix II	100
Appendix III	100
Appendix IV.....	101
Appendix V	102
Appendix VI.....	103
Appendix VII.....	105
Appendix VIII	106
Appendix IX.....	108

List of Tables

Table 1.1 Physical properties and toxicity data of some chocking agents.....	5
Table 1.2 Physical properties and toxicity data of GB and GA	7
Table 1.3 Physical properties and toxicity data of some blood agents.....	8
Table 1.4 Physical properties and toxicity details of Sulfur Mustard	9
Table 2.1 Atmospheric stability classification based on Monin-Obukhov length	37
Table 2.2 Height of the planetary boundary layer depending on the atmospheric stability	37
Table 2.3 The turning angle of the wind at 200 m reference height under various stability conditions	40
Table 2.4 Relationship between stability class & temperature lapse rate.....	41
Table 4.1 Summary of DP26 trials used for the model evaluation of HPM.....	72
Table 5.1 Summary of basic meteorological parameter evaluation	75
Table 5.2 Runtimes reported for a potential flow around a hemi spherical hill under various grid resolutions and computer performances.....	82
Table 5.3 Summary of results for each performance measure as shown in the evaluation study of HPM	83
Table 5.4 General Input to Hazard Prediction model for hypothetical simulation of a sarin emission scenario	89
Table 5.5 Source Input to Hazard Prediction model for hypothetical simulation of a sarin emission scenario	90
Table 5.6 Geographical Input to Hazard Prediction model for hypothetical simulation of a sarin emission scenario	90
Table 5.7 Meteorological Input to Hazard Prediction model for hypothetical simulation of a sarin emission scenario (Note that the MEDA stands for the meteorological station and WS, WD, T, P, RH, CC, RF for the hourly averaged wind speed, direction, temperature, pressure, relative humidity, cloud cover and rain fall respectively.).....	90

List of Figures

Figure 1.1 Factors governing the impact of chemical warfare agent release on an exposed individual.....	3
Figure 1.2 The general structures of nerve agents.....	6
Figure 1.3 The diurnal variation of the planetary boundary layer in fair weather conditions.....	12
Figure 1.4 Effect of turbulent eddies on a gas/vapor cloud ⁷	14
Figure 1.5 Evolution of a chemical cloud from a detonation.....	15
Figure 2.1 Description of the grid system	27
Figure 2.2 Summary of inputs and outputs of the meteorological model	29
Figure 2.3 Summarization of the geographical model	52
Figure 3.1 Summary of major input and output of cloud rise and plume rise models	55
Figure 3.2 Schematic diagram of rise and dispersion of material following an instantaneous explosive release	56
Figure 3.3 Schematic diagram of rise and dispersion of a buoyant plume	60
Figure 3.4 Horizontal view of trajectory and growth of a single puff ($l = X, Y, Z$)	62
Figure 4.1 Dipole pride test site with dissemination points (N2,N3,S2,S3), Sampling lines (Line 1-3), MEDA stations (M1, M2, M3, M6, M9, M10, M17, M28), Primary instrumentation positions (BJY, UCC, YFW).....	71
Figure 5.1 Predicted vs Reported values of sensible heat flux.....	77
Figure 5.2 Predicted vs Reported values of Monin-Obukhov length.....	77
Figure 5.3 Predicted vs Reported values of friction velocity	78
Figure 5.4 Numerical simulation of a potential flow around a hemi spherical hill – 3 Dimensional view (the direction of the wind is represented by arrows).....	80
Figure 5.5 Numerical simulation of a potential flow around a hemi spherical hill – 2 Dimensional view (Red and blue arrows represent the numerically simulated wind field and the analytical wind field respectively. The brownish circle in the middle of the figure represents the hill.).....	81
Figure 5.6 Scatter plot of predicted maximum dosages vs observed values for each sampling line	85
Figure 5.7 3-D view of Nevada test site as approximated by HPM	86
Figure 5.8 Dosage color maps produced by HPM for the atmospheric dispersion of agents without chemical processes (a), dispersion of GA (b), GB (c), and HD (d) with Hydroxyl radical reactions. (Note that the red, yellow, green and blue represents dosages above 1050 ppt h, 1050 - 750 ppt h, 750 - 450 ppt h, and 450 - 150 ppt h ranges)	88

Figure 5.9 Output of Hazard Prediction Model for the hypothetical simulation of sarin emission scenario - wind field **(a)**, Dosage color map **(b)** (Note that the red, yellow, green and blue represents dosages above 5000 ppt h, 5000 - 3000 ppt h, 3000 - 1500 ppt h, and 1500 - 400 ppt h ranges).....91

Glossary

A	Pasquill stability category: Extremely unstable
<i>A</i>	Coefficient matrix in wind field divergence minimization
AC	Hydrogen cyanide
α	Surface moisture availability coefficient
α'	Small angle through which the earth must turn to bring the meridian of the interested location directly under the sun (radians)
α_l	The drift term of the stochastic Langevin equation
α_u	Weighing factors for the wind field divergence minimization in X direction
α_v	Weighing factors for the wind field divergence minimization in Y direction
α_w	Weighing factors for the wind field divergence minimization in Z direction
B	Pasquill stability category: Moderately unstable
<i>B</i>	Divergence vector in wind field divergence minimization
β_l	Diffusion term of the stochastic Langevin equation
β_R	Constant involved in plume rise modeling
C	Pasquill stability category: Slightly unstable
<i>c</i>	Ensemble averaged concentration (ppt)
\tilde{c}	Concentration of a substance in the atmosphere (ppt)
χ	Solar elevation angle (radians)
c_0	Observed concentration (ppt)
CK	Cyanogen chloride
C_l	Correction factor reflecting heat loss and impact on the fireball radius
c_p	Specific heat capacity of air at constant pressure (1.006 kJ kg ⁻¹ K ⁻¹ at 1 x 10 ⁵ N m ⁻² pressure)
c_{prd}	Predicted concentration (ppt)
Cl	Chlorine
$c(x, y, z)$	Concentration of agent at location x, y, z (ppt)
D	Pasquill stability category: Neutral
D_C	Molecular diffusion coefficient of the substance
Δt	Small time increment (s)

du'_l	Fluctuation of turbulent velocity over a small time step
$dW_l(t)$	Gaussian white noise process with zero mean and variance of one
$D(z)$	Turning angle of the wind at height Z (deg)
$D(z_{200})$	Turning angle of the wind in clockwise direction at reference height
E	Pasquill stability category: Slightly stable
e	Albedo value
F	Pasquill stability category: Stable
f	Coriolis parameter
F_0	Initial buoyancy of the puff
$FAC2$	Fraction of observations within factors of two observations
$FAC3$	Fraction of observations within factors of three observations
FB	Fractional bias
G	Pasquill stability category: Very stable
G	Divergence of the wind field (s^{-1})
g	Acceleration of gravity (9.81 m s^{-2})
GA	Tabun
GB	Sarin
g'	Reduced gravity (m s^{-2})
H_0	Sensible heat flux (kW m^{-2})
h_{crit}	Critical height for the vertical interpolation of meteorological variables (m)
H_g	Ground heat flux (W m^{-2})
HD	Sulfur mustard
H_l	Latent heat flux (W m^{-2})
H_R	Heat released from an explosion (kJ)
H_r	Net radiation (W m^{-2})
H_{rs}	Incoming solar radiation (W m^{-2})
H_{ri}	Isothermal net long wave radiation (W m^{-2})
$I_{i,j}$	Interpolated variable at computational grid point i,j
$I_{smooth,i,j}$	Smoothed meteorological variable

J_n	Julian day number
κ	von Karaman Constant (0.41)
k_B	Boltzmann constant (1.3807×10^{-23} J K $^{-1}$ molec $^{-1}$)
K_{GA}	Rate constant for the reaction of tabun with hydroxyl radicals (cm 3 molecule $^{-1}$ s $^{-1}$)
K_{GB}	Rate constant for the reaction of sarin with hydroxyl radicals (cm 3 molecule $^{-1}$ s $^{-1}$)
K_{HD}	Rate constant for the reaction of sulfur mustard with hydroxyl radicals (cm 3 molecule $^{-1}$ s $^{-1}$)
k_s	Transfer coefficient
K_x	Turbulent diffusion coefficient in x direction
K_y	Turbulent diffusion coefficient in y direction
K_z	Turbulent diffusion coefficients in z direction
L	Monin-Obukhov length (m)
l	Directional index (X, Y, Z)
λ	Lagrange multiplier
λ'	Vector of corresponding λ values
λ_ζ	Decay time scale for hydroxyl radical reactions (s)
M_0	Initial momentum of m th puff
MG	Geometric mean bias
\overline{M}	Average mass of one air molecule (kg)
N	Cloud cover
N_B	Brunt-Vaisala frequency (s $^{-1}$)
$NMSE$	Normalized Mean Square Error
$O_{obs,m}$	Observed variable at meteorological station m
ω	Angular velocity of the rotation of earth
P	Pressure at a particular height (N m $^{-2}$)
\tilde{p}	Atmospheric pressure (N m $^{-2}$)
P_{ref}	Pressure at the reference height (N m $^{-2}$)
PG	Phosgene
φ	Latitude of the position (decimal degrees)
$P(x,t;x',t')$	Probability density function which describes the probability of finding particles at position (x) at time (t), which were at position x' at time t'

ψ_w	Western longitude (decimal degrees)
Q	Mass of a puff (kg)
r	Radial distance to location x, y, z from the center of hemisphere (m)
r_0	Fireball radius just after the termination of fast adiabatic expansion (m)
r_{hs}	Radius of the hemisphere (m)
ρ_0	Density of the initial fireball (Kg m ⁻³)
ρ_a	Density of air (kg m ⁻³)
$\tilde{\rho}$	Density of atmospheric air (kg m ⁻³)
R_m	Radial distance from station m to the location of grid point i, j (m)
R_{\max}	Maximum radial distance in horizontal meteorological interpolation (m)
r_s	Radius of the source of a semi-continuous release (m)
\tilde{S}_θ	Term representing sources and sinks of the heat
\tilde{S}_C	Term representing sources and sinks of a substance
SD	Solar declination (radians)
σ	Stefan-Boltzmann constant (5.67×10^{-8} W m ⁻² K ⁻⁴)
σ_{IT}^2	Thermal wind turbulent variance
σ_{IM}^2	Mechanical wind turbulent variance
σ_{xn}	Standard deviations of concentration distribution in X direction
σ_{yn}	Standard deviations of concentration distribution in Y direction
σ_{zn}	Standard deviations of concentration distribution in Z direction
$\sigma_l^2(t)$	Velocity variance in direction l
SL	Solar longitude (radians)
$S(x', t')$	Source distribution of material in interest
t	Interested time between sunrise and sunset (hrs)
Γ_d	Dry adiabatic lapse rate (K m ⁻¹)
T_*	Turbulent temperature scale (K)

T_0	Initial temperature of the source material (K)
T_a	Ambient temperature (K)
T_{50}	Temperature at 50 m height (K)
θ	Corrected wind direction (deg)
θ_0	Wind direction observed at 10 m reference level (deg)
$\tilde{\theta}$	Atmospheric temperature (K)
T_{Ll}	Lagrangian time (s)
t_n	Value of the time step n (s)
T_s	Surface temperature (K)
$t_{sunrise}$	Time of the sunrise (hrs)
t_{sunset}	Time of the sunset (hrs)
t_u	Universal time (hrs)
T_w	Wet bulb temperature (K)
T_{z0}	Temperature at surface roughness length (K)
u	Mass consistent wind component in X direction (m s^{-1})
u_0	Mass inconsistent wind component in X direction (m s^{-1})
u_A	Analytic wind component in X direction (m s^{-1})
u_a	Ambient wind speed (m s^{-1})
\tilde{u}	Component of wind velocity in X direction (m s^{-1})
u_c	Magnitude of the initial wind flow (m s^{-1})
\bar{u}_l	Mean wind in direction l (m s^{-1})
u'_l	Turbulent velocity component in direction l (m s^{-1})
$\overline{u'c'}$	Concentration flux in direction X
ν_a	Coefficient of kinematic viscosity of air
u_*	Friction velocity (m s^{-1})
$(u_*)_0$	Surface friction velocity (m s^{-1})
$u(z)$	Wind speed at height z (m s^{-1})

V	Volume of the fluid (m^3)
v	Mass consistent wind component in Y direction (m s^{-1})
v_A	Analytic wind component in Y direction (m s^{-1})
\tilde{v}	Component of wind velocity in Y direction (m s^{-1})
$\overline{v'c'}$	Concentration flux in direction Y
VG	Geometric variance
v_0	Mass inconsistent wind component in Y direction (m s^{-1})
W	Amount of chemical warfare agent used (kg)
w	Mass consistent wind component in Z direction (m s^{-1})
W_A	Entrapped weight of airborne chemical warfare agent (kg)
w_A	Analytic wind component in Z direction (m s^{-1})
\tilde{w}	Component of wind velocity in Z direction (m s^{-1})
$\overline{w'c'}$	Concentration flux in direction Z
w_0	Mass inconsistent wind component in Z direction (m s^{-1})
W_0	Emission velocity of material from semi-continuous source (kg s^{-1})
W_{TNT}	TNT equivalent weight of the explosive material (kg)
x_{cn}	The X coordinate of the center position of n th puff (m)
ξ	Computer generated random variable with zero mean and variance of one
$x_l(t)$	Position of puff at time t ($l = X, Y, Z$)
y_{cn}	The Y coordinate of the center position of n th puff (m)
z	Cartesian coordinate in Z direction (m)
z_0	Surface roughness length (m)
z_1	Reference height for wind measurement (m)
z_{200}	Reference height at 200 m
z_{cn}	The Z coordinate of the center position of n th puff (m)
ζ	Chemical warfare agent
z_{fnw}	Equilibrium height of a buoyant puff in the absence of wind (m)
z_g	Ground height (m)

z_I	Initial height of the puff center location (m)
z_m	Height of the atmospheric boundary layer (m)
z_m^n	Vertical position of the m th puff at n th time step (m)
z_{ref}	Reference height at 2 m
z_t	Constant domain height (m)

Chapter one

1 Introduction

Over the last century, the societal awareness of the impact of toxicological air pollutants has been increased. The immense use of toxic chemicals in industry and the increased terrorist activities around the world have made unexpected toxic gas emissions into the atmosphere highly probable. Therefore, the involvement of authorities in maintaining safety regulations and emergency response systems has become very important. In Sri Lanka, among two origins of toxic gas releases, the event that draws the most attention, especially after the Tamil Eelam war, is the terrorist event due to its unpredictable and potentially catastrophic effect on humans. Although attacks with chemical weapons are considered to be low probable nowadays, enough gas attacks on government military forces have been reported during the Tamil Eelam war.* Furthermore, a plot for a mass scale chemical attack was barred and enough evidence was found.† The nature of the terrorism is that it is highly unpredictable. Despite its low probability, the most important aspect is protecting a community and minimizing the impact of an immediate chemical warfare attack by carrying out efficient disaster management activities. Often, disaster management activities are aided by Emergency Response Systems in order to execute them efficiently. In facing a sudden chemical warfare attack, a hazard prediction model can serve as a key component of an Emergency Response System. A hazard prediction model can be viewed as a collection of computerized mathematical simulations which is capable of predicting the disaster following a chemical weapon attack. More precisely, it can predict the dispersion of a chemical warfare agent (CWA) in the atmosphere, quantify the toxicity in effected locations and even to predict the number of human lives at stake. The assistance of such a system for authorities, particularly in saving human lives is immeasurable. Therefore, a Hazard Prediction Tool for a chemical warfare release is an ample necessity of a nation.

* Athas, I.,*The aftermath of Muhamalai confrontation*, <<http://www.asiantribune.com/index.php?q=node/1034>>, 03 March 2012

† LTTE plot for mass scale chemical attack barred, <http://www.defence.lk/new.asp?fname=20090312_05>, 03 March 2012

Implementation of a Hazard Prediction Model leaves two different options, implementing a commercially available software or research and development of an own software. The first is a fast solution with no research and development costs. Errors in the software codes may be minimal since they have been used for some time and tested properly. However, there is a high risk of predicted results as these models have been validated using field tests conducted under different meteorological and geographical conditions. Moreover, implementing commercially available software involves higher costs. In contrast, development of an own software model has the advantage over reliability and cost effectiveness. Researchers have the freedom to develop software which is compatible with existing systems, and to continuously improve the model according to their requirements. Models can be calibrated and optimized with latest field tests making them powerful tools. Considering these facts, it can be concluded that the development of an own software model is the best solution for the timely requirement of a hazard prediction model.

1.1 Behavior and the Impact of a Chemical Warfare Attack

Prior to the modeling of hazard from a sudden chemical warfare attack, it is important to realize the factors governing its impact. Basically, the impact on an individual living in the area of the attack or away from a certain distance primarily depends on three factors. The toxicity of the agent, which is directly related to the type of the chemical warfare agent released; the effective amount present at the location of the victim and the time of exposure. The second is tailored to the amount of agent released, how it reaches the individual's location and the agent loss during the release and spreading. The released amount is decided by the attacker. Weather variables and the mode of dissemination determine the spreading of the agent. The relationship of the above mentioned factors and underlying variables are summarized in Figure 1.1.

In next sub sections, details on chemical warfare agents, their dissemination and the spreading are presented. Further, special considerations related to the terrorism are also discussed.

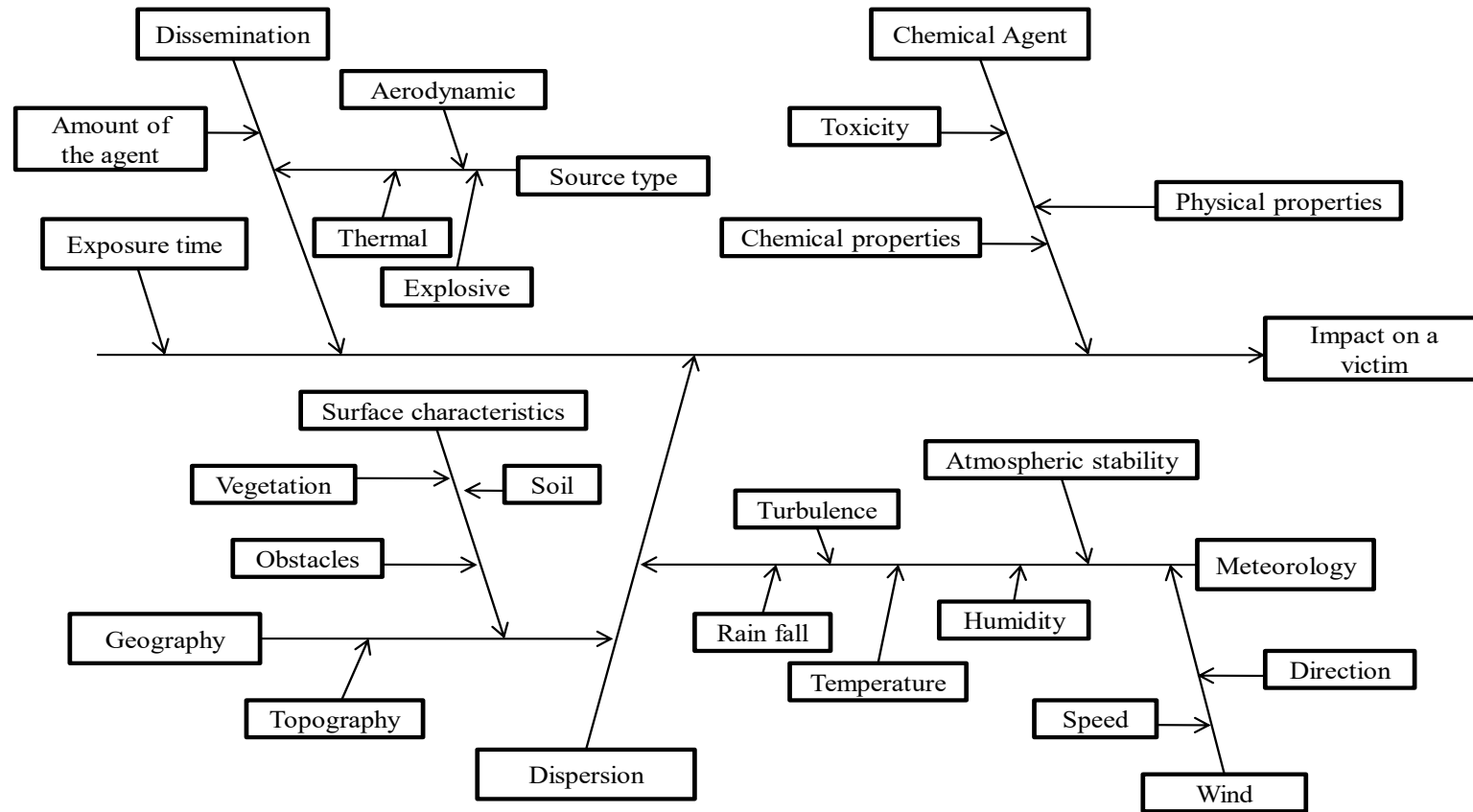


Figure 1.1 Factors governing the impact of chemical warfare agent release on an exposed individual

1.1.1 Chemical warfare agents and the terrorism

A chemical warfare agent can be defined as a chemical compound that can be used to kill, seriously harm or incapacitate humans. These agents are mainly classified depending on the physical properties and the physiological action on victims. According to the physical classification, an agent can be a solid, liquid or a gas depending on its physical state. Based on the physiological action, these compounds are classified as blood agents, nerve agents, chocking agents, blister agents and incapacitating agents.¹

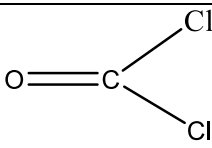
Chemical warfare agents can affect exposed humans in various ways. They may enter into the body through the respiratory system, eyes, skin or wounds and scratches on the body surface and through the digestive system. Chemical vapor and aerosols released into the atmosphere reaches the lung through nose and throat upon inhaling. Chocking agents, blood agents and some nerve agents cause hazard via this route of exposure. Chemical agents such as blister agents are sensitive to sweated surface of the body. Sweated skin, eyes absorb the agent vapor allowing to cause damages to the surface. Some nerve agents dispersed in the aerosol form can deposit on the body surface, penetrate in to the body via wounds and scratches. Most persistent agents can contaminate with foods or water and absorb into the body through gastrointestinal tract upon consumption.

In considering the impact on an exposed individual, a yardstick is needed to quantify the toxicity. In toxicology, the dosage is defined as the amount of a substance the body takes in. If the substance is toxic it can be called as toxic dosage. It is expressed as mg/kg of the body weight of a person. Regarding the toxicity of chemical warfare agents, median lethal dosage and median incapacitating dosage are important. For a liquid chemical agent, LD₅₀ is defined as the amount of a liquid agent required to kill 50% of the exposed group of individuals. Median incapacitating dosage for a liquid agent (ID₅₀) is defined as the amount of liquid agent required to incapacitate 50% of the exposed group of individuals. Two major indicators which are related to routes of the exposure can be found in the literature. For the inhalation of vapor and aerosols, median lethal dosage and median incapacitating dosage is expressed using LC_{t50} and IC_{t50} indicators where LC_{t50} is the product of the concentration of a chemical agent and the exposure time that is lethal to 50 percent of an exposed unprotected group of personnel at an assumed breath rate. IC_{t50} is defined in the same manner for the incapacitating effect. For the exposure through skin and eyes, these two indicators are defined considering the surface area of the skin instead of the breath rate.

1.1.1.1 Chocking agents

Chocking agents are also known as lung damaging agents, which affect mainly the respiratory tract of the victim. These include chemical compounds such as phosgene (PG), diphosgene (DP), chlorine (Cl) and chloropicrin (PS). Among all chocking agents, PG and Cl are considered to be very important chemical warfare agents which have been widely used in the battlefield in the history. Both PG and Cl are gasses at the room temperature. They can be disseminated using pressurized vessels, explosives or thermal devices. When released, both gasses are carried by the wind but tend to accumulate near the ground due to the high molecular weight. If the release is from a pressurized container, the agent hugs the ground and spreads. Some physical properties and toxicity data of PG and Cl are shown below.

Table 1.1 Physical properties and toxicity data of some chocking agents^{1,2}

Chemical Agent	Phosgene	Chlorine
Molecular Structure		Cl—Cl
Molecular weight (g/mol)	98.92	70.9
Appearance	Colorless gas	Greenish yellow gas
Boiling point (°C)	7.6	-34
Vapor pressure (mmHg)	1173 (at 20 °C)	5168 (at 21°C)
Vapor density (Compared to air)	3.4	2.5
LCT ₅₀ (mg min/m ³)	3200	No data available
ICT ₅₀ (mg min/m ³)	1600	No data available

When an unprotected individual inhaled a chocking agent, irritation occurs in the nose, throat and especially in lungs. Cell membranes of effected tissues are swelled and liquids are accumulated in air sacs of the lung making it difficult to breathe. Therefore, victims die due to lack of oxygen. Mild eye irritation is also possible. However, if a PG release occurs during a rainy condition, its effectiveness will be reduced due to rapid hydroxylation. According to defense specialists, PG

and Cl has a higher probability to be used in a terrorist event due to two reasons.[§] First, both these chemicals are widely used in industry. Cl is used in manufacturing processes such as agrochemical, pharmaceutical, polymer products and also used as a disinfectant. PG is used in the manufacturing of pesticides and preparation of precursor chemicals for the manufacturing of polymers (polyurethane). In addition to the ease of accessibility, both these chemicals do not need an expertise in adopting them into chemical weapons. Therefore, Cl and PG are important choking agents in considering a terrorist event.

1.1.1.2 Nerve agents

Chemical warfare nerve agents are derived from either phosphoric or phosphonic acids and are chemically related to organophosphate pesticides. These agents are classified into two types known as ‘G’ agents and ‘V’ agents. The primary difference between two types is their chemical structure, where ‘G’ agents contain fluorine or cyanide in its molecular formula and ‘V’ agents are either phosphorothioates or phosphonates. The general structures of two types of nerve agents are as follows.



Figure 1.2 The general structures of nerve agents

‘G’ agents include tabun (GA), sarin (GB), soman (GD), cyclosarin (GF) where as ‘V’ agents include VX, VE, VG and VM. All the nerve agents are viscous liquids in its pure form but differ in some physical properties.³ ‘G’ agents are more volatile than ‘V’ agents and are mostly vapor hazards. Agents such as GB and GD are disseminated explosively or thermally causing large vapor clouds in the battlefield. When an exposed individual inhaled this chemical vapor, moist surfaces in the lung absorb it causing serious health problems. ‘V’ agents are oily liquids with a low volatility and are primarily contact hazards. When these agents are disseminated using explosive delivery systems aerosol clouds and small droplets are formed. The fat soluble agent droplets deposit on the skin or on eyes of an exposed individual, retain longer and can penetrate through the surface into the body. ‘V’ agents are persistent in the environment and some of them

[§] Bowman, S. R., *Weapons of Mass Destruction: The Terrorist Threat*. Washington D.C., USA . UNT Digital Library. <<http://digital.library.unt.edu/ark:/67531/metacrs3666/>>. June 18, 2012.

might cause a limited amount of vapor which is sufficient to become a vapor hazard. Agent GA can also be a contact hazard as it has a low volatility. However, it should be noted that these physical properties can be changed by adding solvents or thickeners.¹ All the nerve agents have the same physiological action on a victim regardless of the type of the hazard. Similar to the organophosphate pesticides, a nerve agent absorbed into the body disrupts the functioning of the nervous system of a human by effecting enzymes which are essential in the neurotransmission process. Exposed individuals may suffer from difficulty in breathing, dimness of vision and many other health problems in the case of a low dose exposure. However, an exposure to a lethal dose can cause death for an individual within several minutes.

Starting from the mass production of GA, GB and GD in Germany during World War II, many countries have produced and stocked various nerve agents, but were rarely used in the battlefield. Although most of the countries have disposed these chemical agents, they are likely to be used in terrorist events. Some defense specialists argue that the synthesis of nerve agents is difficult due to barriers in obtaining precursor chemicals and involving higher costs and a risk.[§]

Table 1.2 Physical properties and toxicity data of GB and GA1

Chemical Agent	Tabun	Sarin
Molecular Structure	$\text{CH}_3\text{CH}_2-\text{O}-\text{P}(=\text{O})(\text{CN})-\text{N}(\text{CH}_3)_2$	$\text{CH}_3-\text{P}(=\text{O})(\text{F})-\text{O}-\text{CH}(\text{CH}_3)_2$
Molecular weight (g/mol)	162.13	140.10
Appearance	Colorless to brown liquid	Colorless liquid
Boiling point (°C)	220-246 at 760 mmHg	158
Vapor pressure (mmHg)	0.037 at 20 °C	2.10 at 20 °C
Vapor density (Compared to air)	5.63	4.86
LCT ₅₀ – respiratory (mg min/m ³)	Approximately 400	100
ICT ₅₀ – respiratory (mg min/m ³)	Approximately 300	75
LCT ₅₀ – Percutaneous (mg min/m ³)	Unknown	12,000 for a naked person
ICT ₅₀ – Percutaneous (mg min/m ³)	Unknown	8000 for ordinary clothing

However, it should be noted that chemical agents such as GB, which is considered to be hard to synthesize was used in two terrorist attacks during 1994-1995 in Japan. Nerve agent GA is also likely to be used in a terrorist event as it is much easy to produce.³ Moreover, there are chemical

production companies in Asia, which has the ability to produce precursor chemicals such as thionyl chloride and trimethyl phosphite.^{**} Considering these facts, primarily nerve agents GB and GA were considered in this study. Physical properties and toxicity data of agents GB and GA are shown in Table 1.2.

1.1.1.3 Blood agents

A majority of the blood agents are cyanide containing compounds. These include hydrogen cyanide (AC), cyanogen chloride (CK) and salts of cyanides in solution form. Cyanide blood agents with low boiling points are highly volatile. They are disseminated using explosive devices which immediately aids the agent to cause a colorless toxic vapor just after the burst. An exposed individual is affected upon the inhalation of toxic vapor within seconds or the death in minutes at worst. The major mechanism of cyanide poisoning is the disruption of cytochrome oxydase system, which is responsible for the transfer of oxygen from blood to body tissues.¹

Table 1.3 Physical properties and toxicity data of some blood agents¹

Chemical Agent	Hydrogen Cyanide	Cyanogen Chloride
Molecular Structure	H — C ≡ N	Cl — C ≡ N
Molecular weight (g/mol)	36.46	61.46
Appearance	Colorless liquid	Colorless liquid
Boiling point (°C)	25.7	12.8
Vapor pressure (mmHg)	612 at 20 °C	1000 at 25 °C
Vapor density (Compared to air)	1.007 (at 27 °C)	2.1
LCT ₅₀ (mg min/m ³)	Varies with the concentration ^{††}	11000
ICT ₅₀ (mg min/m ³)	Varies with the concentration ^{††}	7000

This in turn prevents the cell respiration in tissues causing various health problems including unconsciousness (agent AC), irritation of the respiratory tract and in eyes, chocking effects (agent CK) and the death at a higher dose. Physical properties and toxicity details of AC and CK are shown in Table 1.3.

^{**} *Chemical Overview*, <<http://www.nti.org/country-profiles/india/chemical/>>, April 05 2012

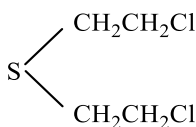
^{††} The human body detoxifies AC at a high rate which is highly dependent on exposed concentration.

The use of cyanide containing blood agents in terrorist events is highly probable. Blood agent AC can be purchased in bulk since it is readily available from industrial organizations. CK is a moderately utilized chemical compound in industry, which has been allowed to produce in bulk quantities by the chemical weapons convention.^{‡‡} The relative cheapness of material, easy to acquire and high lethal and incapacitating toxic effects make these two blood agents ideal for terrorist activities.⁴ Moreover, a less effort is required in adapting them into weapons. Therefore, it is very important to concern blood agents AC and CK as likely substances in the terrorism.

1.1.1.4 Blister agents

Blister agents are primarily skin damaging agents. They include sulfur mustard (HD), nitrogen mustards (HN) and arsenicals (arsenic containing blister agents). Although, there exist various chemical compounds of these types, none of the blister agents have been used in any of the reported terrorist events so far.

Table 1.4 Physical properties and toxicity details of Sulfur Mustard¹

Molecular Structure	
Molecular weight (g/mol)	159.08
Appearance	Yellow-Brown oily liquid
Boiling point (°C)	228 (Sometimes 217)
Vapor pressure at 25 °C (mmHg)	0.0996
Volatility at 25 °C (mg/l)	0.958
LCT ₅₀ –Inhalation (mg min/m ³)	1500
ICT ₅₀ –Inhalation (mg min/m ³)	150
LCT ₅₀ –Percutaneous (mg min/m ³)	10000
ICT ₅₀ – Percutaneous (mg min/m ³)	2000 or less

However, HD is likely to attract terrorists due to several reasons. It can be synthesized in a laboratory much easily in comparison to Nerve agents.[§] Also, precursor chemicals such as 2-chloroethanol and thiodiglycol can be obtained from industrial organizations. HD is highly persistent, and lasts in the environment for a long time. Its vapor can be carried for a long distance by the wind. Due to these reasons HD is an ideal choice for terrorists who are planning to attack a large group of civilians.⁵ The physical properties and toxicity data of HD are presented above. HD is disseminated in the form of aerosols and vapor using spray systems or explosive

^{‡‡} *Blood Agent: Cyanogen Chloride (CK),*<<http://cbwinfo.com/Chemical/Blood/CK.shtml>> , March 03 2012

devices. When an unprotected individual exposed to these aerosols, small droplets are deposited on the skin causing a severe burn as long as they are in contact. Inhalation of the agent vapor also causes inflammation of the respiratory tract. In the case of eye contamination victims suffer from irritation and inflammation of eyes. The dispersed agent may persist for several hours to 2-3 days if it is not hydrolyzed. In the presence of strong oxidizing agents, HD produces corresponding sulphoxide and the sulphone.⁴ The resulting sulphone can also cause blister effects on exposed individuals. Therefore, HD is a severe hazard if dispersed in the atmosphere.

1.1.2 Dissemination of chemical warfare agents in the atmosphere

Chemical warfare agents are disseminated in the form of vapor, aerosol or liquids in the atmosphere. The mode of dissemination is considered to be one of the key factors of efficient chemical warfare dissemination. In a chemical warfare release, only the behavior of the released material in the first 30 second is depend on the characteristics of the mode of dissemination.⁶ Thereafter, weather variables such as wind, temperature, humidity, stability condition of air and rainfall mainly govern the dispersion of agents in the atmosphere. Modes of dissemination include explosive dissemination, thermal dissemination and aerodynamic dissemination. Explosive dissemination involves release of the agents from bursting munitions such as bombs. In thermal dissemination systems, pyrotechnics are used to disseminate the agent. Projectiles such as mortar cartridges are examples of thermal munitions. Aerodynamic dissemination involves dissemination of the agent from spray tanks carried by aircrafts.

In considering the explosive dissemination, chemical agents immediately form vapor clouds from bursting munitions. First, the cloud expands and rises above due to the heat supplied by the explosion. If the density of the released material is less than that of the air, lifting is rapid. The cloud becomes heavy and cools down as it moves up and finally stabilizes to a certain height. If the vapor density of the chemical agent is denser than that of the air, the cloud turns in to a flat shape and moves down closer to the earth surface.⁵ This vapor cloud then travels in the downwind direction. Aerosol clouds may be formed by thermal munitions, spray tanks or as a byproduct of bursting munitions. Initially, an aerosol cloud resulting from thermal munitions or bursting munitions has a high temperature. The heated cloud rises to a certain height immediately at the point of the release, but sinks back to earth as it is heavy.⁵

⁵⁵ Chemical Weapons Delivery, <<http://www.fas.org/programs/bio/chemweapons/delivery.html>>, May 12 2012

Explosive and thermal disseminations can be treated as the most important dissemination modes in considering a terrorist event. However, weapons may be vague. A bottle of liquid agent or a cylinder of gas packed with explosives is an easily prepared chemical weapon. Advanced terrorists may have the ability to adapt a chemical agent in to traditional munitions. Therefore, in developing a hazard prediction model for a terrorist event, a generalization is required rather than just considering traditional munitions.

1.1.3 Dispersion of chemical warfare agents in the atmosphere

As soon as the dissemination is over, atmospheric dispersion of the cloud formed by the chemical agent begins. Meteorological parameters are the key factors which mainly govern its dispersion in the atmosphere. They include the wind speed and the direction, atmospheric turbulence, temperature, atmospheric stability, humidity and the rainfall. Moreover, geographic characteristics such as topography, vegetation and the nature of the soil are also important.⁵ Prior to the discussion on the dispersion phenomena of chemical warfare agents, it is essential to realize the structure of the atmosphere and underlying concepts of meteorology.

1.1.3.1 The structure of the earth's atmosphere

The earth's atmosphere is divided into a few layers depending on the vertical temperature profile. The lowest layer, which is known as the troposphere is where all the weather dynamics and atmospheric processes take place. In considering the dispersion of a substance released from the surface of the earth, the lower part of the troposphere which is known as the Planetary Boundary Layer (PBL) is rather interested.⁷ The Planetary Boundary Layer is directly influenced from earth's surface and responds to them quickly. Turbulence, evaporation, heat transfer, topography and emission of air pollutants always cause the changes within the boundary layer. Its thickness depends on the time of the day and the meteorological conditions. As a day progresses, three major parts can be observed in the boundary layer. They are known as the mixing layer, the residual layer and the nocturnal boundary layer. In addition, the lowest layer which is in contact with the surface is called the surface layer.

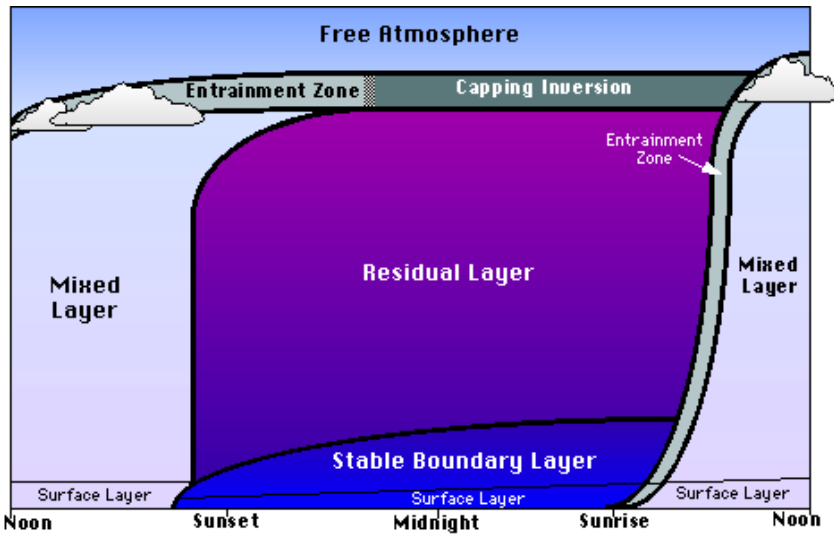


Figure 1.3 The diurnal variation of the planetary boundary layer in fair weather conditions***

Regardless of the time of the day, it occupies about 10% of the boundary layer height. The diurnal variation of the planetary boundary layer is depicted in the following figure. During the day time, as the earth's surface is heated from the radiation of sun, warm air parcels near the surface begin to rise. Therefore, the boundary layer becomes unstable and is characterized by intensive mixing of air masses. This turbulent dominated boundary layer is called the mixing layer. Its upper limit acts as a stable boundary which does not allow further vertical movement of air parcels into the atmosphere located above.⁷ The air pollutants released from the earth surface move with the air parcels and are trapped within the mixing layer. Therefore, in studying the day time dispersion of any substance released from earth surface, meteorology of the mixing layer is the most important aspect to consider.

As the sunset takes place, the surface of the earth becomes cooler than the atmospheric air. The air parcels near the surface also become cold resulting in a positive vertical temperature gradient in the lower part of the boundary layer. The upper part remains with a negative vertical temperature gradient which is much similar to mixing layer. Therefore, two layers can be observed within the planetary boundary layer during the night time. The lower layer, which is in contact with the surface, is called the nocturnal boundary layer whereas the upper is called the residual layer. Nocturnal boundary layer has some small turbulence near the surface. Its upper limit is defined as the height at which the turbulence intensity is low in compared to turbulence intensity near the surface. However, this height increases over the night as the air becomes cooler. During the night time, the substances that are emitted from the earth surface are poorly

*** *The Planetary Boundary Layer*, <<http://www.envi.hufs.ac.kr/gwlee/session7/session7.html>>, November 08 2012

dispersed in the vertical direction resulting in high concentrations within the nocturnal boundary layer.

1.1.3.2 Atmospheric turbulence

Atmospheric turbulence can be defined as continuous fluctuation of moving air in its speed and the direction due to the presence of eddies. These eddies are responsible for the atmospheric dispersion of a substance, which is effective more than 1000 times compared to molecular diffusion.⁸ Atmospheric turbulence can be generated either mechanically or thermally. The mechanical turbulence occurs due to the resistance of the earth surface as the wind blows. When the wind blows over obstacles on the earth surface, the speed decreases resulting in a velocity gradient. This velocity gradient totally depends on the upper wind speed and the roughness of the surface. In order to compensate the resistance force, a downward turbulence flux of momentum is caused. Thermal turbulence occurs due to the heating of earth surface. As the earth surface is heated by solar radiation, the hot air near the surface begins to rise which causes an upward turbulent flux. During the day time, both thermal and mechanical turbulence can be observed in the mixing layer. In the nocturnal boundary layer, only mechanical turbulence can take place.

1.1.3.3 Atmospheric stability

When a heated parcel of dry air moves upwards, it will expand with the decreasing pressure. If the temperature of the surrounding air is less than that of the parcel, the surrounding atmosphere is called an unstable atmosphere. In such a situation, the parcel will tend to accelerate upwards. When the atmospheric temperature is higher than the air temperature inside the parcel, it will be forced downwards. This atmospheric condition is named as a stable atmosphere. If both of them have the same temperature, the atmospheric condition is called neutral. When this situation prevails, the parcel will move with the surrounding air. Unstable atmospheric condition is dominant in the mixed layer whereas the nocturnal boundary layer has a stable atmospheric condition. Atmospheric stability directly influences the impact of a cloud of released chemical warfare agent. During the day time, a release chemical warfare cloud rises to higher altitude reducing the ground level concentration. In contrast, the stable atmospheric condition during the night time will cause high ground level concentrations and the chemical agent travels longer distance.

1.1.3.4 Dispersal of chemical warfare agents

Vapor/gas clouds are more susceptible to meteorological parameters. Just after the release, the temperature of the cloud nearly equals to the temperature of the air, and travels in the downwind

direction with the same speed of surrounding air. Turbulent forces in the atmosphere take over the dispersal of the material. The atmospheric turbulence contains a large range of sizes of the turbulent eddies which extends from few millimeters to several hundreds of meters. This turbulent eddies of different sizes act differently on a vapor/gas cloud.

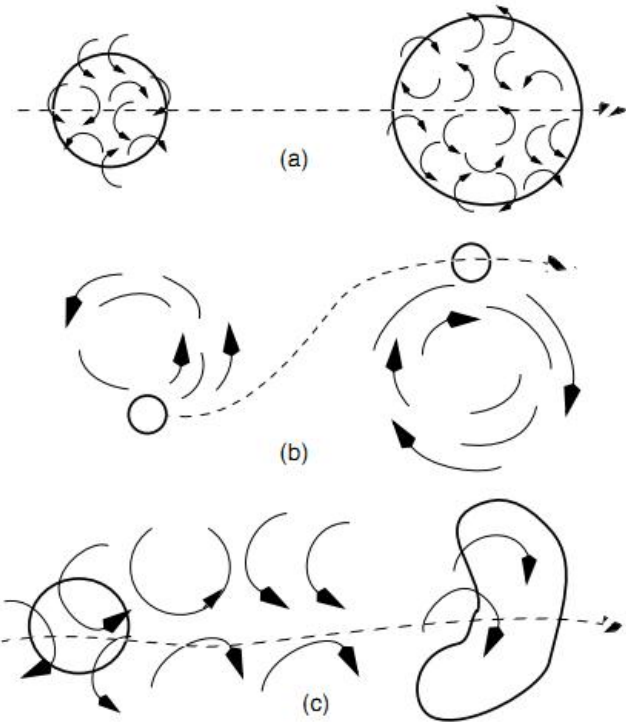


Figure 1.4 Effect of turbulent eddies on a gas/vapor cloud ⁷

- (a) Turbulent eddies are smaller than the size of the cloud
- (b) Turbulent eddies are larger than the size of the cloud
- (c) Turbulent eddies are in the same size of the cloud

Turbulent eddies which are smaller than the size of the cloud will contribute to its growth by uniformly dispersing the material inside (Figure 1.4a). Turbulent eddies which are larger than the size of the cloud will displace it without changing the shape (Figure 1.4b). Eddies of the same size of the cloud will change its shape and increase the size (Figure 1.4c). As the size of the cloud is increased, it will be split creating sub clouds. These sub clouds are affected in the same manner as discussed. Unlike vapor clouds, aerosol clouds are not much affected by the meteorological parameters due to its integrity. However, they travel in the downwind direction while larger, heavier droplets are falling out of the cloud. These droplets deposit on the vegetative or ground

surfaces and stick to them. Depending on the agent properties and the temperature of the environment, they have a finite life time on the surfaces, and can be evaporated back to atmosphere creating a secondary cloud.^{†††} Figure 1.5 illustrates the evolution of a chemical agent cloud resulted from a detonation. Note that the cloud contains both vapor and aerosol.

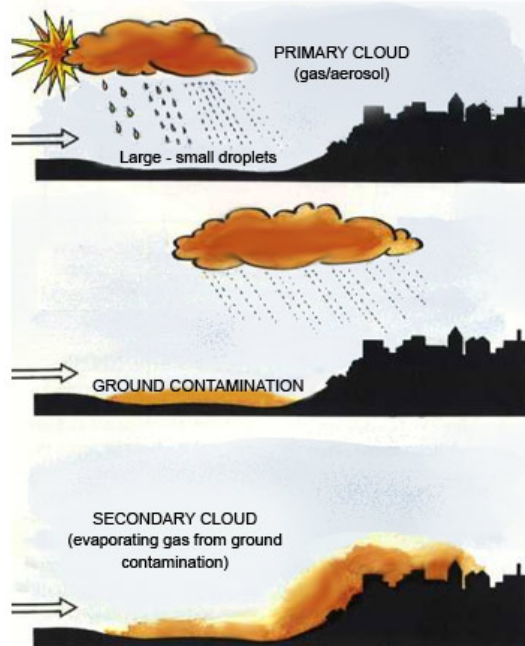


Figure 1.5 Evolution of a chemical cloud from a detonation^{†††}

Finally, the concentration of the agent is reduced below effective levels as it is diluted by atmospheric turbulence. The fate of the chemical agent in the environment is decided by several processes. They include, hydrolysis, photochemical reactions, thermal decomposition and reactions with other compounds in the environment. However, these processes are not so important for an immediate hazard prediction model unless they are significant within the interested time period.

1.2 Modeling of Chemical Warfare Release

Assessing the chemical hazard from an immediate chemical warfare release involves the parameterization of underlying key physical processes taking place in the atmospheric boundary layer which governs the transportation of the material. Moreover, it is essential to form mathematical equations from which these processes can be expressed. At this point, one might

^{†††} *Dispersal and Fate of Chemical Warfare Agents*, <
<http://www.noblis.org/missionareas/nsi/backgroundonchemicalwarfare/chemicalwarfareagentsandchemicalweapons/pages/dispersalchemicalwarfareagents.aspx>>, June 20 2012

argue that the behavior of chemical warfare agents is similar to dense gasses as most of them have higher vapor pressures and molecular weights than the air. However, most hazard prediction models developed so far are passive dispersion models in which agent clouds are assumed to be positively or neutrally buoyant. Some of those models assume that the agent cloud resulting from explosive/thermal releases behave positively buoyant and rise into the atmosphere until it cools.⁹ They further assume that the rapid mixing of the agent and the air results in a neutrally buoyant cloud. This assumption is justifiable for vapor clouds and for some aerosol clouds in the far field (depending on the volatility, aerosol clouds form secondary clouds). Modeling a chemical warfare release scenario from a terrorist attack is a complex event since weaponry is vague. Due to this reason, calculating the density of the initial cloud is not possible and an exact decision on its state is difficult to make. Therefore, assumptions such as mentioned above are required in modeling. In this section, mathematical formulation considering the transportation of passive material is presented.

The physical processes in the atmospheric boundary layer which govern the dispersion of a substance are described using conservation laws of mass, energy, motion, water, gaseous and aerosol substances. The mathematical equations which express these laws include the continuity equation, energy equation, motion equations and transport equations. They can be derived considering an Euler rectangular coordinate system in which axes OX, OY, OZ pointed in the directions east, north and upward respectively.¹⁰ Assuming a dry atmosphere and that the atmospheric turbulent movements are incompressible the set of equations can be written as follows.

The continuity equation,

$$\frac{\partial}{\partial x} \tilde{u} + \frac{\partial}{\partial y} \tilde{v} + \frac{\partial}{\partial z} \tilde{w} = 0 \quad (1.1)$$

where \tilde{u} , \tilde{v} , \tilde{w} are the components of wind velocity in OX, OY and OZ directions.

The energy equation:

$$\frac{\partial \tilde{\theta}}{\partial t} + \tilde{u} \frac{\partial \tilde{\theta}}{\partial x} + \tilde{v} \frac{\partial \tilde{\theta}}{\partial y} + \tilde{w} \frac{\partial \tilde{\theta}}{\partial z} = \tilde{S}_{\theta} \quad (1.2)$$

where $\tilde{\theta}$ is the potential temperature and \tilde{S}_{θ} is a term representing sinks and sources of heat.

The motion equations are;

$$\frac{\partial \tilde{u}}{\partial t} + \tilde{u} \frac{\partial \tilde{u}}{\partial x} + \tilde{v} \frac{\partial \tilde{u}}{\partial y} + \tilde{w} \frac{\partial \tilde{u}}{\partial z} = 2\omega(\tilde{v} \sin \varphi - \tilde{w} \cos \varphi) - \frac{1}{\tilde{\rho}} \frac{\partial \tilde{p}}{\partial x} + v_a \left[\frac{\partial^2 \tilde{u}}{\partial x^2} + \frac{\partial^2 \tilde{u}}{\partial y^2} + \frac{\partial^2 \tilde{u}}{\partial z^2} \right] \quad (1.3.1)$$

$$\frac{\partial \tilde{v}}{\partial t} + \tilde{u} \frac{\partial \tilde{v}}{\partial x} + \tilde{v} \frac{\partial \tilde{v}}{\partial y} + \tilde{w} \frac{\partial \tilde{v}}{\partial z} = -2\omega \tilde{u} \sin \varphi - \frac{1}{\tilde{\rho}} \frac{\partial \tilde{p}}{\partial y} + v_a \left[\frac{\partial^2 \tilde{v}}{\partial x^2} + \frac{\partial^2 \tilde{v}}{\partial y^2} + \frac{\partial^2 \tilde{v}}{\partial z^2} \right] \quad (1.3.2)$$

$$\frac{\partial \tilde{w}}{\partial t} + \tilde{u} \frac{\partial \tilde{w}}{\partial x} + \tilde{v} \frac{\partial \tilde{w}}{\partial y} + \tilde{w} \frac{\partial \tilde{w}}{\partial z} = -g + 2\omega \tilde{u} \cos \varphi - \frac{1}{\tilde{\rho}} \frac{\partial \tilde{p}}{\partial z} + v_a \left[\frac{\partial^2 \tilde{w}}{\partial x^2} + \frac{\partial^2 \tilde{w}}{\partial y^2} + \frac{\partial^2 \tilde{w}}{\partial z^2} \right] \quad (1.3.3)$$

where \tilde{p} is the atmospheric pressure, $\tilde{\rho}$ is the density of atmospheric air, φ is the latitude of the position, ω is the angular velocity of earth rotation, g is the gravitational constant and v_a is the coefficient of kinematic viscosity of air.

The transport equation is,

$$\frac{\partial \tilde{c}}{\partial t} + \tilde{u} \frac{\partial \tilde{c}}{\partial x} + \tilde{v} \frac{\partial \tilde{c}}{\partial y} + \tilde{w} \frac{\partial \tilde{c}}{\partial z} = D_C \left[\frac{\partial^2 \tilde{c}}{\partial x^2} + \frac{\partial^2 \tilde{c}}{\partial y^2} + \frac{\partial^2 \tilde{c}}{\partial z^2} \right] + \tilde{S}_C \quad (1.4)$$

where \tilde{c} is the concentration of the substance in the atmospheric air defined as the ratio of the mass of the substance to the volume of air in consideration, D_C is the molecular diffusion coefficient of the substance and \tilde{S}_C is a term representing sinks and sources of the substance.

In quantifying the amount of a chemical warfare agent present at a particular location, one should solve above set of equations. However, it is not possible to solve them unless further simplifying assumptions and modifications are introduced. These modifications consist of techniques known as averaging procedures and closure procedures. Averaging procedures include ensemble averaging and volume averaging techniques whereas closure procedures differ from each other by the order of closure. Based on different simplifying assumptions, averaging and closure procedures, various forms of equations for above processes could be obtained. Generally, the transport equation is isolated from the rest of the equations and treated separately, which forms the foundation to develop stand alone transport models known as atmospheric dispersion models. The rest of the equations which describe the atmospheric processes lead to the development of meteorological models. Different mathematical models of atmospheric dispersion and meteorology based on above mentioned modifications and assumptions can be found in the literature. In the next subsections, a review of existing dispersion models, meteorological models and source modeling related to chemical warfare release scenarios are presented. Moreover, their strengths and weaknesses are evaluated in adopting them as immediate hazard prediction tools.

1.2.1 Atmospheric dispersion models

There is uncountable number of dispersion models available and in use, which are differing from each other by underlying mathematical model. These mathematical models can be categorized in to various ways according to the modifications introduced to basic transport equations, the type of reference frame/coordinate system used and etc. In this study, it was tried to differentiate available mathematical models on the basis of the coordinate system been used.

Atmospheric dispersion models can either be based on Eulerian or Lagrangian coordinate systems. The Eulerian approach describes the diffusion or dispersion of a substance in a turbulent flow referring to a coordinate system located at a fixed point at a particular time. That is the concentration of the material in question $c(x, t)$ and the velocity of the fluid $u(x, t)$ are described with respect to a fixed point at time t . The dispersion/diffusion of a substance is a random process due to complex three dimensional turbulent motions in the atmosphere. Therefore as mentioned earlier, the prediction of instantaneous concentration readily from the transport equation is impossible unless averaging and closure procedures are introduced. By applying the widely used ensemble averaging procedure, equation (1.4) becomes,

$$\frac{\partial c}{\partial t} + u \frac{\partial c}{\partial x} + v \frac{\partial c}{\partial y} + w \frac{\partial c}{\partial z} = D_c \left[\frac{\partial^2 c}{\partial x^2} + \frac{\partial^2 c}{\partial y^2} + \frac{\partial^2 c}{\partial z^2} \right] - \left(\frac{\partial \bar{u}'c'}{\partial x} + \frac{\partial \bar{v}'c'}{\partial y} + \frac{\partial \bar{w}'c'}{\partial z} \right) + S_c \quad (1.5)$$

where c is the ensemble averaged concentration, u, v, w are the ensemble averaged wind components and $\bar{u}'c', \bar{v}'c', \bar{w}'c'$ are the components of the concentration fluxes.

In order to calculate average concentration from equation (1.5), one should determine components of the concentration fluxes. That is closure procedures are required. For example, the easiest and the most widely used first order closure procedure which involves the gradient transfer hypothesis can be applied. According to this hypothesis, the concentration fluxes are proportional to the gradients of the average concentration in each direction.

$$\bar{u}'c' = -K_x \frac{\partial c}{\partial x} \quad (1.6.1)$$

$$\bar{v}'c' = -K_y \frac{\partial c}{\partial y} \quad (1.6.2)$$

$$\overline{w'c'} = -K_z \frac{\partial c}{\partial z} \quad (1.6.3)$$

where K_x, K_y, K_z are the turbulent diffusion coefficients in x, y and z directions

The equation (1.5) can be rewritten by substituting equations (1.6.1)-(1.6.3) and neglecting molecular diffusion terms as follows.

$$\frac{\partial c}{\partial t} + u \frac{\partial c}{\partial x} + v \frac{\partial c}{\partial y} + w \frac{\partial c}{\partial z} = \left(\frac{\partial}{\partial x} \left(K_x \frac{\partial c}{\partial x} \right) + \frac{\partial}{\partial y} \left(K_y \frac{\partial c}{\partial y} \right) + \frac{\partial}{\partial z} \left(K_z \frac{\partial c}{\partial z} \right) \right) + S_c \quad (1.7)$$

This equation can be solved either numerically or analytically by introducing further simplifying assumptions. The numerical models of this type are known as first order K theory models. Assuming that the atmospheric turbulence is homogeneous and stationary, turbulent diffusion coefficients (K_x, K_y and K_z) in equation (1.7) can be turned into constants. At this point, it is possible to derive well known Gaussian analytical equations to obtain the mean concentration. Such mathematical equations have been derived even considering the nature of the emission scenario.⁸ Numerous Eulerian mathematical models based on different averaging procedures and higher order closures can be found in literature. Some of them have been employed in hazard prediction modeling of chemical warfare releases. In 1980s Eulerian Gaussian models played an important role in predicting the hazard from chemical warfare agents. The D2PC¹¹ by US army, ATP-45 dispersion model¹² of NATO are good examples of such models. The HPAC modeling system used by defense threat reduction agency of United States includes a dispersion model known as SKIPUFF¹³, which is an Eulerian second order closure model. However, it is worth to mention, that the use of Eulerian numerical models as immediate hazard prediction models is rare, as they are computationally inefficient even with the fast computers available nowadays.

Hazard prediction models based on the Lagrangian mathematical framework are equally available and in use.

The Lagrangian approach describes the atmospheric dispersion/diffusion of a substance referring to a coordinate system attached to a fluid particle/hypothetical fluid parcel which is moving with the flow field. The transport equation (1.4) in the Lagrangian framework is given by the following equation.¹⁴

$$\frac{d\tilde{c}}{dt} = D_C \left[\frac{\partial^2 \tilde{c}}{\partial x^2} + \frac{\partial^2 \tilde{c}}{\partial y^2} + \frac{\partial^2 \tilde{c}}{\partial z^2} \right] + \tilde{S}_C \quad (1.8)$$

In high turbulent flows, the effect of the molecular diffusion on the concentration is negligible. Neglecting the molecular diffusion term and the source term, the above equation becomes,

$$\frac{d\tilde{c}}{dt} = 0 \quad (1.9)$$

Equation (1.9) implies that the concentration is conserved as a fluid particle moves through the fluid. This gives rise to the concept of marked fluid particles/parcels moving though the fluid where, the change in the concentration is described as the redistribution of such marked particles all over the fluid. If a substance in interest is dispersed in this fluid flow, its concentration field can be described by the statistics of marked fluid particles and the distribution of sources and sinks. For example, the ensemble averaged concentration of a substance in a turbulent flow is given by,

$$c(x, t) = \int_{-\infty}^t \int_V P(x, t; x', t') S(x', t') dx' dt' \quad (1.10)$$

where V is the volume of the fluid, $P(x, t; x', t')$ is the probability density function which describes the probability of finding particles at position (x) at time (t) , which were at position x' at time t' and $S(x', t')$ is the source distribution of material in interest.

As far as the dispersal of a non reactive substance is concerned, the probability density function of equation (1.10) depends only on the meteorological parameters. However, one should apply closure procedures in evaluating its value and calculation of the average concentration requires further simplifications.

Various mathematical models developed under Lagrangian framework can be found in literature. Similar to Eulerian Gaussian models, Lagrangian Gaussian models have also been derived using equation (1.10) by approximating Gaussian distribution to the probability density function and with further assumptions.¹⁰ In Lagrangian box models the coordinate system is assumed to be attached to a moving column of air in the space. The most advanced Lagrangian models which are very popular nowadays: Lagrangian stochastic models treat the dispersing substance as a collection of particles representing the mass of the substance. And their trajectories in the space are determined with the aid of stochastic Langevin equation. Finally, the concentration is

determined by counting particles at a particular grid volume at a time of interest. However, the requirement of a large number of particles to represent an emission has made this approach much inefficient. To overcome this problem, approaches such as puff/particle methods were developed where clusters are concerned instead of particles.^{15,16}

Numerous hazard prediction models applicable in chemical warfare releases developed on the basis of Lagrangian mathematical models are in use. The VLSTRACK dispersion model¹³ is a Lagrangian Gaussian puff model used by US Navy. A trend can be seen among modern hazard prediction models towards the Lagrangian stochastic models. The NBC defense model developed by Swedish Ministry of Defense¹⁷, NARAC dispersion model¹⁸ used by US department of energy, NEWS model^{***} developed in Germany are good examples for such models. Perhaps, this is due to the fact that Lagrangian particle models have strengths in various aspects in comparison to other available mathematical models.

Lagrangian stochastic models are suitable for modeling chemical warfare release scenarios in many aspects. The ability to incorporate any source configuration and simulating the dispersion under any meteorological condition in complex terrains are their primary strengths. Specially, it is very straightforward to introduce chemical reactions and deposition processes which are essential features of hazard prediction from chemical warfare agents. Moreover, stochastic models are capable of simulating the dispersion at any spatial scale. Being derived from the Lagrangian framework, they do not involve problems of numerical diffusion occurring in Eulerian numerical K theory models.⁸ These strengths of Lagrangian stochastic models fulfill the key requirements and features of a hazard prediction models applicable in chemical warfare releases.¹⁹ Therefore, Lagrangian stochastic mathematical models can be treated as the most suitable mathematical model to simulate dispersion and assess the hazard following a chemical warfare agent release.

1.2.2 Meteorological models

The predictions made by the atmospheric dispersion models are solely based on the provided meteorological input. Wind speed and the direction, temperature, stability condition of the atmosphere, height of the atmospheric boundary layer and turbulence parameters are some of the essential parameters that they demand. In brief, the role of a meteorological model is to provide

*** NEWS,<<http://www.tms-bonn.de/en/products/news/>>, April 28 2012

all the meteorological parameters that govern the dispersion of a substance in the atmosphere. Several approaches of modeling meteorology can be found in literature. They can be categorized as traditional methods, meteorological preprocessors and flow models.

The most straightforward and the oldest methods are the traditional methods. They use empirical relationships to calculate required meteorological variables from measurements made by weather stations. For example, the vertical wind profile is determined using the so called power law method and the atmospheric stability condition is decided by simple observations. Meteorological preprocessors, which are more advanced in comparison to traditional methods, were then developed. They include a set of algorithms to calculate vertical wind profile, temperature profiles and other meteorological parameters characterizing the boundary layer. Unlike traditional models, preprocessors attempt to parameterize simple terrain features and incorporate their effect in calculations.²⁰ Meteorological preprocessors usually require hourly averaged measurements made by weather stations. However, both traditional models, and meteorological preprocessors can only power simple Eulerian models such as Gaussian dispersion models which demand a simple meteorological input.

Flow models; diagnostic meteorological models and prognostic models can provide high resolution 3D meteorological fields. Most diagnostic wind models available in literature are mass consistent models. These models are consisting of 3D grid systems and algorithms to calculate meteorological parameters either based on traditional schemes or meteorological preprocessor schemes. First, meteorological variables are calculated considering each weather station within the grid, and interpolate them to each of the grid points. To generate a high resolution wind field, mass consistent wind models use the mass conservation principle. With the aid of variational calculus, the difference between the interpolated wind vectors at each grid point (i.e. divergence) is minimized considering terrain slopes until the wind field becomes mass consistent.²¹ However, it should be noted that the effectiveness of diagnostic wind models are solely dependent on the number of weather stations available within the grid.¹⁰ In contrast, prognostic models do not suffer from this constraint. They are considered as the most advanced meteorological models, where continuity equations (1.1-1.5) are numerically solved to calculate meteorological parameters. Prognostic models may be driven by a single level weather input or a gridded meteorological input.¹⁰ They are capable of producing meteorological fields with a very high resolution and specially, have the forecasting ability which is not possible with any of the other models. However, the biggest limitations are the inefficiency and the requirement of high computational power and expertise in using them.

In selecting a proper meteorological model to power a hazard prediction model, the degree of accuracy and the speed are key concerns. While traditional methods and meteorological preprocessors powered classic hazard prediction models such as D2PC¹¹ and ATP45¹², diagnostic models can be viewed as the widely used modeling approach in most of the other applications. The use of prognostic meteorological models among hazard prediction models is rare despite its high accuracy and forecasting ability. Definitely, this is due to the facts that a hazard prediction model should be able to execute at least less than 10 minutes after a disaster¹⁹ and generating a rough footprint of areas at risk is sufficient to take immediate disaster management actions.

1.2.3 Source models

Source modeling is one of the major aspects which make a difference between a hazard prediction model and a regular industrial air pollutant dispersion model. The role of a source model is to calculate initial parameters such as initial cloud radius, height of the stabilized cloud etc. as required by the dispersion model. In modeling a chemical warfare release from a terrorist attack, one should consider possible modes of dissemination and select appropriate mathematical models which describe them. As discussed previously, explosive dissemination and thermal dissemination are the most likely dissemination modes in a terrorist event. If the release time of the material is in the order of seconds, the release is termed as an instantaneous release. Otherwise, it may be termed as a quasi-continuous or continuous release. The first should be treated using an instantaneous cloud rise model whereas the latter with a plume rise model. Mathematical models of explosive cloud/plume rise models related to chemical warfare releases are sparse in literature. However, several instantaneous cloud rise models which model dust/gas resulting from explosive sources and enough industrial stack plume rise models can be found. Empirical models such as Church's cloud rise model²², semi empirical models such as Zhang's instantaneous cloud rise model²³, and Brigg's plume rise model⁸ are good examples of widely used models. They can be amended to apply in a chemical warfare release by introducing assumptions and modifications. This approach has been widely used in many of the available hazard prediction models. For example, D2PC11 uses Brigg's plume rise formulas with several modifications. Although it is not possible to obtain accurate results in comparison to specifically developed cloud/plume rise models suited for a chemical warfare release, this approach can be viewed as a good alternative.

1.3 Computer Simulation of Hazard Prediction Models

When the mathematical modeling is over, the next important task is its computational implementation. At this point, one should concern about several facts; selecting an appropriate programming language, proper implementation and after all the predictions of the program (or software) should be evaluated by comparing with existing or new field datasets.

Mathematical models underlying the hazard prediction involve complex calculations which results in complex algorithms requiring extensive computer power in executing them. For example, the divergence minimization step of a diagnostic meteorological model (in establishing a mass consistent wind field) involves solving a large set of linear equations iteratively. Therefore, an appropriate programming language which is consisting of an efficient math library should be a primary concern in implementing a hazard prediction model. Moreover, efficient data storage systems, proper memory management and ease of implementation should also be considered. The user friendliness of the final application can possibly enable users to comfortably run the program during an immediate incident. Visual C# can be treated as one of the best programming languages which facilitate all the above mentioned requirements. Although it is popular as an object oriented language among business application developers, its features are advantageous in developing scientific applications.^{sss} Having derived from .net framework, a rapid application development with an interactive user interface is possible using visual C#. The implementation and the error handling are also trivial. The availability of advanced open source packages such as graphic libraries, map navigation systems are very advantageous particularly for an application like a hazard prediction model. Furthermore, the availability of advanced open source numerical packages allows programmers to implement heavy mathematical calculations without a hassle.

It is essential to evaluate predictions made by a hazard prediction model after the development. For this purpose, field tests can be conducted and collect data or existing datasets can be used. The latter is the most widely used approach in model evaluations since the first is time consuming and involves heavy expenses. Although a variety of field experiments have been conducted, only a few of them can be used in validating a hazard prediction model. The Dipole Pride 26 experiment,²⁴ OLAD field experiment²⁵ and MADONNA field experiment²⁶ can be used to evaluate the atmospheric dispersion from instantaneous sources. To evaluate the dispersal from

^{sss} Gilani,F., *Harness the features of C# to power your scientific computing projects.*
<<http://msdn.microsoft.com/en-us/magazine/cc163995.aspx>>, June 18 2012

a continuous release, field datasets from the Copenhagen²⁷ and Indianapolis²⁷ field experiments are appropriate. However, it should be mentioned that MADONNA field experiment contains data from both instantaneous and semi-continuous releases but the disadvantage is they are available at cost. Moreover, OLAD field test was specifically designed to validate releases from instantaneous line sources such as aerial sprays. Therefore, this field test data is not suitable to use in evaluating a hazard prediction model that specifically designed to apply in a terrorist event.

1.4 Objectives and Scopes of the Research

As stated previously, there is a need to develop a computer model to predict the hazard following an immediate chemical warfare release from a terrorist event. The purpose of this research is to fulfill this need by developing a computer program called “Hazard Prediction Model” or “HPM” using visual C# programming language. The program is capable of simulating the dispersion of chemical agents Cl, PG, GB, GA, AC, CK and HD resulting from explosive and thermal releases. To achieve this task, a Lagrangian puff/particle mathematical model was used. Moreover, a diagnostic meteorological model consisting of a mass consistent wind algorithm was developed in order to provide necessary meteorological input. Possible release types were modeled by amending available mathematical models of cloud and plume rise. Finally, the accuracy of the code and the quality of prediction were evaluated using three approaches. To evaluate the accuracy of the meteorological code, a calculated set of micrometeorological parameters in Indianapolis field experiment was compared with the predictions from the model developed in this work. Furthermore, the accuracy of the mass consistent wind model was tested by comparing the flow field around a hemispherical hill with an analytical solution. Finally, the model predictions were evaluated with Dipole Pride 26 field experiment. The next chapters of this thesis are organized as follows. In the second, third and fourth chapters, the model descriptions of diagnostic meteorological model, dispersion model and model evaluation methodology are presented respectively. Chapter 5 presents the results of model evaluation study and the discussion of results. Finally, Chapter 6 gives the conclusions and suggestions for future improvements.

Chapter Two

2 Computer Model Development

The development of the Hazard Prediction Model primarily consisted of implementing algorithms for the diagnostic wind model, the source model and the dispersion model. In addition, a geographical code was developed in order to provide terrain data fields as required by these sub models. Finally, the model performance was evaluated through several approaches. In this chapter and the following chapters, a comprehensive description of each of these components and model evaluation procedure are presented.

2.1 Grid System

Prior to the formulation of Hazard Prediction Model, a grid system had to be defined and a computational domain had to be established. A nested grid system compatible with Universal Transverse Mercator (UTM) grid was chosen for this purpose.^{****} This nested grid system consisted of a 3D meteorological grid and a 2D concentration grid in which the latter lying inside the first. The purpose of the 3D grid was to define meteorological variables whereas the second was used in calculating the concentration/dose of a substance dispersed in the atmosphere. Both grids were defined at a virtual origin and their X, Y, Z were pointed in the east, north and upward directions respectively.

^{****} U.S. Geological Survey., *The Universal Transverse Mercator (UTM) Grid – Fact sheet 077-01*, <<http://egsc.usgs.gov/isb/pubs/factsheets/fs07701.html>>, July 12 2012

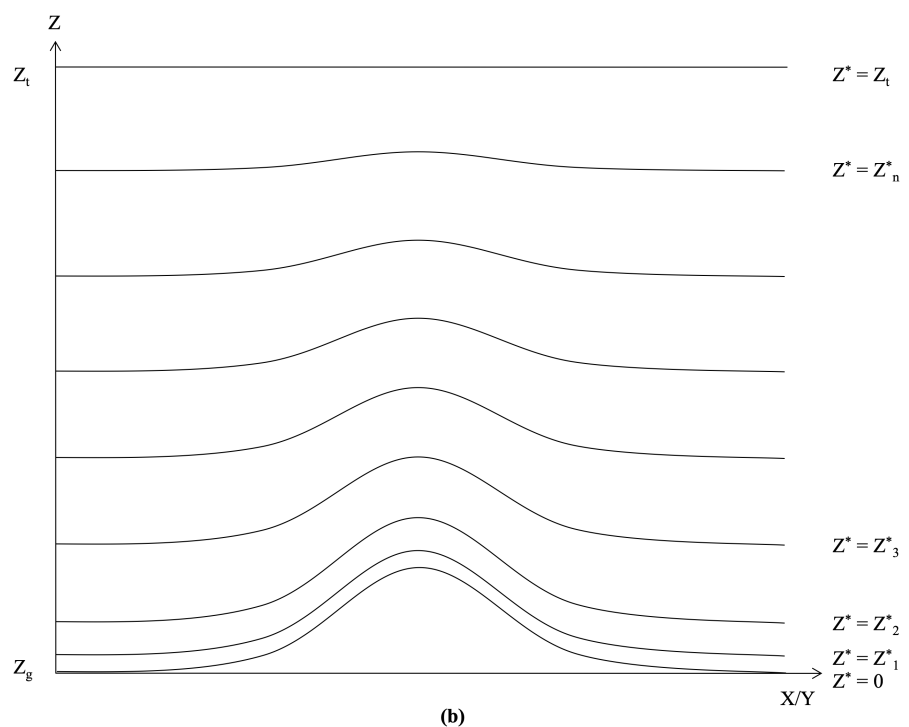
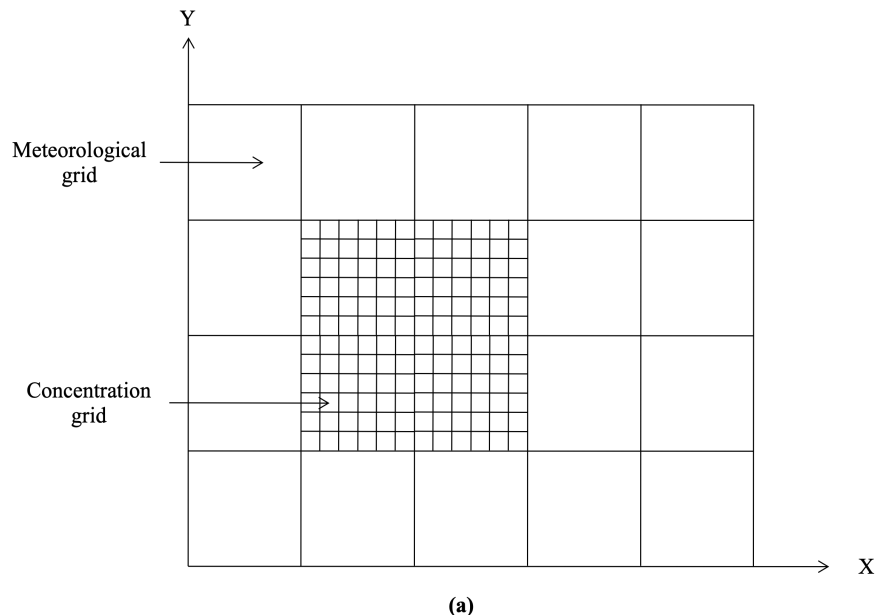


Figure 2.1 Description of the grid system

- (a) Horizontal arrangement of the grids
- (b) Vertical arrangement of the meteorological grid

In the horizontal directions, grids were uniform and the cell dimensions of the meteorological grid were greater than that of the concentration grid. (Figure 2.1a) These cell and grid dimensions were user defined variables. In the vertical direction, the meteorological grid was terrain following, none uniform and was squeezed or expanded with in a constant ceiling height and the varying topography. (Figure 2.1b)

Then the terrain influenced vertical coordinate (z^*) is defined by²¹,

$$z^* = \left(\frac{z - z_g}{z_t - z_g} \right) \times z_t \quad (2.1)$$

where z is the Cartesian coordinate (in m), z_g is the ground height (in m) and z_t is the constant ceiling height (in m)

Meteorological parameters were defined at the center point of a meteorological cell. Concentration/dose values were calculated at center points of the concentration cells. Further details on the use of these grids are presented in the description of meteorological and dispersion models.

2.2 The Meteorological Model

The atmospheric dispersion of a chemical warfare agent primarily relies on meteorological parameters. As mentioned previously, the wind field, temperature, atmospheric stability, turbulence, humidity and rainfall are key parameters responsible for this process. These variables were parameterized by the meteorological model with a minimal data input and provided in the form of 3D or 2D fields for the whole grid where the dispersion took place. Furthermore, some other gridded meteorological data fields which were demanded by the source model were also generated. As the output from a hazard prediction model is expected to generate quickly, the performance of the meteorological model was also important. In other words, the meteorological model had to run quickly and provide sufficiently accurate meteorological fields upon a minimal data input provided. Concerning these facts, the meteorological model was formulated by selecting most appropriate mathematical models from literature. Figure 2.2 summarizes the input required by the meteorological model and the expected output.

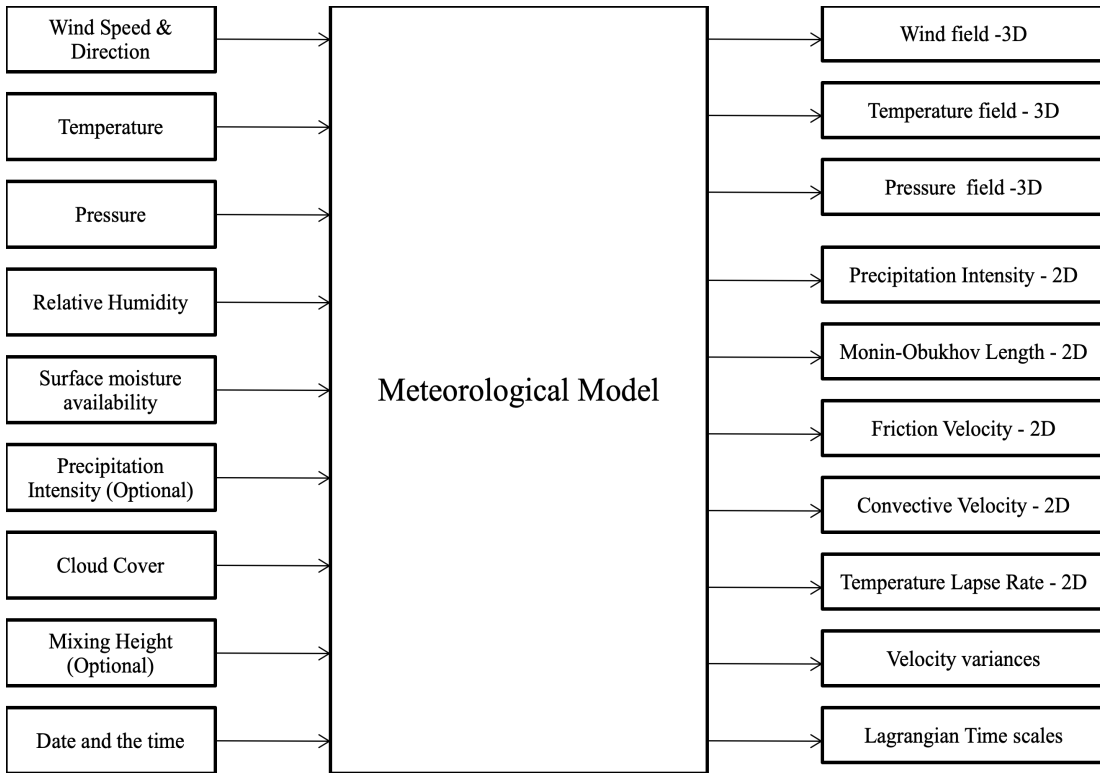


Figure 2.2 Summary of inputs and outputs of the meteorological model

2.2.1 Meteorological input

The Hazard Prediction Model (HPM) was developed with an interactive user interface which allows users to provide necessary data input to the program easily. Unlike many other available hazard prediction models, HPM was developed to allow users to locate a release point in a satellite map viewer, and to mark the release location, and meteorological stations nearby. The meteorological grid was designed to form automatically by the program, covering the release location such a way that it locates on the center of the grid. Hourly averaged observations as reported by surface meteorological stations were required by the model. Wind data at 10 m height, temperature, pressure and relative humidity at 2 m height were the primarily required data. Moreover, cloud cover was required as a percentage which is available from most meteorological stations and airports. Surface moisture availability is a surface characteristic of an interested area, which is close to 100% for wet vegetative surfaces and 0% for dry surfaces. The precipitation intensity (rainfall) and the mixing height observations were optional. However, it should be noted that the mixing height is an important parameter demanded by dispersion models

and the model consisted of an algorithm to estimate this parameter using other meteorological parameters in the absence of real observations. The collection/measurements of data from each meteorological station inside this grid was taken into account and users were required to input above mentioned data that could be obtained from each station.

2.2.2 Description of the meteorological model

The diagnostic meteorological model of HPM was developed on the basis of several widely used mathematical models available in literature. One such model which provided the most important basis is the meteorological pre-processor scheme presented in the yellow book⁸ primarily relied upon the work of Van Ulden, Holtslag and De Bruin.^{20,28,29} This semi-empirical scheme is based on the data collected from the lower part of the boundary layer, and can provide a sufficiently accurate meteorological output for dispersion modeling of surface releases. It is consisting of procedures to determine key atmospheric boundary layer parameters which are essential in the rest of the meteorological modeling. These key parameters include three length scales known as surface roughness length, Monin-Obukhov length, boundary layer height, two velocity scales termed as surface friction velocity, convective scaling velocity and a temperature scale. Although the surface roughness length is considered to be a meteorological variable under this scheme, it has been included under the geographical code in the current work. Further, this scheme was used along with some other supportive algorithms which enhance the quality of the expected output.

The solar elevation angle is the first variable calculated by the meteorological preprocessor scheme. Considering the cloud cover and the solar elevation angle, the day time calculation procedure or the night time calculation procedure is selected to determine the sensible heat flux, Monin-Obukhov length and the friction velocity. Then the calculations are performed to determine temperature scale, boundary layer height and the convective velocity scale if the atmospheric condition is unstable.

2.2.2.1 Procedure for the estimation of solar elevation angle

Estimation of solar elevation angle was the initial step of the meteorological model in calculating key meteorological parameters. Since all the weather dynamics that takes place inside the boundary layer are affected by solar energy received from the sun, the elevation of the sun is a major concern. The calculation procedure requires the date and the universal time, latitude and the longitude of the position of interest and the cloud cover.

The solar elevation angle is described by the following equation;

$$\chi = \arcsin \left\{ \sin(SD) \sin\left(\varphi \frac{\pi}{180}\right) + \cos(SD) \cos\left(\varphi \frac{\pi}{180}\right) \cos(\alpha') \right\}$$

(2.2)

where χ is the solar elevation angle (radians), φ is the latitude of the location (decimal degrees), SD is the solar declination (radians) and α' is the smallest angle through which the earth must turn to bring the meridian of the interested location directly under the sun in radians.

The value of α' can be obtained from the following relationship.

$$\alpha' = \psi_w \frac{\pi}{180} + 0.043 \sin(2.SL) - 0.033 \sin(0.0175J_n) + \pi \left(\frac{t_u}{12} - 1 \right) \quad (2.3)$$

where ψ_w is the western longitude (decimal degrees), SL is the solar longitude (radians), J_n is the Julian day number (see Appendix I for the estimation), t_u is the universal time in hours.

The solar declination is calculated by;

$$SD = \arcsin(0.398 \sin(SL)) \quad (2.4)$$

and the solar longitude is determined using;

$$SL = 4.871 + 0.0175J_n + 0.033 \sin(0.0175J_n) \quad (2.5)$$

It is reported that the scheme is capable of estimating the solar elevation angle within an accuracy of 0.05 radians.

2.2.2.2 Procedure for the estimation of sensible heat flux, Monin-Obukhov length and surface friction velocity

The stability of the atmospheric boundary layer is determined by the ratio between thermal to mechanical turbulence. This ratio can be expressed as a characteristic length scale called Monin-Obukhov length and it is given by;

$$L = -\frac{\rho_a c_p T_a u_*^3}{\kappa g H_0} \quad (2.6)$$

where L is the Monin-Obukhov length (m), ρ_a is the density of air, c_p is the specific heat of air at constant pressure (1.006 kJ kg⁻¹ K⁻¹ at 1 x 10⁵ N m⁻² pressure), T_a is the ambient temperature (K), κ is the Von Karaman constant (0.41), g is the acceleration of gravity (9.81 m s⁻²), H_0 is the sensible heat flux (kW m⁻²) defined as the vertical flux of sensible heat transferred by the turbulence to or from the earth surface and u_* is the friction velocity (m s⁻¹) which is a measure of the contribution of mechanical turbulence to the total turbulence.

The Monin-Obukhov length is a measure of atmospheric stability. It can also be interpreted as the height at which the atmospheric turbulence is generated more by buoyancy than by wind shear. In calculating its value from equation (2.6) one should evaluate sensible heat flux, friction velocity and for this an iterative procedure is needed.

The value of the friction velocity is given by;

$$u_* = \frac{u_a(a)}{f\left(\frac{z}{z_0}, L\right)} \kappa \quad (2.7)$$

where $u_a(a)$ is the wind speed at 10 m height and $f\left(\frac{z}{z_0}, L\right)$ is an empirical function.

This empirical function is defined as;

$$f\left(\frac{z}{z_0}, L\right) = \ln \frac{z}{z_0} + 5 \frac{(z - z_0)}{L} \quad \text{for } \left(\frac{1}{L} > 0\right) \quad (2.8a)$$

$$f\left(\frac{z}{z_0}, L\right) = \ln \frac{z}{z_0} - \psi\left(\frac{z}{L}\right) + \psi\left(\frac{z_0}{L}\right) \quad \text{for } \left(\frac{1}{L} \leq 0\right) \quad (2.8b)$$

where $\psi\left(\frac{z}{L}\right)$ is an empirical function.

$$\psi\left(\frac{z}{L}\right) = 2 \ln\left(\frac{1+\psi'}{2}\right) + \ln\left(\frac{1+\psi'^2}{2}\right) - 2 \arctan(\psi') + \frac{\pi}{2} \quad (2.8c)$$

Function ψ' is defined as;

$$\psi' = \left(1 - 16 \frac{z}{L}\right)^{1/4} \quad (2.8d)$$

where $z = 10$ m and z_0 is the surface roughness length calculated by the geographical code.

Calculation of the sensible heat flux is done using either day time calculation procedure or the night time calculation procedure. The first should be used under neutral and unstable conditions whereas the latter should be in stable conditions. To select the appropriate procedure and initiate the calculation, criteria based on the solar elevation angle and cloud cover can be used.²⁰

According to this criterion, the incoming solar radiation is calculated first. This is given by;

$$H_{rs} = (990 \sin \chi - 30) \times (1 - 0.75N^{3.4}) \quad (2.9)$$

where H_{rs} is the incoming solar radiation (in W m^{-2}) χ is the solar elevation angle (in radians) and N is the cloud cover as a fraction

Then the net radiation (in W m^{-2}) is calculated according to;

The net radiation (H_r) is given by;

$$H_r = \{(1-e)H_{rs} + 5.31 \times 10^{-13} T_a^6 - \sigma T_a^4 + 60N\}/1.2 \quad (2.10)$$

where e is the Albedo value or the reflection coefficient calculated by the geographical code, T_a is the atmospheric temperature in (K), N is the cloud cover as a fraction, σ is the Stefan-Boltzmann constant ($5.67 \times 10^{-8} \text{ W m}^{-2} \text{ K}^{-4}$) and H_{rs} is the incoming solar radiation

To discriminate between day time and night time, the value of net radiation can be used. For day time conditions, the value of the net radiation is greater than zero. (That is $H_r > 0$) In opposite, negative values of net radiation indicate night time conditions. (That is $H_r < 0$)

Day time calculation procedure for sensible heat flux

If the net radiation is positive (i.e. day time), the sensible heat flux is calculated as⁸;

$$H_0 = \frac{(1-\alpha)+\gamma}{1+\gamma} (0.9H_r) - 20\alpha \quad (2.11)$$

where H_0 is the day time sensible heat flux (in W m^{-2}), α is the surface moisture availability as a fraction, γ is the ratio calculated from Table A-2. (See Appendix II) and H_r is the net radiation

After calculating the daytime sensible heat flux from equation (2.11), the Monin-Obukhov length and the surface friction velocity are obtained by solving equations (2.6), (2.7) and (2.8b) iteratively. The iteration initiates by estimating the value of u_* from equation (2.6) for $\left(\frac{1}{L} = 0\right)$.

Generally, Monin-Obukhov length can be obtained with 5% accuracy after 3 iterations.

Night time calculation procedure for sensible heat flux

In the absence of solar radiation from the sun, the atmospheric condition of the planetary boundary layer is governed by the remaining energy. That is the summation of heat fluxes should be zero. Thus, the night time sensible heat flux is estimated using the following heat balance equation.

$$H_0 + H_l + H_g - H_r = 0 \quad (2.12)$$

where H_0 is the night time sensible heat flux (in W m^{-2}), H_l is the latent heat flux (in W m^{-2}), H_g is the ground heat flux (in W m^{-2}), H_r is the net long wave radiation (in W m^{-2}).

The night time sensible heat flux H_0 can be calculated from;

$$H_0 = -\rho_a c_p u_* T_* \quad (2.13)$$

where T_* is the turbulent temperature scale (in K).

The turbulent temperature scale is defined as;

$$T_* = \frac{u_*^2 T_a}{\kappa g L} \quad (2.14)$$

The net long wave radiation is given by;

$$H_r = H_{ri} + 4\sigma T_{50}^3 (T_{50} - T_s) \quad (2.15)$$

where H_{ri} is the isothermal net long wave radiation (in W m^{-2}), T_{50} is the temperature (in K) at 50 m and T_s is the surface temperature (in K).

The temperature at 50 m can be calculated from the following equation with $z_2 = 50$ m and $z_1 = 2$ m.

$$T_a(z_2) - T_a(z_1) = \frac{T_*}{\kappa} \left\{ f\left(\frac{z_2}{z_1}, L\right) - \Gamma_d(z_2 - z_1) \right\} \quad (2.16)$$

where Γ_d is the dry adiabatic lapse rate (0.011 K m^{-1}) and the function $f\left(\frac{z_2}{z_1}, L\right)$ is defined by equation 2.8a.

The surface temperature is defined as;

$$T_s = T_{z0} - T_* \left(10 + \frac{4.2}{u_*} \right) \quad (2.17)$$

where T_{z0} is the temperature at surface roughness length calculated from equation 2.16 with $z_2 = 2$ m and $z_1 = z_0$

The isothermal net long wave radiation is given by;

$$H_{ri} = -\sigma T_{50}^4 \left(1 - 9.35 \times 10^{-6} T_{50}^2 \right) + 60N \quad (2.18)$$

where all the terms have their usual meanings.

The ground heat flux is determined according to;

$$H_g = 1.2 \left(\frac{H_{ri}}{3} - \frac{H_0}{4} \right) \quad (2.19)$$

The latent heat flux is given by;

$$H_l = \frac{\frac{1}{1+\gamma} (H_r - H_g) + \rho_a c_p (T_a - T_w) k_s u_*}{1 + \frac{500\gamma}{1+\gamma} k_s u_*} \quad (2.20)$$

where T_w is the wet bulb temperature (see Appendix III for the estimation) and k_s is the transfer coefficient.

The transfer coefficient defined as;

$$k_s = \frac{T_*}{T_a - T_s} \quad (2.21)$$

Calculation of night time sensible heat flux, Monin-Obukhov length and the friction velocity was done via an iterative procedure. This was performed using the method of false position (See Appendix IV) with $1/L = 0$ & $1/L = 1$ as initial values. First, u_* from equation (2.7) and the value of the equation (2.12) were determined considering initial values. Then new value of $1/L$ was obtained using the false position method and u_* and heat balance equation were reevaluated. This procedure was carried out until the value of the heat balance equation becomes less than a specified tolerance. In the current study, a value of 10^{-5} was used as the tolerance.

2.2.2.3 Procedure for the estimation of convective scaling velocity and boundary layer height

In unstable atmospheric conditions, the total turbulence is the summation of thermal and mechanical turbulence. While the friction velocity measures the contribution of mechanical turbulence to the total turbulence, the convective velocity scale measures the contribution of thermal turbulence.

The convective scale velocity (w_*) is defined by²⁰;

$$w_* = \sqrt[3]{\frac{gH_0 z_m}{\rho_a c_p T_a}} \quad (2.22)$$

where z_m is the atmospheric boundary layer height (in m).

The height of the atmospheric boundary layer is highly dependent on the stability condition. However, most modeling schemes to calculate the mixing height are empirical formulations which use traditional stability categories such as Pasquill stability classes. At this point, it was necessary to adopt a classification of atmospheric stability which relates Monin-Obukhov length to the traditional stability classes. Table 2.1 presents the atmospheric stability classification used in the current study.³⁰

Table 2.1 Atmospheric stability classification based on Monin-Obukhov length

Monin-Obukhov length (m)	Stability condition	Stability class
-100 < L < -50	Extremely unstable	A
-200 < L < -100	Moderately unstable	B
-500 < L < -200	Slightly unstable	C
L > 500	Neutral	D
500 > L > 200	Slightly stable	E
200 > L > 50	Stable	F
50 > L > 10	Very stable	G

Then, the boundary layer heights can be obtained using the following empirical schemes⁸ given in Table 2.2.

Table 2.2 Height of the planetary boundary layer depending on the atmospheric stability⁸

Stability class	Boundary layer height (m)
A , B, C	1500
D (if $1/L = 0$)	Smallest value of 500 or $0.2 \frac{u_*}{f}$
D (if $1/L > 0$), E, F,G	$0.4 \sqrt{\frac{u_*}{f}} L$

where f is the Coriolis parameter.

The Coriolis parameter can be determined according to;

$$f = 14.54 \times 10^{-5} \sin \varphi \quad (2.23)$$

where φ is the latitude of the location.

As given in the Table 2.1 it was assumed that the boundary layer height under very stable conditions is given by the same equation used for stable and slightly stable atmospheric conditions.

2.2.2.4 Formulation of gridded meteorological fields

The outputs of diagnostic meteorological model were mostly gridded meteorological fields where the value of each meteorological variable was interpolated over 3D or 2D computational grids. In 3D fields, the meteorological observations were vertically interpolated at each horizontal layer of the grid and then were horizontally interpolated. In 2D fields, the horizontal interpolation was only applied. The vertical interpolation criteria differs between each meteorological parameter whereas as the other did not. However, all the parameters were interpolated at grid points; i.e. center of grid cells. In this section, interpolation procedures used in the formulation of each meteorological variable is discussed.

Horizontal interpolation scheme

An interpolation method called inverse distance method was used in this study. According to this method, the interpolated variable at a particular point is given by;

$$I_{i,j} = \frac{\sum_m \left(\frac{O_{obs,m}}{R_m^2} \right)}{\sum_m \left(\frac{1}{R_m^2} \right)} \quad (2.24)$$

where $I_{i,j}$ is the interpolated variable at computational grid point i, j , $O_{obs,m}$ is the observed value at meteorological station m , R_m is the radial distance from station m to the location of grid point i, j

In addition, a maximum radial distance (R_{\max}) was employed in determining effective meteorological stations which influence a particular cell. The maximum radial distance was treated as a user option with a default value of 2500 m. If the value of R_m is less than R_{\max} , the meteorological station was considered to be influential. In the absence of any meteorological station within the maximum radial distance, the code increased its values by 500 m until an influential station was found.

Except in the case of wind field modeling, the terrain effects were considered in the interpolation of other meteorological parameters. (Cartesian interpolation) That is, if the ground height of a meteorological station is greater than the height of a grid point, the station was considered to be non influential. In the absence of any influential stations, a critical height (h_{crit}) was employed. Similar to maximum radial distance discussed above, h_{crit} was a user option with a default value of 100 m. If no influential stations were available for a grid point, the value of h_{crit} was increased by 50 m and the code looked for a meteorological station located within the new critical height above the grid point.

Vertical interpolation of wind speed and the direction

After obtaining formula for the friction velocity, it is very straightforward to estimate wind speed at upper levels using the profile method. By rearranging equation (2.7) and substituting required heights to z , corresponding values of wind speed can be obtained.

$$u(z) = u(z_1) \begin{cases} f\left(\frac{z}{z_0}, L\right) \\ \frac{f\left(\frac{z_1}{z_0}, L\right)}{f\left(\frac{z}{z_0}, L\right)} \end{cases} \quad (2.25)$$

where $u(z)$ is the wind speed at height z (in m s^{-1}), z_1 is the reference height for wind (10 m), $u(z_1)$ is the wind speed at 10 m height (in m s^{-1}), functions $f\left(\frac{z}{z_0}, L\right)$ & $f\left(\frac{z_1}{z_0}, L\right)$ are defined by equation (2.8a) and (2.8b)

In unstable and neutral conditions, the above equation is used in combination with equation (2.8b) for heights up to mixing height. In stable conditions, equation (2.8a) is used for heights up to Monin-Obukhov length. Otherwise, equation (2.25) is used with the function (2.8a) redefined as follows.²⁰

$$f\left(\frac{z}{z_0}, L\right) = \ln \frac{z}{z_0} + 17 \left(1 - e^{\left(-0.29 \frac{z}{L}\right)}\right) \quad (2.26)$$

As the height changes, the direction of the mean wind is also varied. Then the magnitudes of the wind components in X, Y directions are affected. Due to this fact, the turning angle of the wind with varying height has to be considered in modeling the vertical wind profile. Although, literature regarding this matter is sparse, the meteorological pre-processor scheme by van Ulden and Holtstag²⁰ presents a method to model the turning of mean wind for heights up to 200 m above the ground level.

According to this method, the turning angle of wind ($D(z)$) at a height less than 200 m is given by;

$$D(z) = 1.58 \times D(z_{200}) \left(1 - e^{\left(-\frac{z}{z_{200}}\right)}\right) \quad (2.27)$$

where z is the height above the ground (in m), z_{200} is a reference height of 200 m, $D(z_{200})$ is the turning angle at reference height in the clockwise direction calculated from Table 2.3

Table 2.3 The turning angle of the wind at 200 m reference height under various stability conditions

Monin-Obukhov length (m)	Reference turning angle (deg)
-30	12
-100	10
-370	9
10^4	12
350	18
130	28
60	35
20	38
9	39

In calculating the correct turning angle from equation (2.27), the value of reference turning angle was obtained from the above table by interpolating Monin-Obukhov lengths. Then the equation (2.27) was solved for the reference height of wind measurements (10 m) and for the height in interest. The corrected wind direction (θ) at height z was then calculated by;

$$\theta = \theta_0 + D(z) - D(10) \quad (2.28)$$

where θ_0 is the wind direction observed at 10 m reference level (deg), $D(z)$ is the turning angle of wind at height z (deg), $D(10)$ is the turning angle of wind at 10 m height as calculated by equation (2.27)

Since the method is limited for heights between (20 – 200) m, θ_0 was employed up to 20 m height and the value of θ at 200 m was employed for heights beyond 200 m.

Vertical interpolation of temperature

The temperatures observed at surface level stations were extrapolated into upper layers using the following scheme. Under stable conditions, the temperature at an upper level is calculated using equation (2.16). In neutral and unstable conditions, the same equation is used with the function $f(z_2/z_1, L)$ defined by equation (2.8b). However, under any atmospheric condition the dry adiabatic lapse rate (Γ_d) is obtained from Table 2.4.

Table 2.4 Relationship between stability class & temperature lapse rate^{31,32}

Atmospheric stability class	Dry adiabatic lapse rate (K m ⁻¹)
A	-0.020
B	-0.018
C	-0.016
D	-0.010
E	0.005
F	0.016
G	0.0625

Vertical interpolation of pressure and relative humidity

Surface pressure measurements can be extrapolated in the vertical direction using the following equation on the hydrostatic assumption; where compression of the atmosphere due to gravity is assumed to be balanced by the pressure gradient force.³³

$$P = P_{ref} e^{-\left(\frac{(z-z_{ref})\bar{M}g}{k_B T_a}\right)} \quad (2.29)$$

where P is the pressure (in N m^{-2}) at height z , P_{ref} is the pressure at the reference height (in N m^{-2}), z_{ref} is the reference height of the pressure observation (2 m), \bar{M} is the average mass of one air molecule (in kg), k_B is the Boltzmann constant ($1.3807 \times 10^{-23} \text{ J K}^{-1} \text{ molec}^{-1}$) and all the other terms have their usual meanings.

Smoothing procedures and gridded meteorological fields

The formulation of gridded meteorological variables was started by vertical interpolation of wind speed and direction, the temperature and the pressure. Then, the horizontal interpolation was applied for these variables at the center of grid cells. In the case of horizontal interpolation of the wind, the mean wind was decomposed in to X, Y, Z directions at each horizontal layer prior to the interpolation. As described previously, the terrain effects were not considered during the horizontal interpolation of wind components since they were accounted by divergence minimization algorithm. Other meteorological variables including Monin-Obukhov length, friction velocity, convective scaling velocity, temperature lapse rate, precipitation intensity were horizontally interpolated in a similar fashion.

After interpolating each of the parameters, a horizontal smoothing procedure was applied in order to avoid abrupt changes between adjacent cells in a horizontal layer. According to this procedure, the changes which may have occurred due to selection of meteorological stations and terrain effects should be removed in order to obtain a smooth meteorological field.

The quantity of a smoothed variable is given by³¹ ;

$$I_{smooth,i,j} = 0.5I_{i,j} + 0.125(I_{i+1,j} + I_{i-1,j} + I_{i,j+1} + I_{i,j-1}) \quad (2.30)$$

where $I_{smooth,i,j}$ is the smoothed meteorological variable, i and j are the indices of grid cell in X and Y directions

In the current computer model, smoothing procedure was applied for all the meteorological fields by default. However, this was allowed to change according to user's preference.

When the smoothing procedure had been applied, the gridded meteorological variables except wind components were possible to use in dispersion predictions. In addition to the smoothing, the wind field requires a special treatment so that it accounts for terrain and obstacle effects. For example, the wind should turn near mountains and obstacles. This effect can be achieved through the mass conservation principle. In this procedure, the smoothed wind field is considered to be a mass inconsistent field and a mass consistent wind field is achieved as follows.

Formulation of the mass consistent wind field

Formulation of the mass consistent wind field involves adjusting divergent; i.e. mass inconsistent wind field until the mass conservation principle is satisfied at every grid point. A procedure is applied to smoothed wind field to take terrain features in to account and adjust the magnitude of individual wind components until the most reasonable solution (non-divergent solution) is found. In order to achieve this objective, a mathematical technique called variational calculus which finds a minimal (or maximal) solution for an integral can be used. The technique was originally developed for a Cartesian coordinate system and its derivation including underlying theory can be found in literature. The use of a terrain influenced coordinate systems such as described in section 2.1 eases the implementation of this technique under complex topography. The variational calculation technique for wind field problems has been derived under such coordinate systems and was concerned in this study.²¹

In the formulation of mass consistent wind field, smoothed wind components were transformed in to a terrain following wind. Since the system was uniform in horizontal directions, a change wasn't required for u , v wind components so that their notations are kept unchanged in the following discussion. The terrain following vertical wind component (w^*) is defined by²¹;

$$w^* = \frac{1}{h} (w - S_x u - S_y v) \quad (2.31a)$$

where h , S_x , S_y terms are defined by equations (2.31b), (2.31c) and (2.31d)

$$h = \left(\frac{z_t - z_g}{z_t} \right) \quad (2.31b)$$

$$S_x = (z^* - z_t) \frac{\partial h}{\partial x} \quad (2.31c)$$

$$S_y = (z^* - z_t) \frac{\partial h}{\partial y} \quad (2.31d)$$

where all the terms in above equations have usual meanings as defined previously.

The incompressible mass continuity equation in terrain following z^* coordinate system is given by;

$$G = \frac{1}{h} \left[\frac{\partial(hu)}{\partial x} + \frac{\partial(hv)}{\partial y} + \frac{\partial(hw^*)}{\partial z^*} \right] = 0 \quad (2.32)$$

where G is termed as the divergence of the wind field.

If u, v, w and u_0, v_0, w_0 are mass consistent and mass inconsistent wind components respectively, the adjustment required to establish the mass consistency is given by;

$$I = \int [\alpha_u^2 (u - u_0)^2 + \alpha_v^2 (v - v_0)^2 + \alpha_w^2 (w - w_0)^2] dv \quad (2.33)$$

where $\alpha_u, \alpha_v, \alpha_w$ are the weighing factors in X, Y, Z directions

It is necessary to find the wind field u, v, w which satisfy the mass continuity equation (2.32) and minimize the integral given by equation (2.33). This minimization problem can be solved with the aid of variational theorem and the corresponding integral can be written as follows.

$$J(u, v, w^*, \lambda) = \int [\alpha_u^2 (u - u_0)^2 + \alpha_v^2 (v - v_0)^2 + \alpha_w^2 (hw^* + S_x u + S_y v - w_0)^2 + \lambda G(u, v, w^*)] h dx dy dz^* \quad (2.34)$$

where $J(u, v, w^*, \lambda)$ is the functional to be minimized, λ is the Lagrange multiplier

Minimizing functional $J(u, v, w^*, \lambda)$ involves the derivation of Euler-Lagrange equations for u, v, w^*, λ from equation (2.34) and the formulation of associated boundary conditions. After some mathematics, resulting Euler-Lagrange equations for u, v, w^* were obtained as;

$$u = \frac{1}{2\alpha_u^2} \left[\frac{\partial \lambda}{\partial x} - \frac{(z^* - z_t)}{h} \frac{\partial h}{\partial x} \frac{\partial \lambda}{\partial z^*} \right] + u_0 \quad (2.35a)$$

$$v = \frac{1}{2\alpha_v^2} \left[\frac{\partial \lambda}{\partial y} - \frac{(z^* - z_t)}{h} \frac{\partial h}{\partial y} \frac{\partial \lambda}{\partial z^*} \right] + v_0 \quad (2.35b)$$

$$w^* = \frac{1}{2h^2} \left[\frac{1}{\alpha_w^2} + \frac{(z^* - z_t)^2}{\alpha_u^2} \left(\frac{\partial h}{\partial x} \right)^2 + \frac{(z^* - z_t)^2}{\alpha_u^2} \left(\frac{\partial h}{\partial x} \right)^2 \right] \frac{\partial \lambda}{\partial z^*} - \frac{(z^* - z_t)}{2\alpha_u^2 h} \frac{\partial h}{\partial x} \frac{\partial \lambda}{\partial z^*} - \frac{(z^* - z_t)}{2\alpha_v^2 h} \frac{\partial h}{\partial y} \frac{\partial \lambda}{\partial z^*} + w_0^* \quad (2.35c)$$

By substituting equations (2.35a)-(2.35c) in equation (2.32) and differentiating yields the Euler-Lagrange equation for λ . Letting $\alpha_u = \alpha_v = \alpha_h$ and rearranging terms, the resulting Euler-Lagrange equation for λ is given by;

$$\frac{\partial^2 \lambda}{\partial x^2} + \frac{\partial^2 \lambda}{\partial y^2} + F_1 \frac{\partial^2 \lambda}{\partial z^{*2}} + F_2 \frac{\partial \lambda}{\partial z^*} - R_x \frac{\partial^2 \lambda}{\partial z^* \partial x} - R_y \frac{\partial^2 \lambda}{\partial z^* \partial y} = \frac{-2\alpha_h^2}{h} G_0 \quad (2.36a)$$

$$F_1 = \frac{1}{h^2} \left(\frac{\alpha_h}{\alpha_w} \right)^2 + (z^* - z_t)^2 (z_x^2 + z_y^2) \quad (2.36b)$$

$$F_2 = 2(z^* - z_t)(z_x^2 + z_y^2) \quad (2.36c)$$

$$R_x = 2(z^* - z_t)z_x \quad (2.36d)$$

$$R_y = 2(z^* - z_t)z_y \quad (2.36e)$$

$$z_x = \frac{1}{h} \frac{\partial h}{\partial x} \quad (2.36f)$$

$$z_y = \frac{1}{h} \frac{\partial h}{\partial y} \quad (2.36g)$$

The associated boundary conditions which satisfy above Euler-Lagrange equations are;

$$\lambda = 0 \text{ (At horizontal boundaries)} \quad (2.37a)$$

$$\frac{\partial \lambda}{\partial z^*} = 0 \text{ (At the top boundary)} \quad (2.37b)$$

$$\frac{\partial \lambda}{\partial z^*} = -\frac{z_t h \left(\frac{\partial h}{\partial x} \frac{\partial \lambda}{\partial x} + \frac{\partial h}{\partial y} \frac{\partial \lambda}{\partial y} \right)}{\left\{ \left(\frac{\alpha_h}{\alpha_w} \right)^2 + z_t^2 \left[\left(\frac{\partial h}{\partial x} \right)^2 + \left(\frac{\partial h}{\partial y} \right)^2 \right] \right\}} \text{ (At the bottom boundary)} \quad (2.37c)$$

It should be noted that in deriving vertical boundary conditions, it is assumed that the w^* , w_0^* in equation (2.35c) are zero. Isolating $\frac{\partial \lambda}{\partial z^*}$ term on the left side and substituting $z^* = z_t, z^* = 0$ for top and bottom boundaries respectively, conditions (2.37b) and (2.37c) were obtained.

In order to achieve a mass consistent wind field, one should solve equation (2.36) for λ and calculate adjusted wind field through equations (2.35a)-(2.35c). However, the system should be solved numerically, subjected to boundary conditions (2.37a)-(2.37c). This involves numerical discretization of the governing set of equations.

Equation (2.36) is an elliptic partial differential equation, which yields a set of linear equations upon discretization. However, this has to be performed on a 3D mesh which is uniform in horizontal directions and non-uniform in vertical direction. In a 1-D uniform mesh, the first and second derivatives of a function f can be expressed through;

$$\frac{\partial f}{\partial x} = \frac{f_{i+1} - f_{i-1}}{2\Delta x} \quad (2.38a)$$

$$\frac{\partial^2 f}{\partial x^2} = \frac{f_{i+1} - 2f_i + f_{i-1}}{\Delta x^2} \quad (2.38b)$$

Similarly, for a 1-D non-uniform mesh³⁴;

$$\frac{\partial f}{\partial x} = \frac{h_i^2 f_{i+1} - (h_i^2 - h_{i+1}^2) f_i - h_{i+1}^2 f_{i-1}}{h_i h_{i+1} (h_i + h_{i+1})} \quad (2.39a)$$

$$\frac{\partial^2 f}{\partial x^2} = \frac{2[h_i f_{i+1} - (h_i + h_{i+1}) f_i + h_{i+1} f_{i-1}]}{h_i h_{i+1} (h_i + h_{i+1})} \quad (2.39b)$$

$$h_i = x_i - x_{i-1} \quad (2.39c)$$

$$h_{i+1} = x_{i+1} - x_i \quad (2.39d)$$

Applying these approximations in equation (2.36) and solving further, the left hand side of the equation was resulted in;

$$\begin{aligned} L.H.S = & \left(\frac{1}{\Delta x^2} + \frac{R_x H}{2\Delta x} \right) \lambda_{i+1,j,k} + \left(\frac{1}{\Delta y^2} + \frac{R_y H}{2\Delta y} \right) \lambda_{i,j+1,k} + \left(\frac{1}{\Delta x^2} - \frac{R_x H}{2\Delta x} \right) \lambda_{i-1,j,k} + \left(\frac{1}{\Delta y^2} - \frac{R_y H}{2\Delta y} \right) \lambda_{i,j-1,k} \\ & - \left(\frac{2}{\Delta x^2} + \frac{2}{\Delta y^2} + \frac{2F_1}{h_k h_{k+1}} + F_2 H \right) \lambda_{i,j,k} + \left[\frac{2F_1}{h_{k+1}(h_k + h_{k+1})} + F_2 H_1 \right] \lambda_{i,j,k+1} + \left[\frac{2F_1}{h_k(h_k + h_{k+1})} - F_2 H_2 \right] \lambda_{i,j,k-1} \\ & - \frac{R_x H_1}{2\Delta x} \lambda_{i+1,j,k+1} + \frac{R_x H_1}{2\Delta x} \lambda_{i-1,j,k+1} + \frac{R_x H_2}{2\Delta x} \lambda_{i+1,j,k-1} - \frac{R_x H_2}{2\Delta x} \lambda_{i-1,j,k-1} \\ & - \frac{R_y H_1}{2\Delta y} \lambda_{i,j+1,k+1} + \frac{R_y H_1}{2\Delta y} \lambda_{i,j-1,k+1} + \frac{R_y H_2}{2\Delta y} \lambda_{i,j+1,k-1} - \frac{R_y H_2}{2\Delta y} \lambda_{i,j-1,k-1} \end{aligned} \quad (2.40a)$$

$$H_1 = \frac{h_k}{h_{k+1}(h_k + h_{k+1})} \quad (2.40b)$$

$$H = \frac{(h_k - h_{k+1})}{h_k h_{k+1}} \quad (2.40c)$$

$$H_2 = \frac{h_{k+1}}{h_k(h_k + h_{k+1})} \quad (2.40d)$$

$$h_k = z_{i,j,k}^* - z_{i,j,k-1}^* \quad (2.40e)$$

$$h_{k+1} = z_{i,j,k+1}^* - z_{i,j,k}^* \quad (2.40f)$$

where grid cell i,j,k is in interest and the rest of 14 indices represent neighbor points.

Similarly, the right hand side of the equation was obtained as;

$$R.H.S = \frac{-2\alpha_h^2}{h} \left[\begin{array}{c} \frac{(hu)_{i+1,j,k} - (hu)_{i-1,j,k}}{2\Delta x} + \frac{(hv)_{i,j+1,k} - (hv)_{i,j-1,k}}{2\Delta y} + H_1(hw^*)_{i,j,k+1} - H(hw^*)_{i,j,k} \\ - H_2(hw^*)_{i,j,k-1} \end{array} \right] \quad (2.41)$$

In the implementation of boundary conditions, λ value was simply set to zero at horizontal boundaries. In the case of vertical boundaries, forward and backward difference schemes were used to discretize equations (2.37c) and (2.37b) respectively.

To obtain corresponding values of λ for the whole domain, the system can be implemented in the matrix form;

$$A\lambda' = B \quad (2.42)$$

where A is the coefficient matrix, λ' is the vector of corresponding λ values, B is the divergence vector resulting from equation (2.41)

The set of linear equations given by (2.42) had to be iteratively solved for λ . However, this was a challenging task since matrix A was a non-symmetric and extremely large square matrix. A majority of its elements were zero values. In the computational implementation of this matrix, it was necessary to use a numerical package which has the capability of implementing sparse matrices. Moreover, a computationally efficient iterative technique had to be chosen in solving the system. Considering these facts, an open source numerical package called dnAnalytics was selected.^{††††} Matrix A was implemented as a sparse matrix and the Bi-Conjugate Gradient Stabilized method in combination with diagonal preconditioning technique was used to solve the above linear problem.³⁵ (See Appendix V) The method is advantageous in comparison to many other available non-symmetric matrix solving techniques and the use of preconditioning technique accelerates its convergence.

When the system (2.42) was solved and corresponding λ values were obtained, the adjusted wind field was computed through equations (2.35a)-(2.35c). Then the divergence of the adjusted wind field was calculated again and the system (2.42) was solved. This iterative procedure was carried out until the divergence of the wind field dropped below a user specified maximum divergence value. By default, the maximum allowed divergence has been set to 10^{-4} s⁻¹.

^{††††} dnAnalytics (2003-2009), BSD license, <[http://dnalytics.codeplex.com](http://dnanalytics.codeplex.com)>, 08 August 2012

However, it should be noted that this value is a critical factor of the total computational time of the divergence minimization algorithm.

When the wind was non-divergent, the vertical wind components were transformed back to Cartesian coordinates using the rearranged form of equation (2.31). The resulting mass consistent wind field was then provided for dispersion calculations.

2.2.2.5 Turbulence parameterization scheme

Turbulence parameters are an important input demanded by most dispersion models. For Lagrangian stochastic models, standard deviations of wind velocity and a measure of persistence of wind flow known as Lagrangian time scale are key parameters. Turbulence parameter schemes may be based on spectral distribution of turbulent kinetic energy or data obtained from field experiments. When coupled with Lagrangian stochastic dispersion models, schemes based on the first has found to show better performance in comparison to the latter.³⁶ Due to this reason, a scheme known as Taylor turbulence parameterization scheme based on the analysis of turbulent kinetic energy was chosen in this study.³⁷ It presents formulas to calculate standard deviations of wind velocities and Lagrangian time scales under different atmospheric stability conditions.

As mentioned earlier, the total atmospheric turbulence is the summation of thermal and mechanical turbulence. Then, the velocity variances of wind can be modeled as a combination of thermal and mechanical turbulent kinetic energy. The total turbulent wind velocity variance (σ_l^2) is given by;

$$\sigma_l^2 = \sigma_{IT}^2 + \sigma_{IM}^2 \quad (2.43)$$

where l is the wind components in X, Y, Z directions, σ_{IT}^2 is the thermal wind turbulent variance, σ_{IM}^2 is the mechanical wind turbulent variance

The thermal wind turbulent variance is defined by;

$$\sigma_{IT}^2 = \frac{1.06 c_l \psi_\varepsilon^{2/3} w_*^2 \left(\frac{z}{z_m} \right)^{2/3}}{\left[(f_m^*)_l^c \right]^{2/3}} \quad (2.44)$$

Mechanical wind turbulent variance as defined by;

$$\sigma_{IM}^2 = \frac{2.32 c_l [\phi_\varepsilon]^{2/3} u_*^2}{[(f_m^*)_l^{n+s}]^{2/3}} \quad (2.45)$$

The Lagrangian time scale (T_{Ll}) can be calculated from;

$$T_{Ll} = \frac{z}{\sqrt{c_l}} \left\{ \frac{0.14 \left[\left(-\frac{\bar{L}}{z_m} \right) \left(\frac{z_m}{-L} \right) \right]^{0.5}}{\left[(f_m^*)_l^c \right]^{2/3} w_* \left[\psi_\varepsilon \frac{z}{z_m} \right]^{1/3}} + \frac{0.059}{\left[(f_m^*)_l^{n+s} [\phi_\varepsilon]^{1/3} u_* \right]} \right\} \quad (2.46)$$

where $\left(-\frac{\bar{L}}{z_m} \right)$ is the average stability parameter for convective planetary boundary layer

In order to calculate velocity variances from equation (2.43) and Lagrangian time scale from equation (2.46), it is necessary to define unknown terms in equations (2.44)-(2.46). While L, z_m, z, u_*, w_* have their usual meanings, rest of the terms differ according to the stability condition of the atmosphere.

Under extremely unstable and moderately unstable atmospheric conditions, the thermal turbulence is dominated and the total velocity variance is calculated only considering the equation (2.44). In calculating Lagrangian time, the last term in the equation (2.46) is set to zero. Then the following definitions can be used for the calculation.

$$c_u = 0.2578, c_v = c_w = 0.3438$$

$$\psi_\varepsilon^{2/3} = 0.75$$

$$\left(-\frac{\bar{L}}{z_m} \right) = 0.01$$

$$(f_m^*)_l^c = \frac{z}{B_l z_m}$$

$$B_u = B_v = 1.5, \quad B_w = 1.8 \left[1 - e^{\left(\frac{-4z}{z_m} \right)} - 0.0003 e^{\left(\frac{8z}{z_m} \right)} \right]$$

Under slightly unstable conditions, the total wind variance is a summation of both thermal and mechanical components. While same definitions are used for the thermal component as defined above, the rest of the terms can be defined as;

$$\phi_\varepsilon = 1.25, \quad (f_m^*)_{ls}^{n+s} = (f_m^*)_{ls}^n \left(1 + 0.03 a_l \frac{f_c z}{(u_*)_0} \right)$$

Where terms $a_u = 3889, a_v = 1094, a_w = 500$ and $(f_m^*)_{us}^n = 0.045, (f_m^*)_{vs}^n = 0.16, (f_m^*)_{ws}^n = 0.33$

and $(u_*)_0$ is the Surface friction velocity

For the rest of the stability conditions, the contribution from thermal component is omitted. The total wind velocity variance equals to mechanical components calculated by equation (2.45) and the first term in equation (2.46) is set to zero in calculating Lagrangian time. In neutral conditions, the calculation is performed with terms defined above. However for slightly stable and stable conditions, some of the terms are modified.

$$\phi_\varepsilon = 1.25 \left(1 + 3.7 \frac{z}{\Lambda} \right)$$

Where;

$$\Lambda = L \left(1 - \frac{z}{z_m} \right)^{(1.5\alpha_1 - \alpha_2)}$$

$$\alpha_1 = 1.5, \quad \alpha_2 = 1$$

$$(f_m^*)_{ls}^{n+s} = (f_m^*)_{ls}^n \left(1 + 0.03 a_l \frac{f_c z}{(u_*)_0} + 3.7 \frac{z}{\Lambda} \right)$$

This parameterization scheme was programmed as a part of the diagnostic meteorological model. However, the turbulent parameters were not considered as gridded fields like other meteorological parameters. They were calculated simultaneously as the dispersion predictions were in progress and whenever demanded by the dispersion model.

2.3 Geographical Model

The idea behind the formulation of a separate code to process geographical data was merely its use in all the main models. Terrain data such as ground heights, slopes and some other surface parameters required in meteorological calculations were provided by the geographical model. Figure 2.3 summarizes the inputs and outputs of the geographical model.

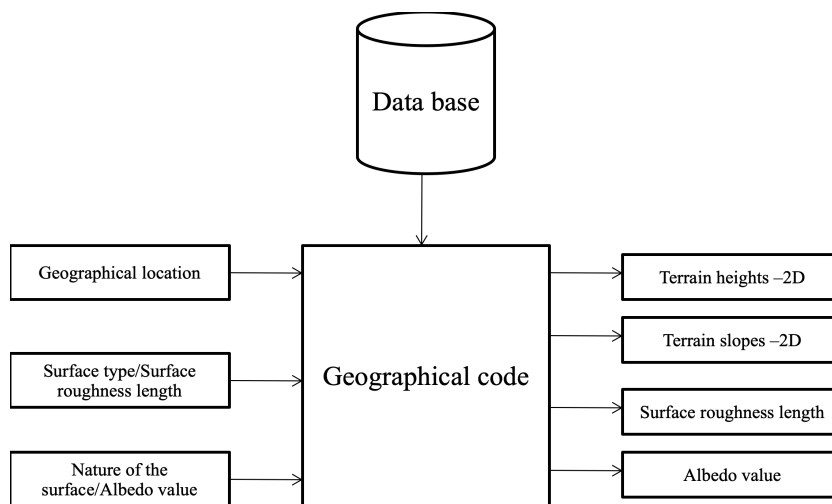


Figure 2.3 Summarization of the geographical model

The implementations of terrain database and grid operations were the most important steps of developing geographical module. To create the terrain database, digital elevation maps³⁸ were processed in ArcGIS 9.03 software³⁹. A massive UTM grid of 510×920 resolution covering the whole island was established using ArcGIS and the information in elevation maps were extracted over the grid. Finally, the data were stored in SQL server database. The algorithms were written in such a way, that grid systems are automatically formed whenever a release point (i.e. the location of terrorist attack) is marked on the satellite map by the user. Based on the location selected, the grid points are generated and terrain heights are interpolated from the database to these points and slopes are calculated at each position.

Although surface roughness length and Albedo values are categorized as weather variables, they were considered as geographical variables in the current study. The surface roughness length

(z_0) is defined as the height at which the wind speed becomes zero. Typically, land areas covered with obstacles have a high roughness length. The geographical model was programmed in such a way that the user is required to select the type of the surface from a given list or insert a value manually. Appendix VII lists types of surfaces and corresponding roughness length values currently being used.

Albedo value is defined as the fraction of incoming solar radiation reflected from the earth surface. Similar to surface roughness length, the Albedo values may be chosen from a classification available in the program (See Appendix VII) or insert manually. The importance of these data fields generated by geographical module has been proved in the meteorological model description presented so far. Moreover, their immense use in source and dispersion modeling can be found in the next chapter.

Chapter Three

3 Modeling Explosive Releases of Chemical Warfare Agents and Dispersion in the Atmosphere

Modeling the atmospheric dispersion of a substance involves the formulation of appropriate models for sources of the substance and turbulent dispersion within the planetary boundary layer. Selecting the most appropriate mathematical models and their correct implementation are critical in describing the dispersion of the substance. This is a very challenging task in the case of a chemical warfare agent dispersion model in comparison to a regular air pollutant dispersion model. Due to the lack of mathematical formulations, one should formulate new mathematical models or modify and take the available models. As the first option is expensive and time consuming, the latter was chosen for the development of Hazard Prediction Model (HPM). In this chapter, the selected models, their modifications and implementation within the HPM are described. Moreover, special considerations on modeling chemical warfare agents are also discussed.

3.1 Modeling the Sources of Chemical Warfare Agents from Terrorist Events

As mentioned previously, explosive sources and thermal sources are the most likely sources would be used in chemical warfare attacks. Although there may be significant differences in terms of the chemical agent in use, source and geometry etc. a generalization is required in modeling of this problem. Due to this necessity, the sources were categorized as instantaneous sources and semi continuous/continuous sources. Sources which terminate the release in less than 15 seconds were considered as instantaneous sources where as the latter release times are greater than that. Moreover, it was assumed that the explosive sources behave as instantaneous releases whereas thermal sources as semi-continuous/continuous sources. The first source type was modeled using an instantaneous cloud rise model and the latter using a plume rise model. Figure 3.1 depicts two types of source models, their major input and the output.

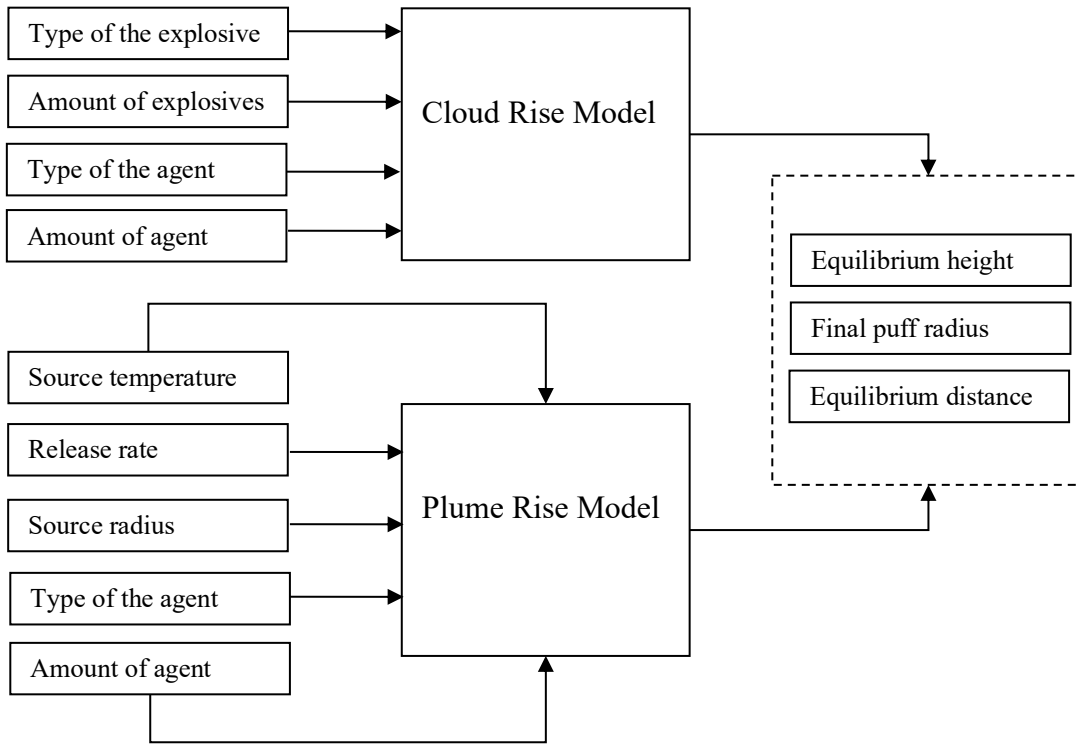


Figure 3.1 Summary of major input and output of cloud rise and plume rise models

Note that the plume rise model demands several source specific input parameters. Calculating these parameters readily from the amount and type of explosives/ agent was problematic since the literature regarding this context was very sparse. Due to this reason, they were considered as input parameters supplied by the user.

3.1.1 Modeling instantaneous explosive releases

An instantaneous cloud rise model which was originally developed to model dust and gas clouds resulting from a chemical explosion was chosen for the Hazard Prediction Model.²³ According to this model, the instantaneous dispersion of material following a chemical explosion is summarized into three processes; the detonation phase, buoyant puff rise phase and the dispersion phase. (See Figure 3.2)

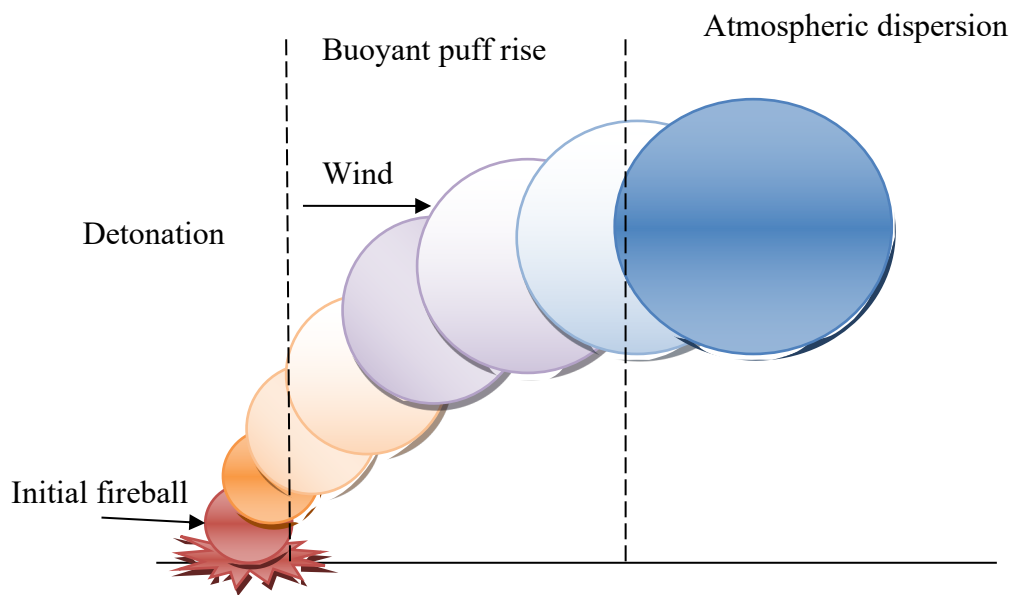


Figure 3.2 Schematic diagram of rise and dispersion of material following an instantaneous explosive release

expansion of the cloud to near atmospheric conditions. Most of the chemical energy stored in explosive material is converted into thermal energy and a fireball is formed. To describe all the processes taking place at this stage, it was assumed that all the energy stored in explosives is contributed to the growth of this fireball and the chemical agent entrains into the fireball after that. The model formulation started by taking its geometric parameters into account and further assuming;

- the geometric shape of the puff is spherical
- all the gasses inside the fireball follow the perfect gas law
- the chemical agent is immediately converted into gasses/vapor/aerosol by the initial blast wave and extreme heat produced
- the effect of dust is negligible
- the shell parts have been ejected far away from the fire ball.

By defining initial puff radius r_0 as the fireball radius just after the termination of fast adiabatic expansion and before the chemical agent is entrained into the puff, following equation can be derived.

$$r_0 = C_l \left(\frac{3H_R}{4\pi\rho_a c_p T_a} \right)^{1/3} \quad (3.1)$$

where C_l is a correction factor reflecting the heat loss and the impact on the fireball radius, H_R is the heat released from the explosion (in kJ) and all the other terms have their usual meanings. It should be noted that the correction factor in the above equation is a coefficient smaller than unity, and was kept as a user option in the current program. By default, its value has been set to unity.

After the formation of initial fireball, a fraction of chemical agent was assumed to be entrained in to puff volume. Then the mass of the entrapped agent had to be determined using some methodology. An empirical model to determine the airborne fraction and the distribution of particle sizes of an inert material following a chemical explosion was taken from literature.^{40,41} The model is valid for condensed phase explosives and it is reported that the effect of source geometry and the state of the dispersing material (liquid or solid) does not have a large impact on the airborne fraction of material of interest.⁴⁰ This methodology was chosen for the current work to determine the amount of the chemical agent entrained into the fireball. The entrapped weight of airborne chemical warfare agent (W_A) immediately after the detonation is given by⁴¹;

$$W_A = 2.783 \left(\frac{W}{W_{TNT}} \right)^{0.3617} W_{TNT} \quad (3.2)$$

where W is the amount of chemical warfare agent used (in kg), W_{TNT} is the TNT equivalent weight of the explosive material (in kg).

The density of the initial fireball (ρ_0) can be written as;

$$\rho_0 = \frac{W_E + W_A}{V_0} \quad (3.3)$$

where W_E is the weight of explosive (in kg), W_A is the airborne weight of chemical agent (in kg), V_0 is the initial fireball volume calculated by approximating a spherical puff (in m³)

After the agent has been entrained into the initial puff, it is assumed to rise adiabatically to a maximum equilibrium height. The air entrains into the puff as it grows while larger droplets of the agent are falling out of it. Its temperature is same as the surrounding air at the equilibrium height. Thereafter, the atmospheric turbulence governs its dispersion and is modeled by an atmospheric dispersion model. The equilibrium height, final puff radius, mass and the puff center location at equilibrium height are the key variables which are essential in modeling the turbulent dispersion. These variables should be provided by the source model. In the absence of ambient wind, the equilibrium height (z_{fnw}) of the puff is given by²³:

$$z_{fnw} = \left(\frac{3V_0 g'}{\pi \alpha^3 N_B^2} \right)^{1/4} \quad (3.4)$$

where α is the entrainment coefficient (0.28), g' is the reduced gravity (in ms^{-2}), N_B is the Brunt-Vaisala frequency (in s^{-1})

The reduced gravity calculated as;

$$g' = \left(\frac{\rho_a - \rho_0}{\rho_0} \right) g \quad (3.5)$$

The Brunt-Vaisala frequency defined by;

$$N_B = \sqrt{\frac{g}{T_a} \left(\frac{dT_a}{dz} + \frac{g}{c_p} \right)} \quad (3.6)$$

where $\frac{dT_a}{dz}$ is the dry adiabatic lapse rate (in Km^{-1})

The puff radius at the equilibrium height is calculated according to;

$$r_f = \alpha z_f \quad (3.7)$$

The puff center location is assumed to be directly above the release point. In the case of large ambient wind; i.e. $\frac{u_a N_B}{g'} \gg 1$, the equations are changed as follow.

The equilibrium height of the puff is given by;

$$z_f = \frac{g'}{5} \left(\frac{3V_0 \pi^4}{32\alpha^3 u_a^3 N_B^5} \right)^{1/4} \quad (3.8)$$

where u_a is the ambient wind speed (in ms^{-1}) and all the other terms have their usual meanings.

The downwind distance at which the maximum puff rise would occur is calculated by;

$$x_f = \left[5z_f \left(\frac{3V_0}{\pi\alpha^3} \right)^{-1/4} \frac{u_a^2}{g'} \right]^{4/5} \quad (3.9)$$

The puff radius at the equilibrium height can be calculated according to;

$$r_f = \left(\frac{3\alpha V_0}{\pi} \right)^{1/4} x_f^{1/4} \quad (3.10)$$

It should be noted that the equations (3.9) and (3.10) are valid only if $\frac{N_B x}{u_a} \leq \frac{\pi}{2}$.

Furthermore, if the parameter $\frac{u_a N_B}{g'} \leq 1$; i.e. the wind condition is small, the final puff equilibrium height is given by;

$$z_f = z_{fnw} \times \exp \left(-1.2 \sqrt{\left(\frac{u_a N_B}{g'} \right)} \right) \quad (3.11)$$

This cloud rise model is valid only for neutral and stable conditions where the dry adiabatic lapse rate is zero or greater than the value of g/c_p in equation (3.6). Due to this reason, the puff variables under unstable atmospheric conditions were approximated considering a neutral atmosphere.

3.1.2 Modeling continuous/semi-continuous sources

Rise of heated chemical clouds resulting from continuous/semi-continuous thermal sources can be modeled using stack plume rise models. Although many plume rise models were available in literature, it was necessary to choose a model compatible with the type of dispersion model to be developed. Considering this fact, a time dependent plume rise model was selected in this study.¹⁶ According to this model, a plume can be represented as a collection of spherical puffs. A single

puff is released during a small time step (Δt), and a collection of puffs are released as long as the release occurs. Assuming that the plume rises adiabatically and cools only due to expansion, the trajectory of each puff is calculated as a function of time. As a puff reaches the equilibrium height, the dispersion is governed by the turbulent dispersion and is modeled by the dispersion model. The rise and dispersion of a buoyant plume is depicted in Figure 3.3.

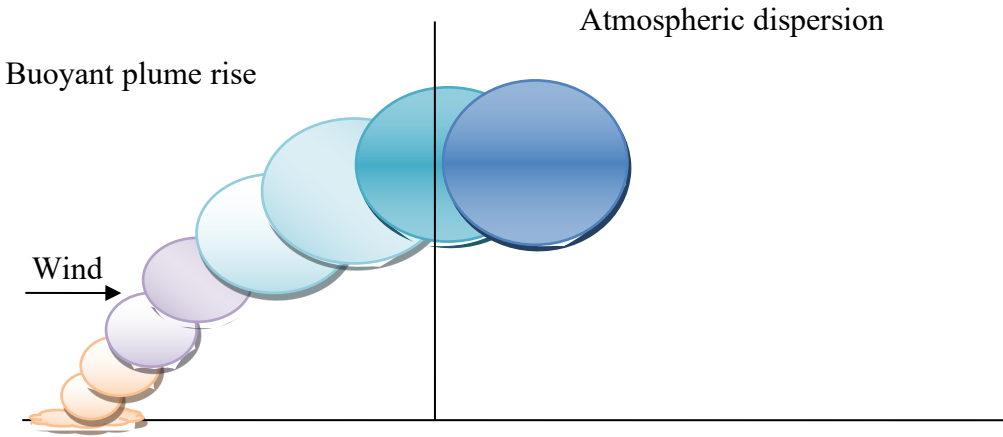


Figure 3.3 Schematic diagram of rise and dispersion of a buoyant plume

Under convective and neutral conditions, the trajectory of each puff was calculated according to¹⁶;

$$z_m^{n+1} = \left\{ \left(z_m^n \right)^3 + \frac{3}{u_a \beta_R^2} \left[M_0 (t_{n+1} - t_n) + \frac{F_0}{2} (t_{n+1}^2 - t_n^2) \right] \right\}^{1/3} \quad (3.12)$$

where z_m^{n+1} is the vertical position of the m^{th} puff at time step $n+1$ (in m), z_m^n is the vertical position of the m^{th} puff at n^{th} time step (in m), M_0 is the initial momentum of the m^{th} puff, F_0 is the buoyancy of puff, β_R is a constant and t_{n+1} , t_n are the values of time steps $n+1$ and n respectively

The value of constant β_R varies with the atmospheric stability condition. For stable/neutral conditions it is 0.5 and is 0.6, 0.65, 0.7, 0.75 for stability categories D, C, B, A respectively.

The initial momentum of m^{th} puff is calculated as;

$$M_0 = \frac{W_0^2 r_s^2 T_a}{T_0} \quad (3.13)$$

where W_0 is the emission velocity (in kg s^{-1}), r_s is the source radius (in m) and T_0 is the initial temperature of source material (in K)

The Buoyancy of puff is given by;

$$F_0 = g W_0 r_s^2 \left(1 - \frac{T_a}{T_0} \right) \quad (3.14)$$

The equilibrium height of a puff is considered to be the height at which the plume dissipation rate $\left(\frac{1.5 W_m^3}{z_m} \right)$ equals to the ambient dissipation rate, $\left(0.6 \frac{w_*^3}{z_m} \right)$.

Under stable conditions, plume variables are obtained by integrating the following set of equations.

$$\frac{dF}{dt} = -N^2 M \quad (3.15a)$$

$$\frac{dM}{dt} = F \quad (3.15b)$$

$$\frac{dz_p}{dt} = W_p \quad (3.15c)$$

$$M = W_p u_a \beta_R^2 z_p^2 \quad (3.16)$$

Set of equations (3.15a)-(3.16) was solved using Euler's method with a time step of $\Delta t/10$. Initial values for the integration were calculated from equations (3.13), (3.14) in combination with the following.

$$r_0 = r_s \left(\frac{T_a W_0}{T_0 u_a} \right)^{\frac{1}{2}} \quad (3.17)$$

$$z_I = \frac{r_0}{\beta_R} \quad (3.18)$$

where z_l is the initial height of the puff center location (in m)

3.2 Modeling the Dispersion of Chemical Warfare Agents in the Atmosphere

After the source parameters have been calculated and the dispersion is totally governed by the atmospheric turbulence, the transportation of chemical warfare agents can be described by a passive dispersion model. In the current study, a Lagrangian puff particle model was chosen for this purpose.¹⁶ According to this model, plume of air pollutants resulting from continuous/semi-continuous release is treated as a collection of puffs. The center of a puff is treated as a particle and is allowed to move during a small time step Δt . The puff grows as it moves during the small time step. (See Figure 3.4) The model assumes that the velocity components in X, Y, Z directions are mutually independent. Moreover, it is assumed that the velocity and position of each puff evolves as a Markov process. A Markov process is a process of which the future can be described solely based on its current state without having knowledge of its previous states.

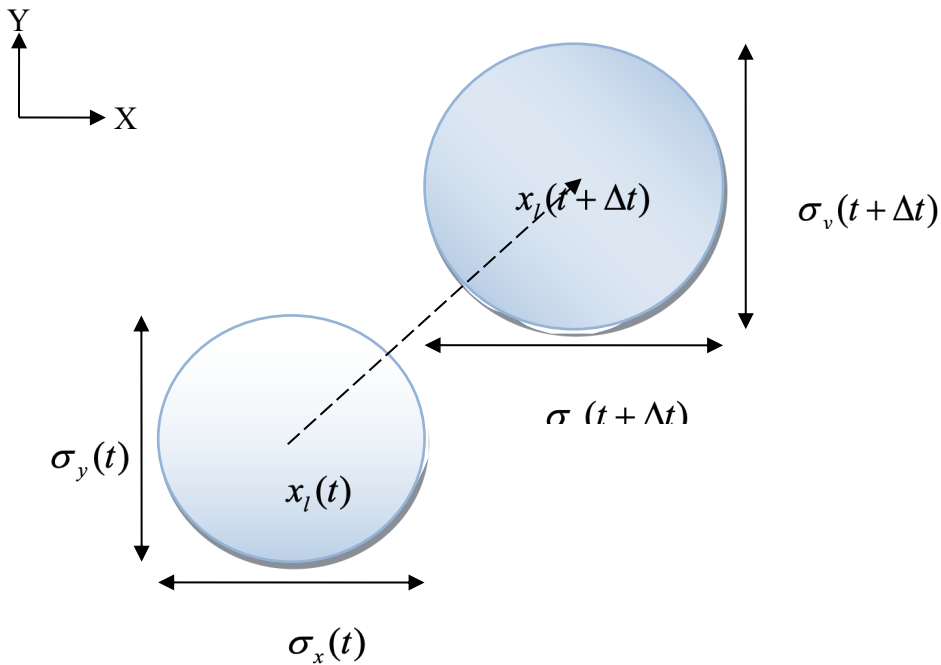


Figure 3.4 Horizontal view of trajectory and growth of a single puff ($l = X, Y, Z$)

The trajectory of a puff can be calculated according to;

$$x_l(t + \Delta t) = x_l(t) + (\bar{u}_l + u'_l) \Delta t \quad (3.19)$$

where l is the direction ($l = X, Y, Z$), $x_l(t + \Delta t)$ is the position of puff at time $t + \Delta t$, $x_l(t)$ is the position of puff at time t , \bar{u}_l is the mean wind in direction l and u'_l is the turbulent velocity component in direction l

The turbulent velocity components are determined using one dimensional Langevin equation and are dependent on the stability condition of the atmosphere. The one dimensional Langevin equation is given by;

$$du'_l = \alpha_l dt + \beta_l dW_l(t) \quad (3.20)$$

where du'_l is the fluctuation of turbulent velocity over a time step, α_l is the drift term determined using the turbulent statistics, β_l is the diffusion term and $dW_l(t)$ represents a Gaussian white noise process with a zero mean and a variance of one. Turbulent statistics are usually described using velocity probability density functions. In the current study, the turbulence was assumed to be homogeneous and isotropic for horizontal dispersion of puffs under any stability condition. Then the equation (3.20) can be written by considering a Gaussian probability density function;

$$du'_l = -\frac{u'_l}{T_{Ll}} dt + \sqrt{\left(\frac{2\sigma_l^2}{T_{Ll}}\right)} dW_l(t) \quad (3.21)$$

For the vertical dispersion of puffs under stable and unstable conditions, the turbulence was assumed to be inhomogeneous and Gaussian. Then, equation (3.20) becomes;

$$du'_l = -\frac{u'_l}{T_{Ll}} dt + \frac{1}{2} \left[1 + \left(\frac{u'_l}{\sigma_l} \right)^2 \right] \frac{\partial \sigma_l^2}{\partial l} dt + \sqrt{\left(\frac{2\sigma_l^2}{T_{Ll}}\right)} dW_l(t) \quad (3.22)$$

In order to obtain an equation for the time evolution of turbulent velocity from equations (3.21) and (3.22), they had to be integrated. The integrated form of these equations was approximated as;

$$u'_l(t + \Delta t) = u'_l(t) + \alpha_l \Delta t + \sqrt{\left(\frac{2\sigma_l^2}{T_{Ll}}\right)} \Delta t \xi \quad (3.23)$$

where ξ is a computer generated random number with a zero mean and a variance of one. Note that the α_l in above equation stands for coefficients of dt terms in equations (3.21) and (3.22).

The concentration of the chemical warfare agent within each puff was assumed to be distributed in a Gaussian manner in X, Y and Z directions. Then the concentration of agent at a particular time and a location is given by⁴²;

$$c(x, y, z) = \frac{1}{(2\pi)^{3/2}} \sum_{n=0}^N \frac{Q}{\sigma_{xn} \sigma_{yn} \sigma_{zn}} \exp\left[-0.5 \frac{(x_{cn}-x)^2}{\sigma_{xn}^2}\right] \exp\left[-0.5 \frac{(y_{cn}-y)^2}{\sigma_{yn}^2}\right] \left\{ \begin{aligned} & \exp\left[-0.5 \frac{(z_{cn}-z)^2}{\sigma_{zn}^2}\right] \\ & + \exp\left[-0.5 \frac{(z_{cn}+z-2z_g)^2}{\sigma_{zn}^2}\right] \end{aligned} \right\} \quad (3.24)$$

where $c(x, y, z)$ is the concentration of agent at location x, y, z (in kg m^{-3}), Q is the mass of a puff (in kg), x_{cn}, y_{cn}, z_{cn} are the coordinates of the center position of n^{th} puff (in m), z_g is the ground height (in m) and $\sigma_{xn}, \sigma_{yn}, \sigma_{zn}$ are the standard deviations of concentration distribution in X, Y, Z directions

The standard deviations of the concentration distribution of n^{th} puff were calculated as⁴²;

$$\sigma_{ln}(t + \Delta t) = \sigma_{ln}(t) + \sigma_l \Delta t \quad \text{for } (t \leq 2T_{Ll}) \quad (3.25a)$$

$$\sigma_{ln}^2(t + \Delta t) = \sigma_{ln}^2(t) + 2T_{Ll} \sigma_l^2 \Delta t \quad \text{for } (t > 2T_{Ll}) \quad (3.25b)$$

where l is the direction index ($l = X, Y, Z$), $\sigma_l^2(t)$ is the velocity variances in direction l and T_{Ll} is the Lagrangian time

To model the dispersion of agents released from an instantaneous source, a similar procedure was used. The concentration was calculated from equation (3.24) considering a single puff.

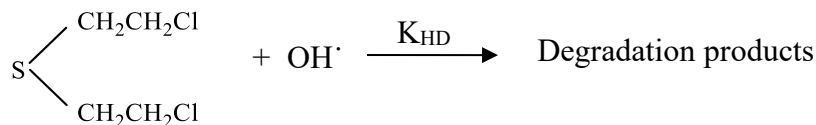
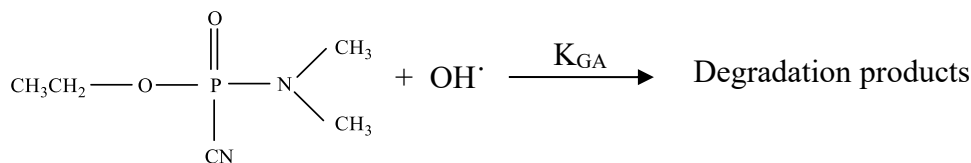
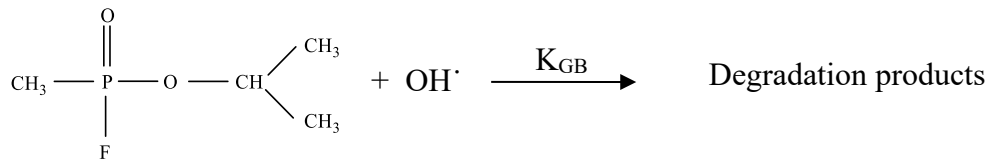
The concentration was calculated at every point of the concentration grid. To evaluate the dose, the time integrated concentration was calculated by integrating equation (3.24) over an interested period of time.

$$Dose = \int_0^t c(x, y, z) dt \quad (3.27)$$

Note that the calculated dose is expressed as an averaged value over a time. (eg: 15 min averaged dosage)

3.3 Modeling chemical reactions

A chemical model which is capable of modeling three important reactions related to GB, GA and HD was developed and incorporated into HPM. All these agents react with radicals in the atmosphere and are converted into toxic/non-toxic substances. During day time, hydroxyl radicals participate in these reactions. Nitrate radicals are the responsible species for their degradation during night time. However, reactions with hydroxyl radicals were only considered due to lack of experimental data on the latter. For releases during night time, agents were assumed to be non-reactive so that downwind dosages were maximized. GB, GA and HD are degraded in the atmosphere by reacting with hydroxyl radicals as follows.



where K_{GB} is the rate constant for reaction of sarin ($4 \times 10^{-11} \text{ cm}^3 \text{ molecule}^{-1} \text{ s}^{-1}$ at 25°)¹³, K_{GA} is the rate constant for reaction of tabun ($4.9 \times 10^{-11} \text{ cm}^3 \text{ molecule}^{-1} \text{ s}^{-1}$ at 25°) ^{####}, K_{HD} is the rate constant for reaction of sulfur mustard ($7.82 \times 10^{-12} \text{ cm}^3 \text{ molecule}^{-1} \text{ s}^{-1}$ at 25°) ^{\$\$\$\$}

These degradations were considered as pseudo first order reactions. For agent ζ ; where $\zeta = GB$, GA and HD, the rate of degradation can be approximated by;

$$\frac{d[\zeta]}{dt} = -K_\zeta [\zeta][OH^\bullet] \quad (3.3.1)$$

where $[\zeta]$ is the concentration of agent ζ , $[OH^\bullet]$ is the concentration of hydroxyl radicals in the atmosphere

Equation (3.4.1) can be rearranged as;

$$\frac{d[\zeta]}{dt} = -[\zeta] / \lambda_\zeta \quad (3.3.2a)$$

where λ_ζ is the decay time scale

The decay time scale is given by;

$$\lambda_\zeta = \left(\frac{1}{K_\zeta [OH^\bullet]} \right) \quad (3.3.2b)$$

The diurnal variation of hydroxyl radical concentration can be expressed through the sine function; $\pi \sin\left(\frac{\pi t}{12}\right) \times 10^6 \text{ molecules cm}^{-3}$ in which t is the time of the day.¹³ Then it is possible to derive an expression for the decay time scale valid for times between sunrise and sunset. The reciprocal decay time scales for agents are given by;

^{####} TABUN CAS RN 77-81-6 – Environmental fate , US National Library of medicine, Available online at <<http://toxnet.nlm.nih.gov/>>, August 13 2012

^{\$\$\$\$} Bis(2-Chloroethyl)sulfide (alias of Sulfur Mustard Gas)– Environmental fate, US National Library of Medicine, Available online at <<http://toxnet.nlm.nih.gov/>>, August 13 2012

$$\frac{1}{\lambda_{GB}} = 2\pi \times 10^{-5} \sin \left[\frac{\pi(t - t_{sunrise})}{(t_{sunset} - t_{sunrise})} \right] \quad (3.3.3a)$$

$$\frac{1}{\lambda_{GA}} = 2.45\pi \times 10^{-5} \sin \left[\frac{\pi(t - t_{sunrise})}{(t_{sunset} - t_{sunrise})} \right] \quad (3.3.3b)$$

$$\frac{1}{\lambda_{HD}} = 3.91\pi \times 10^{-6} \sin \left[\frac{\pi(t - t_{sunrise})}{(t_{sunset} - t_{sunrise})} \right] \quad (3.3.3c)$$

where t is any interested time between sunrise and sunset, $t_{sunrise}$ is the time of sunrise (hours), t_{sunset} is the time of sunset (hours)

To account for the above chemical reactions, equation (3.3.2) was integrated with appropriate decay time scales from equations (3.3.3a)-(3.3.3c). During each time step of the dispersion prediction, residual mass of the puff after the removal of agent due to degradation was calculated. The residual mass was then used in dispersion calculations. The toxicity of any product formed upon the degradation was discarded in dosage calculations.

Chapter Four

4 Model Evaluation Methodology

The most important phase of a computer model development is the evaluation stage. It not only detects subtle coding and logical errors in the model, but also establishes a confidence so that it could be practically applicable. The Hazard Prediction Model (HPM) was also robustly evaluated fulfilling this aim. The model evaluation procedure was carried out as a three stage procedure; evaluation of basic meteorological parameterization scheme, the accuracy of mass consistent wind model and finally the performance of the whole model against a field dataset. This chapter presents detailed information regarding the methodology followed in each stage of the model evaluation procedure. Moreover, details of a study to demonstrate the effect of chemical processes on dispersion are also presented.

4.1 Evaluation of basic meteorological parameterization scheme

Evaluation of basic meteorological parameters calculated by HPM plays an important role in assessing the overall model performance. Since the parameterization scheme consists of complex algorithms, its results should be robustly evaluated. To achieve this task, a meteorological data set available in Modelers Data Archive (MDA) for well known Indianapolis tracer gas experiment was used.²⁷

The Indianapolis field experiment was carried out during 1985 at Perry K Power plant in Indianapolis, USA. While the primary consideration was to study the atmospheric dispersion of tracer gasses, it reports a good set of meteorological data including measured and derived parameters which are valuable in evaluating a meteorological parameterization scheme. The measured meteorological parameters were obtained from three 10 m towers around the site (urban observations), a location at 94 m above the ground level (bank observations), and Indianapolis airport weather station (NWS observations). The dataset contains hourly averaged 170 meteorological observations obtained from each of the locations. Reported data include basic meteorological observations and the derived parameters include Sensible heat flux, Monin-Obukhov length, friction velocity and convective scaling velocity.

To evaluate the performance of meteorological parameterization scheme, the observations made by 10 m towers and airport weather station were chosen. Since the scheme demands meteorological input at 10 m height, the Bank observations were omitted. The location of the site was approximated as 39.8 ° N latitude and -86.2 ° E longitude. It is reported that the values of surface roughness length, Albedo and surface moisture availability are 1.0 m, 0.18, and 50% respectively. In several cases of 170 observations, some basic meteorological parameters were marked as missing values. After omitting these observations, wind speed and direction, temperature, pressure, cloud cover of the rest were used as the input to HPM and values of sensible heat flux, Monin-Obukhov length, and friction velocity were calculated. The calculated values were then compared with derived parameters reported in Modelers Data Archive. The residual analysis technique and the Analysis of Variance (*ANOVA*) were used in discarding outliers and statistically comparing datasets.

4.2 Evaluation of the Mass Consistent Wind Model

The accuracy of mass consistent wind field generated by the meteorological code plays a vital role in the overall dispersion predictions made by the Hazard Prediction Model. The divergence minimization code contains a complex set of algorithms which should be precisely evaluated for its subtle coding and logical errors. Checking the accuracy with experimental wind field datasets does not satisfy this need as complex topographical effects and wind patterns may lead to difficulties in identifying them. Therefore, it is necessary to simulate the wind field for a hypothetical scenario around simple geometrical objects. To fulfill this task, a potential flow was simulated around a hemispherical hill. A mass consistent wind field produces a potential flow when the values of weighing factors $\alpha_u, \alpha_v, \alpha_w$ were set to unity.²¹ When such a flow is numerically simulated around a hemisphere, the analytic solutions can be used to check the accuracy. The magnitude of wind components for a potential flow around a hemisphere are given by the following analytic equations.⁴³

$$u_A = u_c \left[1 + \frac{(y^2 + z^2 - 2x^2)r_{hs}^3}{2r^5} \right] \quad (4.1a)$$

$$v_A = \frac{-3u_c xy r_{hs}^3}{2r^5} \quad (4.1b)$$

$$w_A = \frac{-3u_c xz r_{hs}^3}{2r^5} \quad (4.1c)$$

where u_A, v_A, w_A are the analytic wind components in lateral, horizontal and vertical directions (in $m s^{-1}$), u_c is the magnitude of initial wind flow (in $m s^{-1}$), r_{hs} is the radius of hemisphere (in m) and r is the radial distance to location x, y, z from the center of hemisphere (in m)

To conduct the numerical simulation, the grid resolution of the computational domain was set to $37 \times 37 \times 15$ with a constant cell size of 50 m in horizontal directions. Vertical layers were established with variable heights dividing the height between a constant ceiling height of 1500 m and varying terrain height in a logarithmic fashion. A hemisphere with a radius of 500 m was placed at the center of the computational domain and a constant horizontal wind of $5 ms^{-1}$ was assigned at each grid point ($v = w = 0$). The divergence minimization algorithm was then applied to the field in order to take terrain features into account and adjust the wind field until the

divergence becomes less than 10^{-5} s^{-1} . The numerical simulation took about 28.5 minutes on an Intel Pentium dual core 1.73GHz laptop computer with 1GB ram.

The analytic wind components were calculated at grid points of first horizontal layer of the computational domain. These results were used to evaluate the accuracy of horizontal wind profile obtained from numerical simulation. To evaluate the accuracy of the vertical wind profile, analytic wind components were calculated at grid points in a vertical layer over the summit. Finally, the results were statistically evaluated using analysis of variation.

4.3 Evaluation of the Overall Performance of Hazard Prediction Model

The most important step of the model evaluation phase is checking the accuracy of concentration/dosage predictions made by Hazard Prediction Model. Since concentrations/dosages are the final output, it is necessary to express the performance using some statistic. Such performance statistics may not only show how good the predictions are, but also problems or weaknesses occurred in meteorological, geographical or dispersion codes. To evaluate the overall performance of the model, a simulation was carried out for several instantaneous gas emission scenarios of Dipole Pride field experiment.²⁴

Dipole Pride field experiment

The Dipole Pride field experiment (DP26) was conducted by US Defense Threat Reduction Agency (DTRA) in November 1996 at Yucca flat of Nevada. ($\sim 37^\circ\text{N}$, -116°E) The primary goal of the experiment was to assist the validation of mesoscale hazard prediction models.

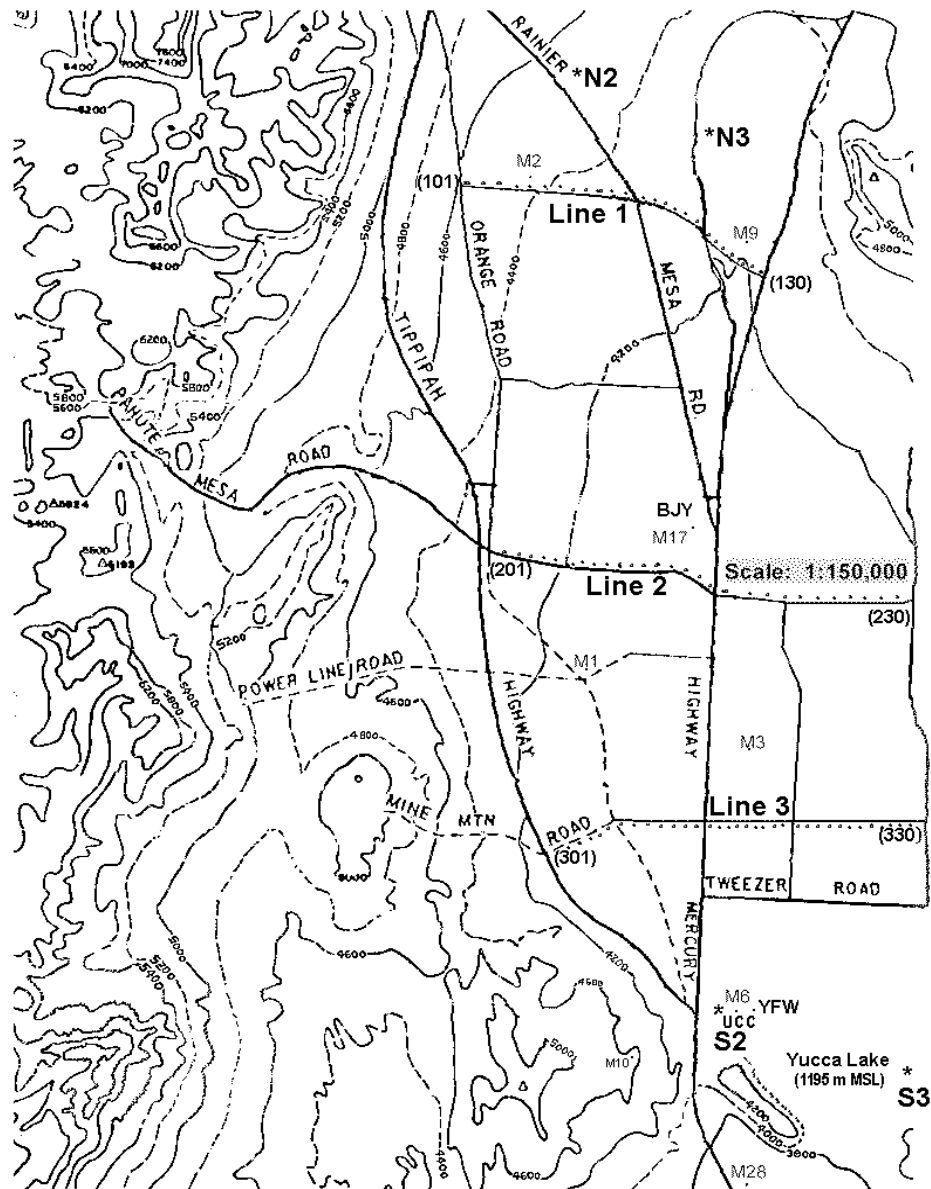


Figure 4.1 Dipole pride test site with dissemination points (N2,N3,S2,S3), Sampling lines (Line 1-3), MEDA stations (M1, M2, M3, M6, M9, M10, M17, M28), Primary instrumentation positions (BJY, UCC, YFW)²⁴

The experiment involved 17 trials of Sulfur Hexafluoride (SF_6) puff releases from disseminators located approximately about 6 m above the ground. These releases were mostly carried out early in the morning or early afternoon hours at one of the four release points located either in North or the South direction of the Yucca flat (N2, N3, S2, and S3 in Figure 4.1). The choice of the dissemination point for a particular release was based on the wind direction. The sampling of emitted SF_6 was primarily conducted using three sampling lines (Line 1, Line 2, and Line 3 in

Figure 4.1); each line consisted of 30 whole air samplers (Tedler Air Sample Bags) positioned 1.5 m above the ground level. The distance between adjacent samplers in each line was about 250 m. These samplers measured 15 min averaged concentrations starting from the time of the release and mostly up to three hours. To obtain surface meteorological observations, eight MEDA stations (M1, M2, M3, M6, M9, M10, and M28 in Figure 4.1) were used. The upper air data was obtained by radiosonde and pilot balloon (Piball) stations (UCC and BJV location in Figure 4.1). While the Piball stations measured only upper wind data, radiosondes collected wind data and temperature data as well. Furthermore, two sonic anemometers were installed YFW and BJV locations. MEDA stations measured 15 min averaged 10 m wind data, temperature, pressure and relative humidity. The DP26 documentation also presents cloud cover measurements related to each trial, and some derived meteorological parameters including surface friction velocity and Monin-Obukhov length. These derived parameters were calculated considering sonic anemometer data. To evaluate the performance of HPM, eight releases of SF₆ conducted under various atmospheric conditions were selected. A summary of the selected trials are shown in Table 4.1.

Table 4.1 Summary of DP26 trials used for the model evaluation of HPM

Trial	Date	Time (PST)	Release location	Mass released (kg)
1	11 Nov	0440	N2	11.6
2	12 Nov	1300	S3	19.3
3	13 Nov	1400	S2	10.4
4	16 Nov	1300	S2	21.1
5	18 Nov	1130	S2	10.8
6	18 Nov	1300	S2	20.2
7	19 Nov	1200	S3	20.3
8	20 Nov	1200	S3	20.4

For each of the selected trials, hourly averaged meteorological data were calculated from observations provided by MEDA stations. These data were used as input to the HPM and 52.5 min averaged dosages were predicted at sampler locations of the three sampler lines. (See Appendix VIII for input data used for the evaluation) The simulations were performed on an Intel Pentium dual core 1.73GHz laptop computer with 1GB ram. Measured concentrations provided by whole air samplers were then integrated and actual dosages at each point were calculated. By selecting the maximum dosage anywhere along a sampling line as the evaluation objective,

predicted and actual dosage values were compared.⁴⁴ The study involved a total of 24 sampling cases where the quantitative performance of the model was assessed using several statistical performance measures. They include fractional bias (*FB*), geometric mean bias (*MG*), normalized mean square error (*NMSE*), geometric variance (*VG*), the fraction of observations within factors of two observations (*FAC2*) and the fraction of observations within factors of three observations (*FAC3*).⁴⁴ These measures are defined as;

$$FB = 2 \frac{(\bar{c}_0 - \bar{c}_p)}{(\bar{c}_0 + \bar{c}_p)} \quad (4.2)$$

$$MG = \exp(\bar{\ln c}_0 - \bar{\ln c}_p) \quad (4.3)$$

$$NMSE = \frac{\overline{(c_0 - c_p)^2}}{c_0 c_p} \quad (4.4)$$

$$VG = \exp\left[\overline{(\ln c_0 - \ln c_p)^2}\right] \quad (4.5)$$

$$FAC2 = \text{Fraction of data for which } \frac{1}{2} \leq \frac{c_p}{c_0} \leq 2 \quad (4.6)$$

$$FAC3 = \text{Fraction of data for which } \frac{1}{3} \leq \frac{c_p}{c_0} \leq 3 \quad (4.7)$$

where c_p, c_0 are predicted and observed concentrations respectively. The over bar represents the mean value.

FB and *MG* are measures of the mean bias whereas *NMSE* and *VG* measure the variance or the random scatter of a data set. Although each measure has its own strengths and weaknesses, *MG* and *VG* are recommended for cases where the observed and predicted data vary in several orders of magnitude.⁴⁴ For a perfect model, *FB* and *NMSE* should equal to zero whereas *MG*, *VG*, *FAC2* and *FAC3* to one. However, it is necessary to establish a minimum threshold concentration level in calculating the latter measures since they consider logarithmic values of concentrations. Therefore a threshold value of 10 ppt was employed in this study. In addition to the above mentioned performance measures, single factor analysis of variance (*ANOVA*) was also used to investigate if there is a significant difference between predicted and observed maximum dosage values.

4.4 Effect of chemical processes on atmospheric dispersion of GB, GA and HD

To demonstrate the effect of chemical reactions on the dispersion of GB, GA and HD four hypothetical puff releases were simulated on the Nevada test site (Same terrain where the DP26 experiment conducted). Same meteorological input used in Trial 4 of DP26 simulations and 20 kg of each agent was chosen. Simulations were performed with and without chemical processes related to each agent. Hourly averaged dosages were calculated along DP26 sampling lines and at all the concentration grid points. Visual observation of dosage color maps and comparison of maximum dosages along sampling lines were used to demonstrate the effect of chemical reactions on the atmospheric dispersion of each agent. The outcomes of the above evaluations are presented in the next chapter.

Chapter Five

5 Results and Discussion

This chapter of the thesis presents the results obtained through model evaluation study and the effect of chemical processes on atmospheric dispersion of GA, GB and HD. Moreover, issues related to each of the results are also discussed.

5.1 Evaluation of Basic Meteorological Parameterization Scheme

The basic meteorological parameterization scheme of HPM was evaluated using the meteorological data reported in Indianapolis field experiment available in Modelers Data Achieve. The study used three important derived meteorological parameters; sensible heat flux, Monin-Obukhov length and friction velocity as evaluation objectives. Surface measurements provided by Indianapolis meteorological stations were used as Input to HPM and predictions for each evaluation objective were made. These predictions were compared with corresponding values of reported data. The statistical analysis of data using single factor *ANOVA* yielded following results. (See Appendix IX for descriptive statistics)

Table 5.1 Summary of basic meteorological parameter evaluation

Parameter	<i>ANOVA</i> statistic (single factor)
Sensible heat flux	$F(1,322) = 1.8986, 0.169, 3.875$
Monin-Obukhov length	$F(1,292) = 0.0605, 0.806, 3.874$
Friction velocity	$F(1,308) = 0.0688, 0.793, 3.872$

Note that in the above table, the *ANOVA* statistic is represented in the format $F(a, b) = c, p, F_{crit}$; where a and b are the between groups and within groups degrees of freedom, c is the F statistic, p is the level of significance and F_{crit} is the critical value for F statistic at 95% confidence level. Single factor *ANOVA* can be viewed as a powerful statistical method to investigate the agreement

between two different data sets. This can be achieved using F statistic along with the level of significance and critical F value in reported *ANOVA* results. If the F statistic is less than the critical F value and the level of significance is greater than 0.05, the two data sets in question can be considered as in good agreement. That is no significant difference between two data sets.

Results obtained from *ANOVA* test for the current study summarized in Table 5.1 shows that the model predictions were in good agreement with reported values of each meteorological parameter. Although the F statistic reported for the sensible heat flux shows a greater value in comparison to F statistics of other two parameters, the model predictions can be still viewed as accurate. First, it meets the criteria to prove that there is no significant difference between predicted and experimentally reported sensible heat flux data. Second, the other two parameters which show a strong agreement with experimental data were calculated with the aid of sensible heat flux. That is Monin-Obukhov length and friction velocity are derived parameters of sensible heat flux.

The variation of each of the predicted meteorological parameters against reported data in the Indianapolis data set have been plotted in Figures 5.1, 5.2 and 5.3.

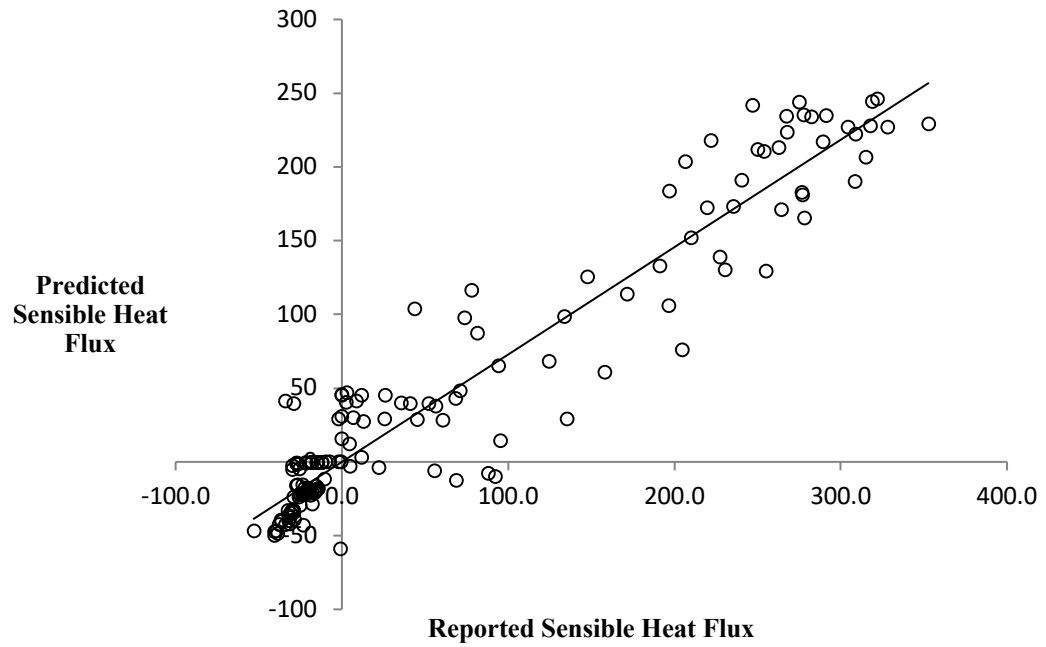


Figure 5.1 Predicted vs Reported values of sensible heat flux

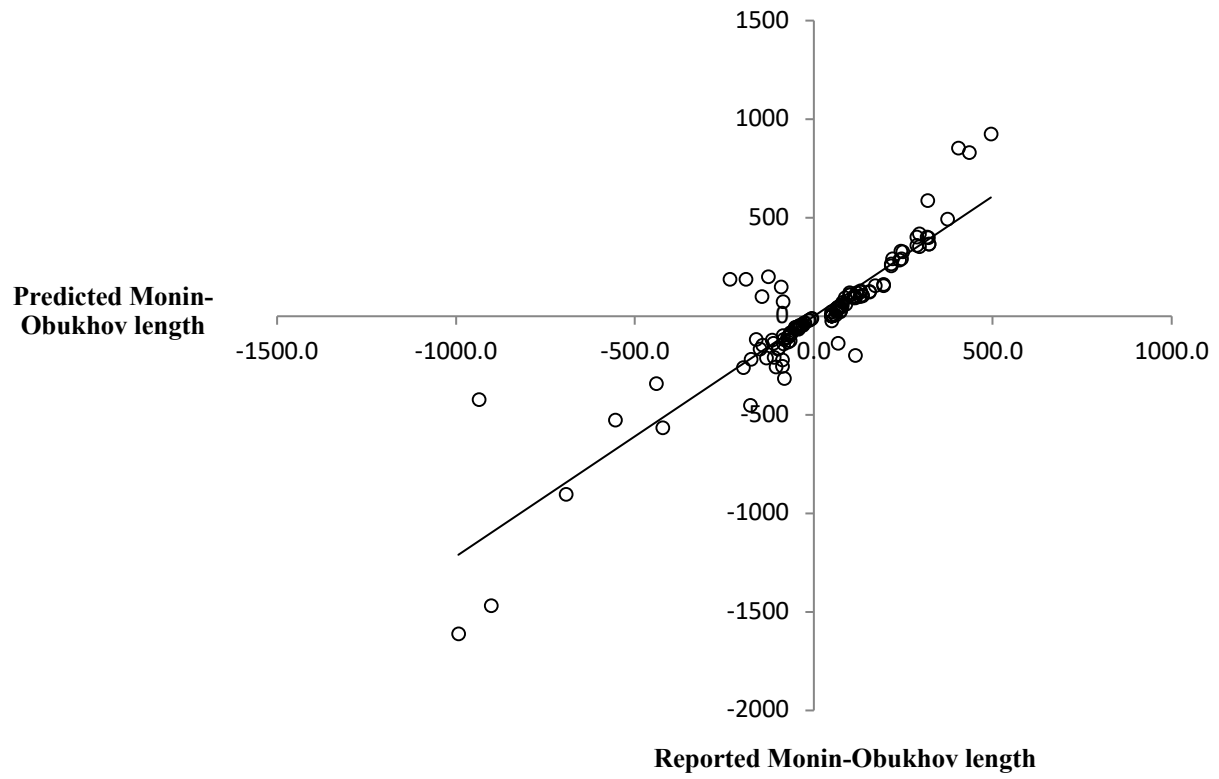


Figure 5.2 Predicted vs Reported values of Monin-Obukhov length

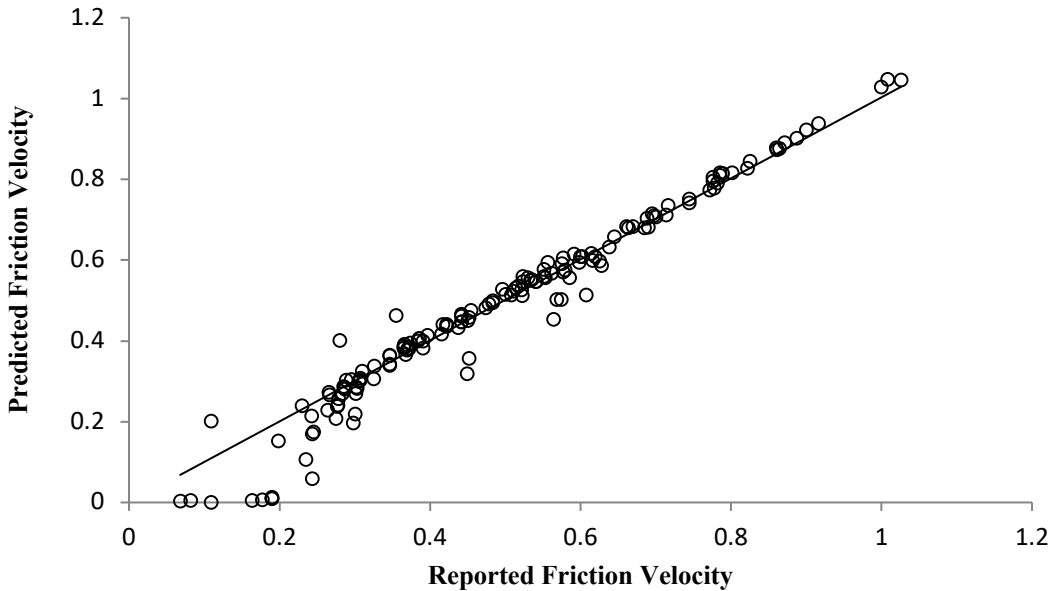


Figure 5.3 Predicted vs Reported values of friction velocity

Figures 5.1-5.3 also show that the model predictions were in good agreement with data reported in Indianapolis experimental dataset. For several cases, the values plotted in Figure 5.1 and 5.2 show negative values whereas the corresponding reported values were positive or vice versa. It should be noted that both sensible heat flux and Monin-Obukhov length are indicators of day and night time. Negative values of sensible heat flux and positive values of Monin-Obukhov length stands for night time and the opposite indicate the day time. The deviation shown in Figure 5.1 and 5.2 may be due to the fact that current study did not account for day light saving time used in USA in solar elevation calculations. However, this problem would have been totally disappeared if the reported data set/experiment was conducted in an equatorial country. In equatorial countries, no day light saving time is employed as they are less affected by seasonal changes. Specially, the predictions made by HPM for an equatorial country such as Sri Lanka would not suffer from above problem.

5.2 Evaluation of the Mass Consistent Wind Model

The accuracy of wind flow generated by mass consistent wind model was evaluated by simulating a potential flow around a hemispherical hill. A constant horizontal wind flow of

5 m s^{-1} was applied over the computational grid and the model was allowed to calculate the correct magnitude and direction of wind components so that the conservation of mass is satisfied. Analytical solutions for a potential flow around a hemispherical hill were used to calculate analytical wind components for the same problem. The obtained solution was compared against the one that generated by HPM. Analysis of variance and visual observation of wind components were used in this comparison. Both methods showed that the mass consistent wind model of HPM is performing well. The *ANOVA* test yielded $F(1, 2448) = 0.4626, p = 0.496, F_{crit} = 3.845$ for the horizontal profile and $F(1, 910) = 0.1145, p = 0.735, F_{crit} = 3.852$ for the vertical wind profile. (See Appendix IX for descriptive statistics) Note that the F statistic is well below the critical F value at 95% confidence level (F_{crit}) and the value of p is greater than 0.05 in both cases.

The accuracy of wind flow simulated by HPM can also be proven by a graphical representation of the wind field. Figure 5.4 depicts 3-dimensional view of wind flow around the hill. The 2-dimensional projection of the same simulation generated by HPM is shown in Figure 5.5. Turning of the wind near obstacles and correct direction of the flow around the hill in Figure 5.5 shows that the model is capable of producing a correct wind flow. Note that the red arrows representing the simulated wind vectors and blue arrows representing analytical wind vectors lie almost top of each other. A higher deviation can be observed near the lower part of the hemisphere. (See the magnified area depicted in Figure 5.5) The coarseness of the grid is relatively higher in this area as the terrain is much steeper. Therefore such a deviation in simulated wind is naturally expected.

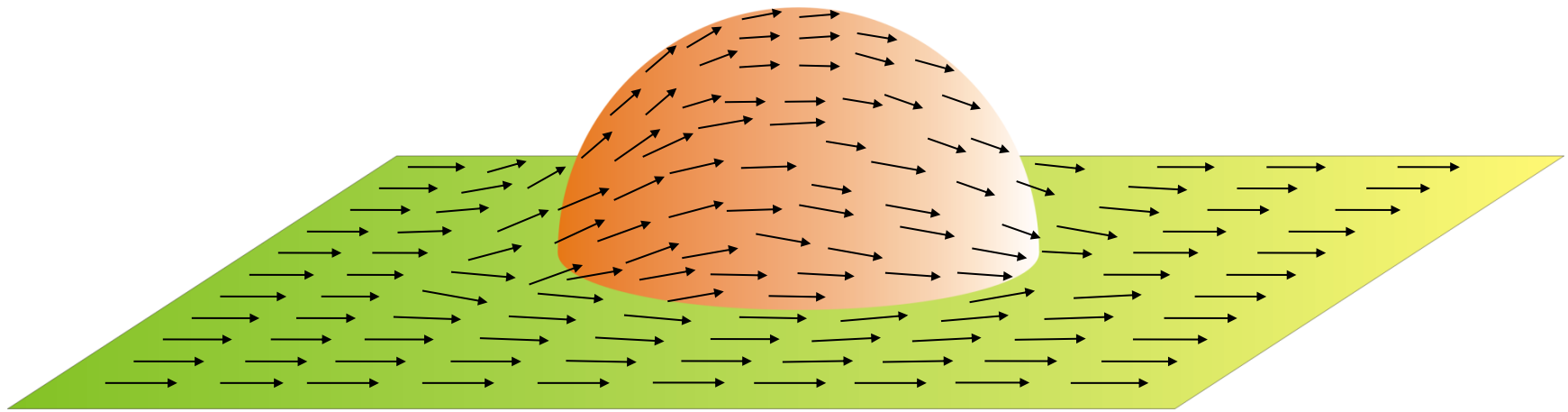


Figure 5.4 Numerical simulation of a potential flow around a hemi spherical hill – 3 Dimensional view (the direction of the wind is represented by arrows)

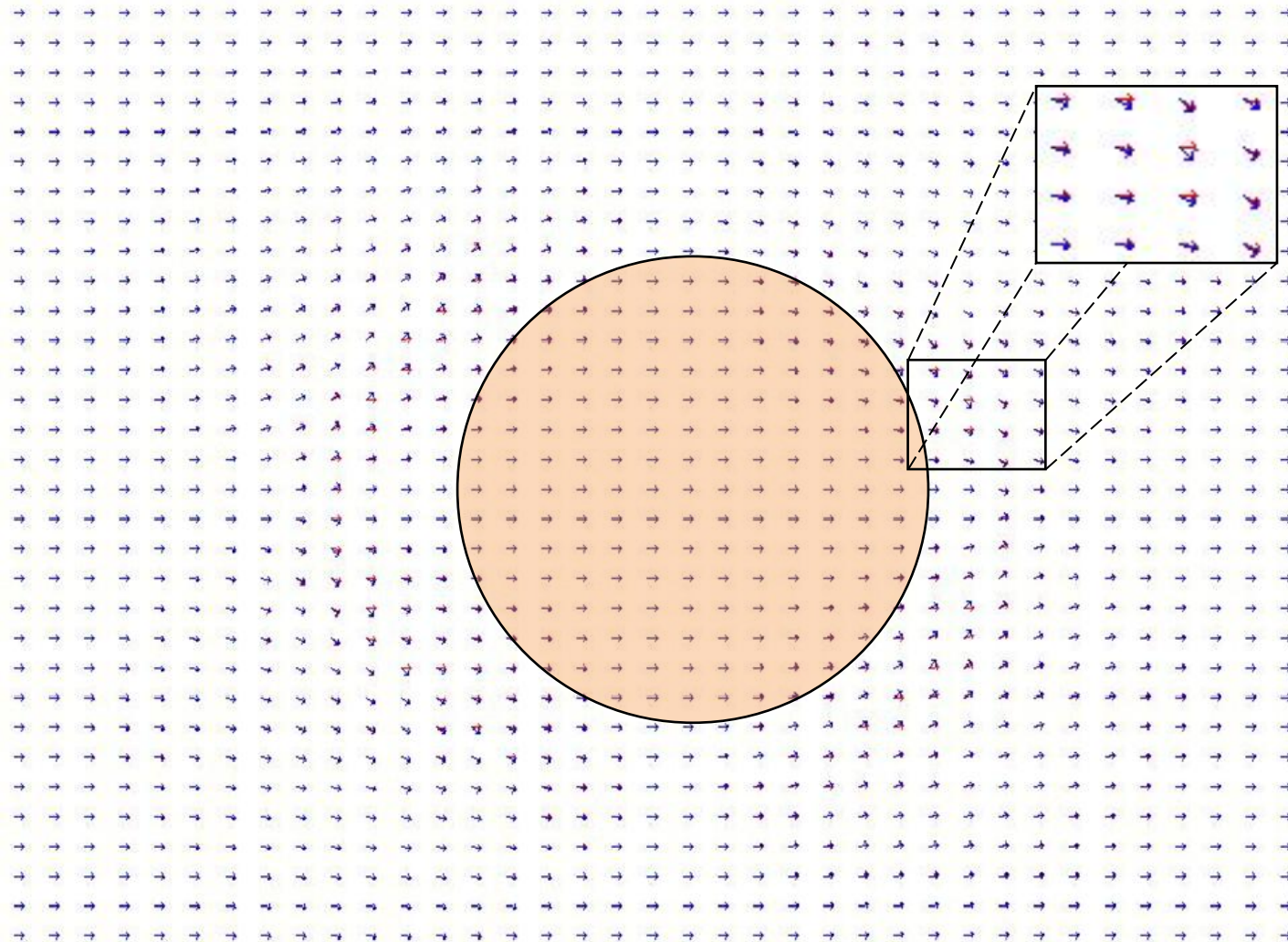


Figure 5.5 Numerical simulation of a potential flow around a hemi spherical hill – 2 Dimensional view (Red and blue arrows represent the numerically simulated wind field and the analytical wind field respectively. The brownish circle in the middle of the figure represents the hill.)

To resolve this problem, the resolution of the computational grid can be increased. Increased grid resolution reduces the coarseness of the grid. However, this has to be considered with care as the resolution is directly related to the total run time of the divergence minimization algorithm. Table 5.2 reports runtimes for the same simulation on two computers with different performance under various grid resolutions.

Table 5.2 Runtimes reported for a potential flow around a hemi spherical hill under various grid resolutions and computer performances

Grid resolution	Run time (s) – 1.73 GHZ	Run time (s) – 3.07 GHZ
	CPU with 1GB ram	CPU with 2 GB ram
$37 \times 37 \times 15$	1719	880
$31 \times 31 \times 15$	862	452
$27 \times 27 \times 15$	419	222

With the times reported in Table 5.2, it is obvious that the runtime for a simulation can be drastically reduced by boosting performance. And a higher gird resolution can be employed under such circumstances. Due to this reason, HPM provides the freedom to adjust its computational grid dimensions according to user's computer performance. This can be viewed as a good feature in comparison to most other available hazard prediction models, where fixed grid sizes are used.

5.3 Evaluation of the Overall Model Performance

The evaluation of overall model performance of HPM involved model simulations for 8 trials of the Dipole Pride 26 field experiment.²⁷ Meteorological and source data reported by DP26 documents were provided as input to HPM and dosages were predicted at the sampling locations where the actual sampling was performed during the experiment. The predicted dosages were then compared with actual dosage values reported by DP26 documentation. Several statistical measures applicable in air pollution model evaluation and analysis of variance (*ANOVA*) were employed in assessing the model performance. The results indicated that the HPM performed well in its predictive capability. They are summarized in Table 5.3. (See Appendix IX for descriptive statistics)

Table 5.3 Summary of results for each performance measure as shown in the evaluation study of HPM

Performance measure	Value
<i>FB</i>	-0.603
<i>NMSE</i>	2.888
<i>MG</i>	0.856
<i>VG</i>	8.537
<i>FAC2</i>	0.542
<i>FAC3</i>	0.625
<i>ANOVA</i>	$F(1,46) = 1.055, p = 0.310, F_{crit} = 4.052$

Although proper model acceptance criteria based on above statistics cannot be found in literature, they can be used to describe the model performance and to benchmark models. The value of fractional bias (*FB*) suggested that the mean bias on a linear scale was about 60% over prediction for HPM. (Note that the negative values of *FB* indicate an over prediction.) Normalized mean square error (*NMSE*) expressed that the under and over predicting errors were about a factor of 2.9 about the mean. The value of geometric mean bias (*MG*) suggested that the mean bias on a logarithmic scale was about 17% over prediction. This value corresponds to random scatter of a factor of 4.3. (Note that this factor was obtained by rearranging the formula for the geometric variance)

FB and *NMSE* indicators suggested that HPM highly over predicted dosages whereas *MG* and *VG* indicated a better performance. This is due to the fact that first two measures are highly influenced by infrequently occurring high predicted and observed values. *FAC2* and *FAC3* values indicated that the fraction of data within $1/2 - 2$ and $1/3 - 3$ factors of observed values were 54% and ~63% respectively. Moreover, analysis of variance showed that the differences between observed and predicted dosages were insignificant. Note that the *F* statistic is clearly below the critical *F* value at 95% confidence level and the value of *p* is greater than 0.05. Considering these facts, it can be concluded that HPM performed well in Dipole Pride simulations with a slight over prediction.

To examine the problem of over prediction more precisely, a scatter plot would be more useful. Predicted values of maximum dosage by HPM versus the observed dosage have been plotted in Figure 5.6. The scatter plot clearly revealed that there was a systemic over prediction. Most of the predictions lied above the symmetric line $y = x$, which was roughly about 60% of the total cases.

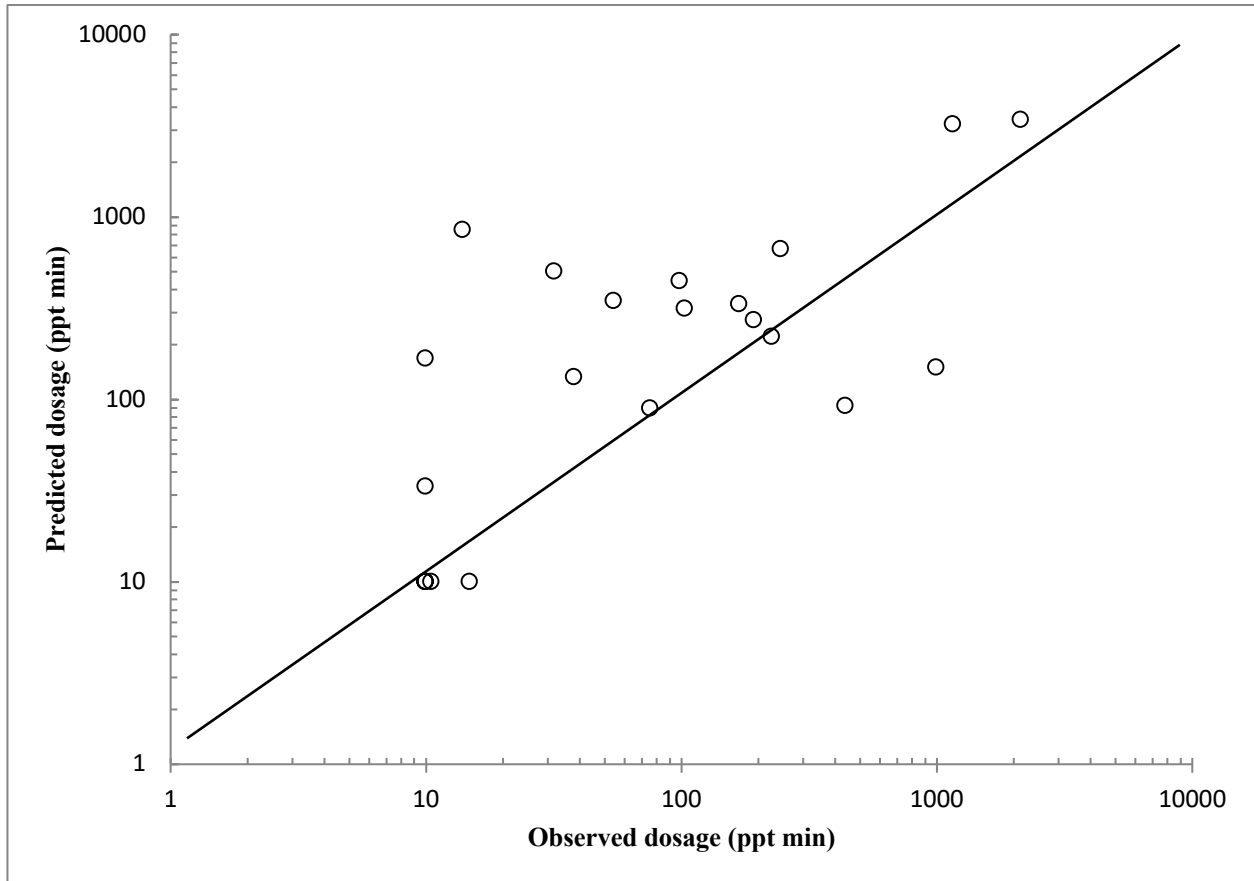


Figure 5.6 Scatter plot of predicted maximum dosages vs observed values for each sampling line

The under/over predictions made by HPM can be either due to under/over prediction of puff dispersion coefficients or the cloud advective speed. Puff dispersion coefficients used in HPM were not specifically developed for instantaneous releases and were similar ones used to model continuous releases. The difference in actual and predicted cloud advective speed can be mainly due to failure of capturing complex wind patterns. There are several possibilities which might have caused this problem. The meteorological algorithm of HPM extrapolated surface wind observations into upper layers of the grid. It would be more accurate if upper wind data from pilot balloons were considered. HPM demanded hourly averaged meteorological input for its predictions which might not reflect instantaneous wind patterns actually taking place. Moreover, the grid resolution had a large impact on the outcome of wind field divergence minimization. The horizontal cell dimensions of the meteorological grid used in the current study was 500×500 m. This may not have truly identified the real topographic effects. Figure 5.4 depicts the Nevada test site as approximated by HPM.

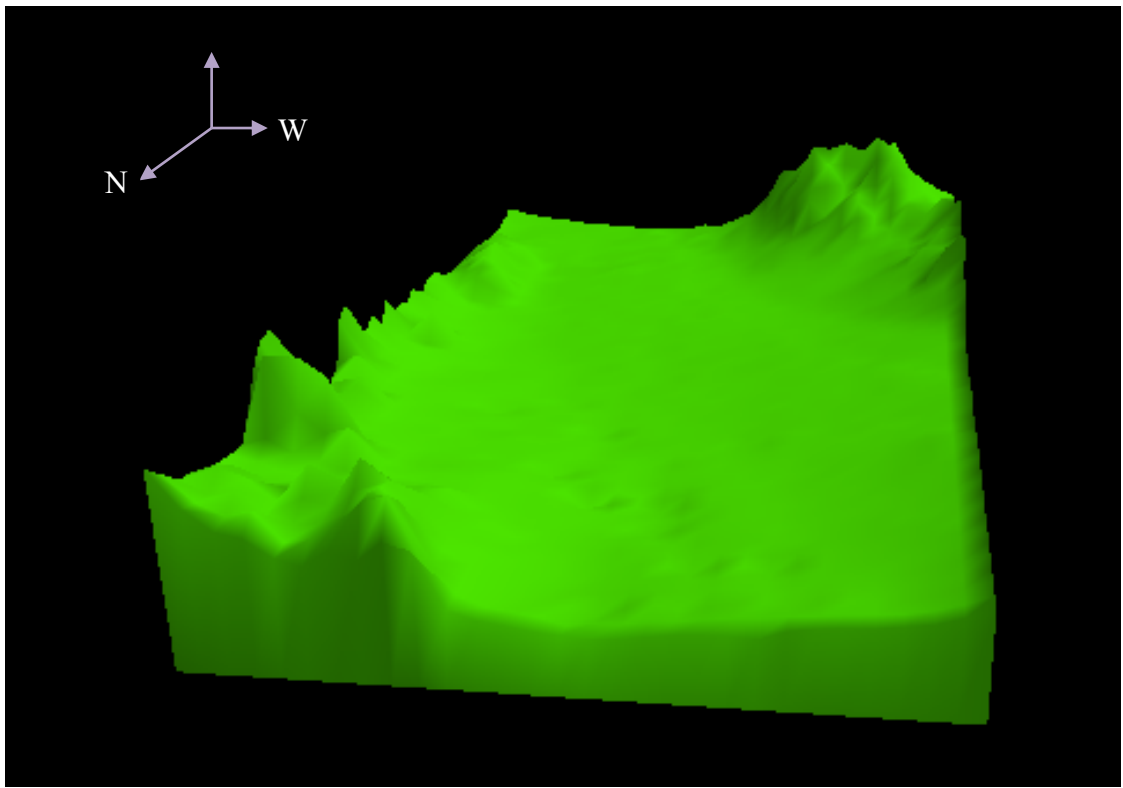


Figure 5.7 3-D view of Nevada test site as approximated by HPM

As shown in Figure 5.7, HPM approximated the Nevada test site as a flat terrain with two hilly areas at lower left and upper right corners of the grid. However, the real terrain is a basin surrounded by a set of hills. Furthermore, meteorological model of HPM did not account for slope flow effects and blocking effects on the wind flow. These factors may have a large impact on the wind field and hence under/over prediction of dosages. However, it is important to emphasize that over/under prediction is natural among all the hazard prediction models available up to date.⁴⁴ The strengths of each model and how advantageous these strengths for a particular emission scenario would determine how successful their predictions are. Based on the performance of Dipole Pride simulations, it is obvious that HPM was able to produce good predictions.

Except the accuracy of predictions, the most important consideration for a hazard prediction model is the run time required for a simulation. In DP26 simulations, the lowest runtime recorded was 24 min whereas the highest around 32 min. More than 80% of the recorded time was consumed by the divergence minimization algorithm and majority of the rest for dosage calculations. These runtimes can be naturally expected as the simulations were carried out on 1.73 GHz laptop with 1GB RAM under $54 \times 30 \times 15$ grid size. However, they would have

dropped down significantly if simulations were performed on a faster computer with fine grid spacing.

5.4 Effect of Chemical Reactions

To assess the importance of hydroxyl chemical reactions in the dispersal of GA, GB and HD, four hypothetical simulations were conducted using HPM. These simulations involved the dispersion of a non-reactive substance and dispersion of GA, GB and HD with reactions. The study showed that the effect of Hydroxyl radical reactions was important on the overall dosage predictions. Dosage color maps produced by HPM for a substance without any chemical reaction, dispersion of GA, GB and HD with hydroxyl radical reactions are depicted by Figure 5.8a to 5.8d respectively.

Visual observation of dosage color maps show that the dosages have been clearly influenced by hydroxyl radical reactions. The sizes of colored areas in Figure 5.8b to 5.8d have been reduced in comparison to Figure 5.8a. The second Figure (color map of GA) shows the highest reduction of colored area in comparison to other two. This is naturally expected as GA quickly reacts with the hydroxyl radicals in the atmosphere. ($K_{GA} = 4.9 \times 10^{-11} \text{ cm}^3 \text{ molecule}^{-1} \text{ s}^{-1}$ at 25°) The color map of GB looks very similar to that of GA but its colored areas are slightly greater than GA. In fact, this is obvious as the rate constants of both agents are much closer but slightly higher for GA. ($K_{GB} = 4 \times 10^{-11} \text{ cm}^3 \text{ molecule}^{-1} \text{ s}^{-1}$ at 25°) Color map of HD depicted that the dosages were less than the original values (i.e. without chemical reactions) but were greater than other two cases. This is reasonable as the reaction rate of HD is less than the other agents. ($K_{HD} = 7.82 \times 10^{-12} \text{ cm}^3 \text{ molecule}^{-1} \text{ s}^{-1}$ at 25°)

These observations were also supported by dosages calculated at DP26 sampling lines. Computed dosages at each sampling line for the dispersion without chemical reactions were the highest. Accounting for the chemical reactions, dosages produced for the same sampling locations were reduced depending on the reactivity with hydroxyl radicals. For example, the maximum hourly averaged dosages predicted along sampling lines for each agent dropped by 7.4 %, 6.6% and 1.7 % for GA, GB and HD respectively. These reductions are compatible with the visual observations of color maps discussed earlier. Therefore, it is clear that HPM correctly accounts for the hydroxyl radical reactions of GA, GB, and HD in modeling their dispersal within the atmosphere which is an important aspect.

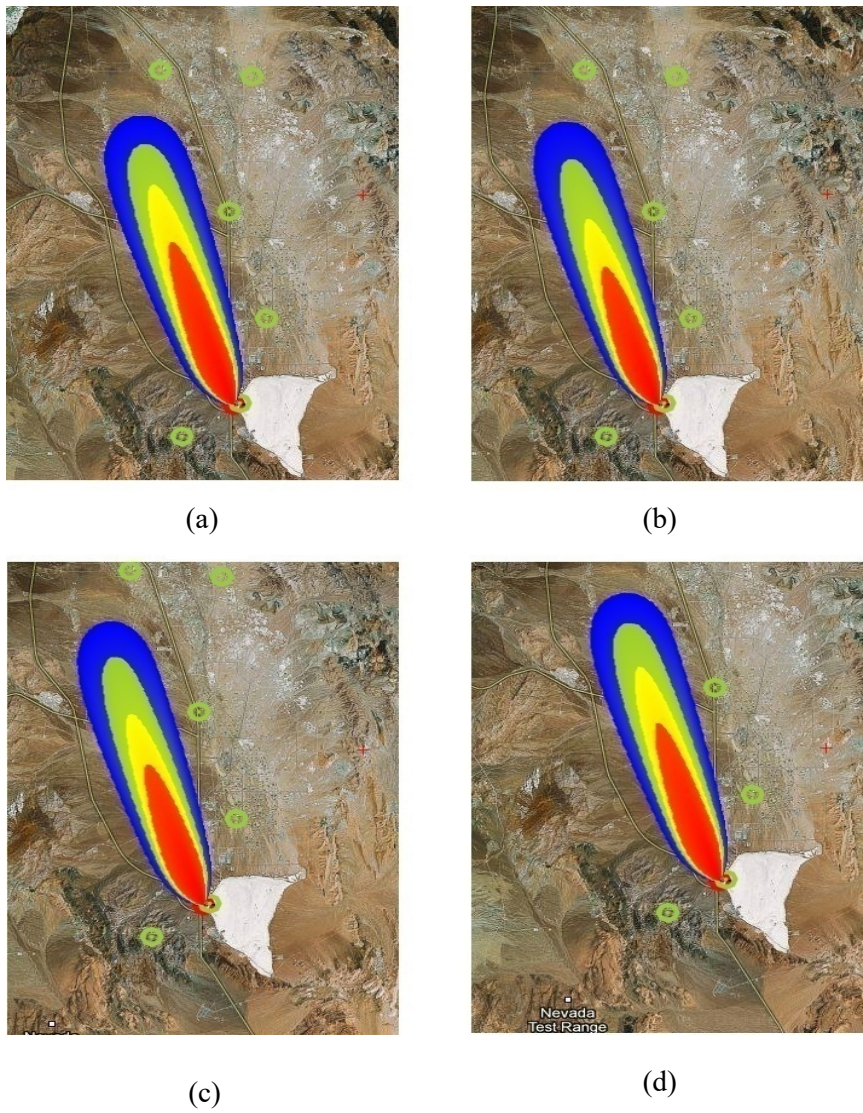


Figure 5.8 Dosage color maps produced by HPM for the atmospheric dispersion of agents without chemical processes (a), dispersion of GA (b), GB (c), and HD (d) with Hydroxyl radical reactions. (Note that the red, yellow, green and blue represents dosages above 1050 ppt h, 1050 - 750 ppt h, 750 - 450 ppt h, and 450 - 150 ppt h ranges)

5.5 Application of Hazard Prediction Model in Sri Lanka

The Hazard Prediction Model has been optimized to use as an immediate modeling tool within Sri Lanka. As mentioned previously, the inbuilt terrain database of the geographical code contains terrain data for a 510×920 UTM grid covering the whole island. Therefore, a release of

chemical warfare attack took place anywhere in Sri Lanka can be simulated using HPM. All the other basic information including time zone has been set as applicable to Sri Lanka by default. Furthermore, several modifications have been made to improve the performance and employ as an immediate modeling tool. First, the minimum allowed divergence in mass consistent wind field generation has been set to 0.0001 by default. This is the same value used in DP26 simulations which aided the divergence minimization algorithm to generate sufficiently accurate results within a reasonable time period. Second, the default grid size has been reduced to $54 \times 30 \times 10$ in order to achieve a higher performance. Third, the resolution of the concentration grid is 540×300 by default, so that the program calculates the concentration/dosage at sampling locations per each 50 m of the grid. Fourth, the graphical representation of concentration/dosage levels using color maps has been done in such a way that the maximum performance is achieved with a minimum video graphic memory. However, it should be noted that HPM allows users to change all these options according to their preference.

To experience all the features of HPM discussed so far, a model simulation for a hypothetical release of chemical warfare agent would be appropriate. This can be performed assuming an explosive release of sarin (GB) near Gampaha in Sri Lanaka ($\sim 7.09^{\circ}\text{N}$, 79.99°E). Furthermore, it is assumed that there are three meteorological stations located in Gampaha district. Hypothetical release locations, meteorological stations and a set of dummy data to run the simulation have been tabulated in Table 5.4 to 5.7.

After providing general input through the smart map navigator (i.e. marking locations tabulated in Table 5.4 on the map), other inputs tabulated in Table 5.5 – 5.7 has to feed through data input window. When the input has been finished, the simulation may run with default configuration.

Table 5.4 General Input to Hazard Prediction model for hypothetical simulation of a sarin emission scenario

Location	Coordinate
Release Point	$\sim 7.09^{\circ}\text{N}$, 79.99°E

Meteorological station 1 (MEDA_1)	7.1080 °N, 79.9923 °E
Meteorological station 2 (MEDA_2)	7.0903 °N, 79.9961 °E
Meteorological station 3 (MEDA_3)	7.0664 °N, 79.9937 °E

Table 5.5 Source Input to Hazard Prediction model for hypothetical simulation of a sarin emission scenario

Input	Value
Date & time	10/13/12, 7.43 PM (Local time)
Source type	Instantaneous
Type of the explosive	Composition B
Amount of the explosive	2 kg
Type of the chemical agent	Sarin (GB)
Amount of the agent	4 kg

Table 5.6 Geographical Input to Hazard Prediction model for hypothetical simulation of a sarin emission scenario

Input	Value
Type of the terrain	Very rough
Type of the surface	Buildings
Surface moisture availability	10 %

Table 5.7 Meteorological Input to Hazard Prediction model for hypothetical simulation of a sarin emission scenario (Note that the MEDA stands for the meteorological station and WS, WD, T, P, RH, CC, RF for the hourly averaged wind speed, direction, temperature, pressure, relative humidity, cloud cover and rain fall respectively.)

Station	WS (m s ⁻¹)	WD (deg)	T (°c)	P (mmHg)	RH (%)	CC (%)	RF (mm)
---------	----------------------------	-------------	--------	-------------	-----------	-----------	------------

MEDA_1	2.0	200	25.0	880.0	40	10	0.0
MEDA_2	2.5	170	24.0	875.0	40	10	0.0
MEDA_3	3.0	145	25.0	880.0	40	10	0.0

The simulation takes approximately 7-8 minutes to run on Intel Dual Core 1.73 GHz laptop with 1 GB RAM. The simulated wind field and dosage color maps with default configuration can be obtained as shown in Figure 5.9.

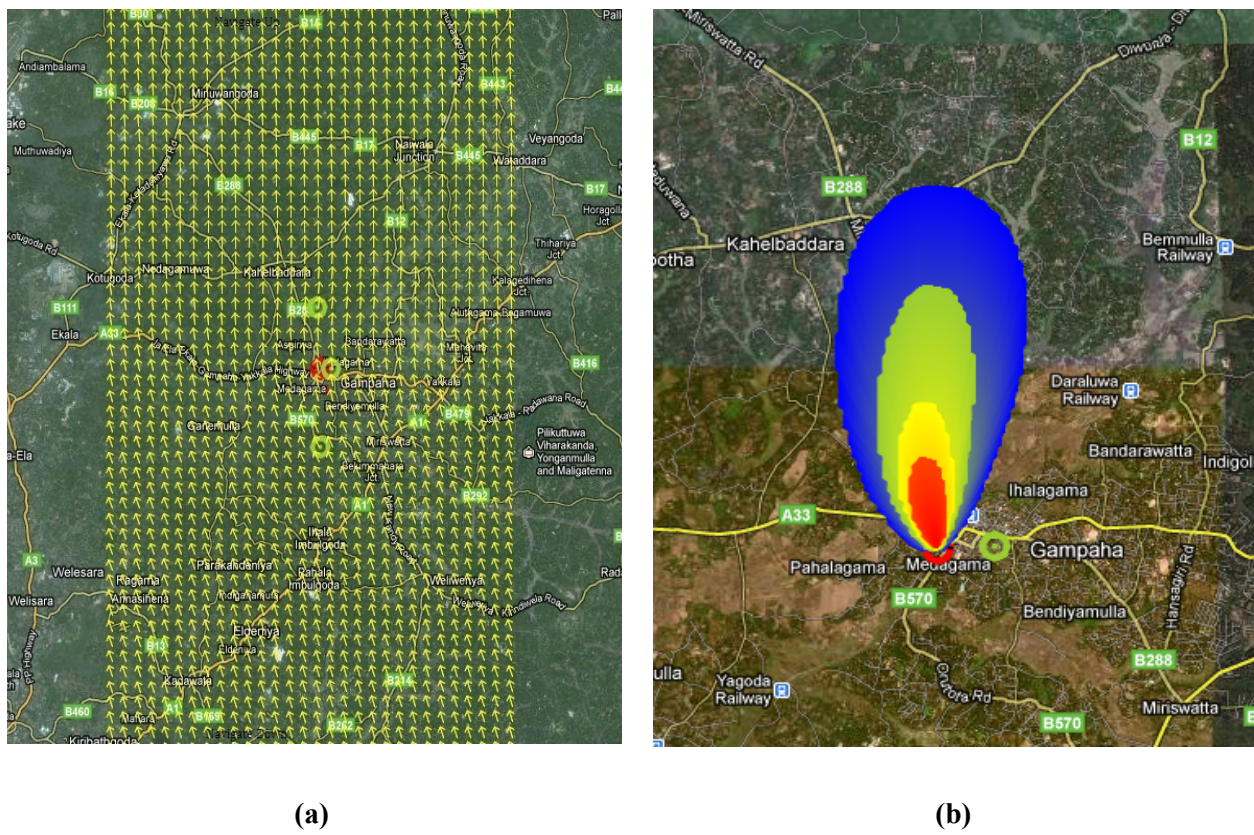


Figure 5.9 Output of Hazard Prediction Model for the hypothetical simulation of sarin emission scenario - wind field **(a)**, Dosage color map **(b)** (Note that the red, yellow, green and blue represents dosages above 5000 ppt h, 5000 - 3000 ppt h, 3000 - 1500 ppt h, and 1500 - 400 ppt h ranges)

Figure 5.9 (a) of the simulated results show that the HPM has produced a mass consistent wind field considering terrain effects and the direction of the wind as reported by each meteorological station. The dosage color map (Figure 5.9b) shows the dispersal of the agent after 1 hour of the release. According to the color map, the northern area of the city is affected by a higher amount of the agent. The color map covers a considerable area of the map, which clearly indicates that the ground level dosages of the agent are high and a higher number of citizens are at stake. This

fact is reasonable as a release take place during the night time increases the ground level concentrations of the agent. During night time, the height of the atmospheric boundary layer is less so that the vertical movement of the agent smoke is poor. This increases the ground level concentration/dosages within the planetary boundary layer and the victims who live in this area would suffer greater levels of consequences. However, the population of the southern part of the city would be least effected or not effected at all. This happens as the wind blows towards northern direction so that the agent material also carried in the same direction. With these reasonable results generated within in a sufficient time, it is obvious that the Hazard Prediction Model can be used to assess the risk following an immediate release of a chemical warfare agent within Sri Lanka.

Chapter Six

6 Conclusions

It is concluded that the Hazard Prediction Model is capable of predicting dosages of Chlorine, Hydrogen Cyanide, Cyanogen Chloride, Sarin, Tabun and Sulfur Mustard agents released into the atmosphere by instantaneous explosive events. These predictions are valid up to times less than one hour. The model can be employed on a fast computer with appropriate selection of grid resolution as a component of an emergency response program. For the day time dispersion of Sarin, Tabun and Sulfur Mustard; it is recommended to consider the effects of chemical processes. To improve the model performance and usefulness, following improvements are suggested for future work. They were not made in the current work due to limited time and resources available for the study.

- A multigrid technique can be introduced to divergence minimization algorithm in order to improve the performance
- The accuracy of the wind field can be increased by introducing slope flow and blocking effects into the meteorological code.
- The model can be extended to other chemical warfare agents by introducing chemical and aerosol deposition processes into existing code.
- Dense gas effects can be introduced into the model
- Instantaneous cloud rise model should be extensively validated with experimental data.
- More work should be done regarding the plume rise model, and the model performance should be evaluated for continuous/semi-continuous releases with a field data set such as MADONNA.
- By introducing appropriate source models, the model can be extended to industrial gas emission scenarios

References

- 1 *Potential Military Chemical/biological Agents and Compounds*; FM 3-9; NAVFAC P-467; AFR 355-7; Department of the Army, Department of the Navy, Department of the Air Force, U.S. Government Printing Office: Washington, DC, 1990.
- 2 Hoenig, S. L., *Compendium of Chemical Warfare Agents*; Springer, 2006, 57-71
- 3 Marrs, T.C., (2007). Toxicology of Organophosphate Nerve Agents. Marrs, T.C., Maynard, R.L., Sidell, F.R.(Eds.). (2007). *Chemical Warfare Agents: Toxicology and Treatment*. (pp. 191-222). John Wiley & Sons, Ltd., New Jersey.
- 4 Ballantyne, B., Bismuth, C., Hall, A. H., (2007). Cyanides: Chemical Warfare Agents and Potential Terrorist Threats. Marrs, T.C., Maynard, R.L., Sidell, F.R.(Eds.). (2007). *Chemical Warfare Agents: Toxicology and Treatment*. (pp. 496-542). John Wiley & Sons, Ltd., New Jersey.
- 5 Maynard, R.L., (2007). Mustard Gas. Marrs, T.C., Maynard, R.L., Sidell, F.R.(Eds.). (2007). *Chemical Warfare Agents: Toxicology and Treatment*. (pp. 375-408). John Wiley & Sons, Ltd.: New Jersey, 2007.
- 6 *Field Behavior of NBC Agents: (including Smoke and Incendiaries)*; FM 3-6; FMFM 7-11-H; AFM 105-7; Department of the Army, Department of the Air Force, United States Marine Corps; U.S. Government Printing Office: Washington, DC, 1992.
- 7 Lazaridis, M., *First principles of meteorology and air pollution*. Springer, 2010, 14-20
- 8 Bakkum, E. A.; Duijm, N. J. Vapor cloud dispersion. In *Methods for the Calculation of Physical Effects: Due to Releases of Hazardous Materials (liquids and Gases) : Yellow Book*; van der Bosch, C.J.H., Weterings, R. A. P. M.; Directorate-General for Social Affairs and Employment, Committee for the Prevention of Disasters: Netherlands, 2005.
- 9 Model Description. *Umatilla Chemical Agent Disposal Facility Quantitative Risk Assessment- Volume 1*; SAIC-00/2641; Science Applications International Corporation: Abingdon, MD, 2002.

- 10 Markiewicz, M., Modelling of the Air Pollution Dispersion. *MANHAZ Monograph: Models and techniques for health and environmental hazard assessment and management, Part 2 - Air Quality Modelling*. Institute of Atomic Energy, Otwock-Swierk, Poland, 2006, 303-347
- 11 Whitacre, C. G.; Griner, J. H.; Myirski, M. M.; Sloop, D. W. *Personal Computer Program For Chemical Hazard Prediction, U.S.Army (D2PC)*; CRDEC-TR-87021; U.S. Army Armament Munitions Chemical Command: Aberdeen Proving Ground, Maryland, 1987.
- 12 Mellsen, S. B. *A Fortran Program for Calculating the Chemical Hazards Using NATO STANAG 2103/ATP-45 Algorithm*; ADA214763; Defense Research Establishment: Suffield, Ralston, Alberta, 1989.
- 13 Applying Meteorological and Dispersion Models. *Modeling and Risk Characterization of US Demolition Operations at the Khamisiyah Pit*; Special Assistant to the Under Secretary of Defense (Personnel and Readiness) for Gulf War Illnesses, Medical Readiness, and Military Deployments, Department of Defense, 2002
- 14 Wilson, J. D., Sawford, B. L., *Bound-Lay Meteorol.* **1996**, 78(1-2), 191–210.
- 15 de Haan, P., Rotach, M. W., *Int. J. Environ. Pollut.* **1995**, 5(3-6), 350–359.
- 16 Andronopoulos, S., Davakis, E., Bartzis, J.G. *RODOS-DIPCOT Model Description and Evaluation*; Report RODOS (RA2)-TN (09)01; EURANOS European Project, 2009.
- 17 Grahn, H., *Modeling of Dispersion, Deposition and Evaporation from Ground Deposition in a Stochastic Particle model*; Defense Research Establishment: Umea, Sweden, 2004
- 18 Nasstrom, J. S., Sugiyama, G., Baskett, R.L., Larsen, S.C. and Bradley, M.M., *Int. J. Emerg. Manage.* **2007**, 4(3), 524–550.
- 19 Kingdon, R. D., Walker, S., (2007). Dispersion Modeling of the Spread of Chemical Warfare Agents. Marrs, T. C., Maynard, R. L., Sidell, F.R.(Eds.). (2007). *Chemical Warfare Agents: Toxicology and Treatment.*(pp. 67-87). John Wiley & Sons, Ltd., New Jersey.
- 20 Van Ulden, A. P., Holtslag, A. A. M., *J.Climate Appl. Meteorol.* **1985**, 29, 1196-1207.
- 21 Ishikawa, H., *J. Appl. Meteorol.* **1994**, 33, 733-743.

- 22 Church, H.W. *Cloud Rise from High Explosive Detonations*; Sc-RR-68-903; Sandia Laboratories: Albuquerque, 1969.
- 23 Brown, R. C.; Kolb, C. E.; Conant, J. A.; Zhang, J., Dussault, D. M. *Source Characterization Model (SCM): A Predictive Capability for the Source Terms of Residual Energetic Materials from Burning and/or Detonation Activities*; Aerodyne Research Inc: Billerica, MA, 2004.
- 24 Biltonft, C. A. *Dipole Pride 26: Phase II of Defense Special Weapons Agency transport and dispersion model validation*; DPG Doc. DPG-FR-98-001; Meteorology and Obscurants Divisions: West Desert Test Center, U.S. Army Dug - way Proving Ground, Dug-way, UT, 1998.
- 25 Biltonft, C. A.; Turley, S. D.; Watson, T. B.; Crescenti, G. H.; Carter, R. G. *Over-Land Along-Wind Dispersion (OLAD) test summary and analysis*; WDTC Doc. WDTC/JCP-99/048; Meteorology and Obscurants Divisions: West Desert Test Center, U.S. Army Dug-way Proving Ground, Dug-way, UT, 1999.
- 26 Cionco, R. M., Kampe, W., Biltonft, C., Byers, J. H., Collins, C. G., Higgs, T. J., et.al., *B. Am. Meteorol. Soc.* **1999**, 80(1), 5-19.
- 27 Olesen, H.R. *User's Guide to the Model Validation Kit*; Research Notes from NERI no. 226; National Environmental Research Institute: Denmark, 2005.
- 28 Holtslag, A.A.M., Van Ulden, A.P., *J.Climate Appl. Meteorol.* **1983**, 22, 517-519.
- 29 Holtslag, A.A.M., De Bruin, H.A.R., *J. Appl. Meteorol.* **1987**, 27, 689-704.
- 30 Gryning, S.E., Batchvarova, E., Brummer, B., Jørgensen, H., Larsen, S., *Bound-Lay Meteorol.* **2007**, 124(2), 251-268
- 31 Andronopoulos, S.; Bartzis, J.G. *Model Description of RODOS Meteorological Pre-Processor*; Report RODOS(RA2)-TN(09)-02; EURANOS European Project, 2009.
- 32 Hey, B. E. *GXQ 4.0 Program Users' Guide*; WHC-SD-SWD-30002; Westinghouse Hanford Company: Richland, Washington, 1994.

- 33 Jacobson, M. Z., *Fundamentals of Atmospheric Modeling*. Cambridge University Press, New York, 34-37 pp., 1999.
- 34 Magnusson, L. *Development and validation of a new mass-consistent model using terrain influenced coordinates*. Department of Earth sciences, University of Uppsala, Sweden, 2005
- 35 Barrett, R., Berry, M., Chan, T.F., Demmel, J., Donato, J.M., Dongarra, J., et.al. (1994), Templates for the Solution of Linear Systems: Building Blocks for Iterative Methods. SIAM, Philadelphia
- 36 Moreira, V.S., Degrazia, G.A., Roberti, D.R., Timm, A.U., Carvalho, J.C., *Atmos. Pollut. Res.* **2011**, 2(3), 384-393.
- 37 Degrazia, G.A., Campos, C.R.J., Carvalho, J.C. Anfossi, D., *Bras. J. Meteorol.* **2001**, 16(2), 123-134
- 38 Jarvis, A.; Reuter, H. I.; Nelson, A.; Guevara, E. *Hole-filled seamless SRTM data V4*; International Centre for Tropical Agriculture (CIAT): Cali, South West Columbia, 2008.
- 39 *ArcMap 9.2*; ESRI (Environmental Systems Resource Institute): Redlands, California, 2009.
- 40 Steindler, M.J.; Seefeldt, W.B. *A method for estimating the challenge to an air cleaning system resulting from an explosive event*. Proceedings of the 16th DOE nuclear air cleaning conference, Harvard air cleaning laboratory, Boston, 1980.
- 41 Halverson, M.A., Mishima, J., *Initial concepts on energetic and mass releases during non-nuclear explosive events in fuel cycle facilities*; NUREG-CR-4539 (PNL-5839); U.S. Nuclear Regulatory Commission, 1986.
- 42 Yamada, T., Bunker, S., *J. Appl. Meteorol.* **1988**, 27, 562-578.
- 43 Chan, S. T.; Sugiyama, G., *A new model for generating mass consistent wind fields over continuous terrain*. 6th tropical meeting of American nuclear society on emergency preparedness and response, San Francisco, CA, 1997.

44 Chang, J. C., Franzese, P., Chayantrakom, K., Hanna, S. R., *J. Appl. Meteorol.* **2003**, 43,
453-466.

Appendix I

Estimation of the Julian day number

Estimating the Julian day number involves determining whether a year is a leap year or not. The following simple procedure can be used to perform this task.

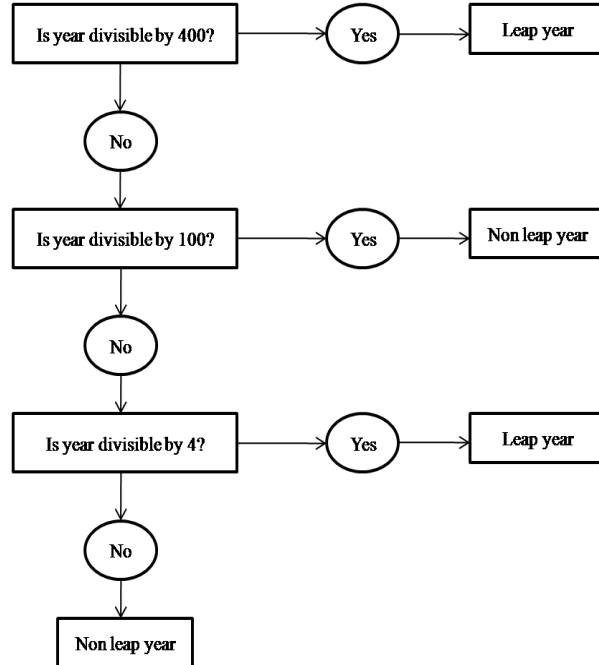


Figure I Procedure to determine whether a year is a leap year

For a leap year, the Julian day number of a month after the February is given by,

$$J_n = DD + X_{MM-1} + 1 \quad (\text{I})$$

In non leap years and up to February of all years,

$$J_n = DD + X_{MM-1} \quad (\text{II})$$

where J_n is the Julian day number, DD is the date, MM is the month and X_{MM-1} is an integer value

The Value of X for above equations can be obtained from the following table.

<i>MM</i>	1	2	3	4	5	6	7	8	9	10	11	12
	Jan	Feb	Mar	Apr	May	Jun	Jul	Aug	Sep	Oct	Nov	Dec
<i>X</i>	031	059	090	120	151	181	212	243	273	304	334	365

Table I Corresponding *X* value for the month

Appendix II

The ratio γ is defined as the ratio of specific heat of air at constant pressure to latent heat of evaporation of water and to the rate of change of the saturation specific humidity with temperature.

$T_a ({}^\circ C)$	γ
-5	2.01
0	1.44
5	1.06
10	0.79
15	0.60
20	0.45
25	0.35
30	0.27
35	0.21

Table II The variation of ratio gamma with the temperature at constant pressure of

$$1 \times 10^5 \text{ N m}^{-2}$$

Appendix III

Estimation of the wet bulb temperature

The wet bulb temperature is defined as the temperature of a parcel of air if it were adiabatically saturated by evaporating water into it with the latent heat supplied by the parcel. Although, its value can be obtained using a wet bulb thermometer or empirical methods, a computationally efficient and accurate iterative procedure which reduces the burden of user input is more appropriate.

According to this procedure, the wet bulb temperature is given by;

$$T_w = (T_a - 273.15) - \left\{ \frac{e_{sw0} - \left(\frac{RH}{100} \times e_s \right)}{6.53 \times 10^{-6} \times p} \right\} \quad (\text{III})$$

where T_a is the dry bulb temperature (K), RH is the relative humidity, p is the atmospheric pressure (Pa), e_s is the saturation vapor pressure and e_{sw0} is the initial saturation vapor pressure

Saturation vapor pressure is calculated from the following equation with $T = T_a - 273.15$;

$$e_s = \exp\left(\frac{21.4T + 494.41}{T + 273.15}\right) \quad (\text{IV})$$

First, the initial saturation vapor pressure is calculated from equation (A-3.3) with $T = T_{w0} = T_a - 288.15$. Value of the equation (A-3.1) was obtained and checks whether $|T_w - T_{w0}| \leq 0.1^\circ\text{C}$ is true. If so, the iteration stops and the value of wet bulb temperature is taken to be T_w . Otherwise, if the value of $(T_w - T_{w0})$ is greater than 0.1°C , T_{w0} is updated as $T_{w0} = T_a - 288.15 + N \times 10^{-3}$. If the value of $(T_w - T_{w0})$ is less than -0.1°C , T_{w0} is updated as $T_{w0} = T_a - 288.15 - N \times 10^{-3}$. After each update, the value of equation (A-3.1) is evaluated, checks for the convergence and the iteration is carried out until the stopping criterion is reached. It should be noted that N is a whole number in above equations, which indicates the order of iterative recurrence required to achieve the stopping criterion. ($N = 1$ is used in this study.)

Appendix IV

The Method of False Position

The iterative procedure of the false position method starts with an initial interval (x_1, x_2) assuming that the function changes sign only once in this interval. Now it is possible to find a x_3 in this interval, which is given by the intersection of the X axis and the straight line passing through $(x_1, f(x_1))$ and $(x_2, f(x_2))$. Then x_3 is given by;

$$x_3 = x_1 - \frac{(x_2 - x_1)f(x_1)}{f(x_2) - f(x_1)}$$

The new interval is either (x_1, x_3) or (x_2, x_3) depending on in which interval the function changes sign. The iteration is carried out until the required accuracy is achieved.

Appendix V

Preconditioned Bi-Conjugate gradient stabilized method

To solve a non-symmetric linear system given by $Ax=b$ the preconditioned Bi-Conjugate gradient stabilized (Bi-CGSTAB) method can be used. To accelerate the convergence the diagonal preconditioner; where preconditioner M consists of the diagonal elements of matrix A is utilized. Pseudocode for the preconditioned Bi-CGSTAB method is given below.

Let $r^{(0)}$ be the residual vector; $r^{(0)} = b - Ax^{(0)}$ for some initial guess $x^{(0)}$

Choose $\tilde{r} = r^{(0)}$

for $i = 1, 2, 3, \dots$

$$\rho_{i-1} = \tilde{r}^T r^{i-1}$$

If $\rho_{i-1} = 0$ method fails

If $i = 1$

$$p^{(i)} = r^{(i-1)}$$

Else

$$\beta_{i-1} = \left(\rho_{i-1} / \rho_{i-2} \right) \left(\alpha_{i-1} / \omega_{i-1} \right)$$

$$\rho^{(i)} = r^{(i-1)} + \beta_{i-1} \left(p^{(i-1)} - \omega_{i-1} v^{(i-1)} \right)$$

End If

Solve $M\hat{p} = p^{(i)}$

$$v^{(i)} = A\hat{p}$$

$$\alpha_i = \rho_{i-1} / \tilde{r}^T v^{(i)}$$

$$s = r^{(i-1)} - \alpha_i v^{(i)}$$

Check norm of s ; If small enough: set $x^{(i)} = x^{(i-1)} + \alpha_i \hat{p}$ and stop

Solve $M\hat{s} = s$

$$t = A\hat{s}$$

$$\omega_i = t^T s / t^T t$$

$$x^{(i)} = x^{(i-1)} + \alpha_i \hat{p} + \omega_i \hat{s}$$

$$r^{(i)} = s - \omega_i t$$

Check convergence; continue if necessary

for continuation it is necessary that $\omega_i \neq 0$

End

Appendix VI

Values of surface roughness length for each surface condition are given by the Devenport classification as shown in the table below.

Table III Devenport classification of surface roughness length

Class		Short terrain description	Zo (m)
1	“Sea”	Open water, Sea or lake (at least 5 km),Snow covered flat plain, featureless desert, tarmac and concrete, with a fetch of several km	0.0002
2	“Smooth”	Featureless land surface without any noticeable obstacles and negligible vegetation; Eg. Beaches, pack ice without large ridges, marsh and snow covered or fallow open country	0.005
3	“Open”	Level country with low vegetation (eg. Grass) and isolated obstacles with separations of at least 50 obstacle heights; eg. Grazing land without windbreaks, heather, moor and tundra, runaway areas of airports. Ice with ridges across-wind.	0.03
4	“Roughly open”	Cultivated or natural areas with low crops or plant covers, or moderately open country with occasional obstacles (eg. Low hedges, isolated low buildings or trees) at relative horizontal distances of at least 20 obstacle heights.	0.10
5	“Rough”	Cultivated or natural area with high crops or crops of varying height, and scattered obstacles at relative distances of 12 to 15 obstacle heights for porous objects (eg. Shelterbelts) or 8 to 12 obstacle heights for low solid objects (eg. Buildings)	0.25
6	“Very rough”	Intensively cultivated landscape with many rather large obstacle groups (large farms, clumps of forest) separated by open spaces of about 8 obstacle heights. Low densely planted major vegetation like bush land. Orchards, young forest. Also, area moderately covered by low buildings	0.5

		with interspaces of 3 to 7 building heights and no high trees.	
7	“Skimming”	Landscape regularly covered with similar-size large obstacles, with open spaces of the same order of magnitude as obstacle heights; eg. Mature regular forests, densely built up area without much building height variation.	1
8	“Chaotic”	City centers with mixture of low-rise and high-rise buildings, or large forests of irregular height with many clearings.	≥ 2

Appendix VII

Albedo values for various types of surfaces are given in the following table.

Table VI Albedo for various surfaces

Surface	Albedo e
Soils (Dark, wet - Light, dry)	0.05 - 0.40
Desert	0.20 - 0.45
Grass (Long [1.0 m] - Short [0.02m])	0.16 - 0.26
Agricultural crops	0.18 - 0.20
Orchards	0.15 - 0.20
Forests	
Decious (bare leaved)	0.15 - 0.20
Coniferous	0.05 - 0.15
Water	0.03 - 1.00
Snow (Old – Fresh)	0.40 - 0.95
Ice	
Sea	0.30 - 0.45
Glacier	0.20 - 0.40
Tarmac, Asphalt	0.05

Buildings	0.20 - 0.45
-----------	-------------

Appendix VIII

Input for the model evaluation study

Table VII presents the hourly averaged meteorological input used for the model evaluation using DP26 field dataset. Note that the MEDA stands for the meteorological station and WS, WD, T, P, RH, CC for the hourly averaged wind speed, direction, temperature, pressure, relative humidity and cloud cover respectively.

Table VII Meteorological input employed in the overall performance evaluation of HPM

Trial	MEDA	WS (ms^{-1})	WD (deg)	T ($^{\circ}\text{C}$)	P (mmHg)	RH (%)	CC (%)
1	1	3.47	301	4.8	870.0	64	100
	2	1.03	296	1.3	869.8	100	100
	3	1.67	252	2.5	870.0	69	100
	6	1.03	172	1.0	880.3	95	100
	9	4.12	345	6.8	880.3	55	100
	10	2.96	319	2.3	880.3	55	100
	17	3.09	352	5.0	880.5	76	100
2	1	3.99	135	4.5	872.5	16	100
	2	2.44	147	1.8	872.8	100	100
	3	4.12	174	5.5	872.5	19	100
	6	3.34	177	4.0	888.1	15	100
	9	2.96	183	2.8	888.1	16	100
	10	2.06	169	1.0	888.1	16	100
	17	4.24	169	6.3	883.5	20	100
3	1	4.24	201	4.8	870.0	25	80

	2	5.79	161	6.5	870.0	100	80
	3	3.99	169	6.0	870.0	22	80
	6	1.93	165	1.8	885.5	22	80
	9	5.40	173	7.0	885.5	21	80
	10	4.12	211	2.8	885.5	21	80
	17	3.22	173	4.0	881.0	27	80
4	2	6.17	172	6.3	865.1	37	20
	3	5.02	161	5.5	865.1	37	20
	6	4.12	151	4.3	880.4	41	20
	9	5.27	171	4.8	880.0	34	20
	10	3.34	201	2.3	880.0	34	20
	17	4.12	160	4.8	876.2	40	20
5	1	2.44	167	1.8	869.6	62	30
	2	3.22	147	3.3	869.6	100	30
	3	2.96	182	1.5	869.6	39	30
	6	2.96	175	2.0	884.9	46	30
	9	2.96	192	2.8	884.9	46	30
	10	3.60	197	2.0	884.9	46	30
	17	2.06	192	2.0	880.6	54	30
6	1	4.37	203	3.3	870	58	20
	2	4.12	158	4.0	868.5	100	20
	3	5.14	167	4.0	885.0	42	20
	6	3.22	191	3.3	883.9	49	20
	9	3.47	191	2.5	885	42	20
	10	6.05	227	4.8	879.5	49	20
	17	3.60	197	2.8	879.5	49	20
7	1	5.02	152	5.0	864.5	46	10
	2	3.47	152	4.5	864.4	37	10
	3	4.89	167	5.3	864.5	37	10
	6	3.34	149	3.5	879.7	38	10
	9	5.79	173	8.0	879.7	36	10
	10	4.12	196	2.5	879.7	36	10

	17	4.63	154	5.0	875.3	37	10
8	1	5.14	129	6.5	868.0	40	10
	2	3.47	147	3.3	863.9	45	10
	3	5.02	163	6.5	863.9	34	10
	6	3.22	186	3.3	879.4	34	10
	9	3.99	180	4.0	875.1	34	10
	10	3.34	196	2.3	864.1	45	10
	17	4.63	161	5.3	874.8	36	10

It should be noted that some MEDA stations reported missing values in several cases. These values were approximated using the values of nearest MEDA station. DP26 documentation reports that the surface roughness length of the Nevada test site varies between 3-6 m. A value of 0.0385 m was chosen by averaging given roughness lengths and 0.3, 0.1 values were assumed for Albedo and surface moisture availability parameters considering the nature of the surface of Nevada test site.

Appendix IX

Descriptive statistics for the evaluation of basic meteorological parameterization

ANOVA test for the Friction Velocity

Anova: Single Factor

SUMMARY

Groups	Count	Sum	Average	Variance
	108			

Column 1	155	74.91677	0.483334	0.053948
Column 2	155	75.935	0.489903	0.043255

ANOVA

<i>Source of Variation</i>	<i>SS</i>	<i>df</i>	<i>MS</i>	<i>F</i>	<i>P-value</i>	<i>F crit</i>
Between Groups	0.003344	1	0.003344	0.068815	0.793246	3.871827
Within Groups	14.96926	308	0.048601			
Total	14.9726	309				

ANOVA test for the Monin-Obukhov length

Anova: Single Factor

SUMMARY

<i>Groups</i>	<i>Count</i>	<i>Sum</i>	<i>Average</i>	<i>Variance</i>
Column 1	147	821.4986	5.588426	86588.79
Column 2	147	1909.9	12.99252	46718.35

ANOVA

<i>Source of Variation</i>	<i>SS</i>	<i>df</i>	<i>MS</i>	<i>F</i>	<i>P-value</i>	<i>F crit</i>

Between Groups	4029.312	1	4029.312	0.060452	0.805956	3.873502
Within Groups	19462842	292	66653.57			
Total	19466871	293				

ANOVA test for the Sensible heat flux

Anova: Single Factor

SUMMARY

Groups	Count	Sum	Average	Variance
Column 1	162	7387.137	45.59961	8228.607
Column 2	162	10016.99	61.83327	14257.21

ANOVA

Source of Variation	SS	df	MS	F	P-value	F crit
Between Groups	21346.06	1	21346.06	1.898625	0.169189	3.8705
Within Groups	3620216	322	11242.91			
Total	3641563	323				

Descriptive statistics for the evaluation of mass consistent wind model

Horizontal profile

Anova: Single Factor

SUMMARY

Groups	Count	Sum	Average	Variance
Column 1	1225	6102.72	4.981812	1.058908
Column 2	1225	6139.481	5.011822	1.325911

ANOVA						
<i>Source of Variation</i>	<i>SS</i>	<i>df</i>	<i>MS</i>	<i>F</i>	<i>P-value</i>	<i>F crit</i>
Between Groups	0.551598	1	0.551598	0.462591	0.49648	3.84526
Within Groups	2919.018	2448	1.192409			
Total	2919.57	2449				

Vertical profile

Anova: Single Factor

SUMMARY						
<i>Groups</i>	<i>Count</i>	<i>Sum</i>	<i>Average</i>	<i>Variance</i>		
Column 1	456	0.000969	2.12E-06	3.06E-07		
Column 2	456	-6.14326	-0.01347	0.722849		
ANOVA						
<i>Source of Variation</i>	<i>SS</i>	<i>df</i>	<i>MS</i>	<i>F</i>	<i>P-value</i>	<i>F crit</i>
Between Groups	0.041394	1	0.041394	0.114531	0.735122	3.851698
Within Groups	328.8962	910	0.361424			
Total	328.9376	911				

Descriptive statistics for the evaluation of overall model performance

Anova: Single Factor

SUMMARY						
<i>Groups</i>	<i>Count</i>	<i>Sum</i>	<i>Average</i>	<i>Variance</i>		
Column 1	24	11262.99	469.2912	824126.6		
Column 2	24	6046.013	251.9172	250803.1		

ANOVA

<i>Source of Variation</i>	<i>SS</i>	<i>df</i>	<i>MS</i>	<i>F</i>	<i>P-value</i>	<i>F crit</i>
Between Groups	567017.3	1	567017.3	1.054985	0.309733	4.051749
Within Groups	24723383	46	537464.9			
Total	25290401	47				